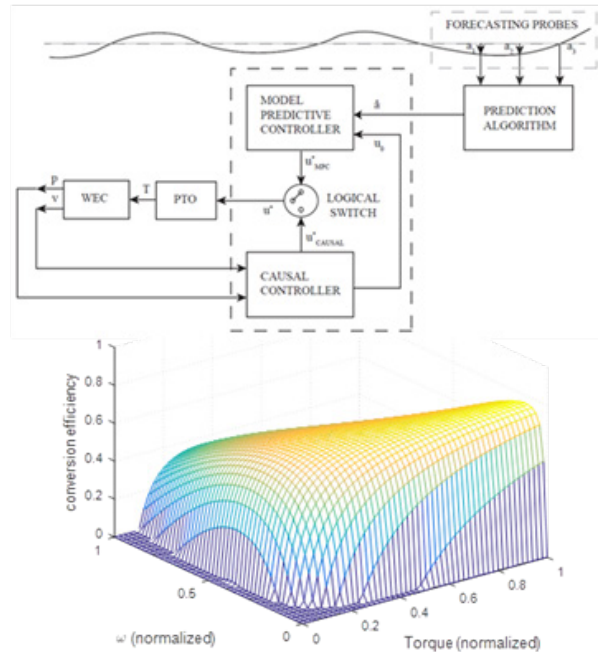
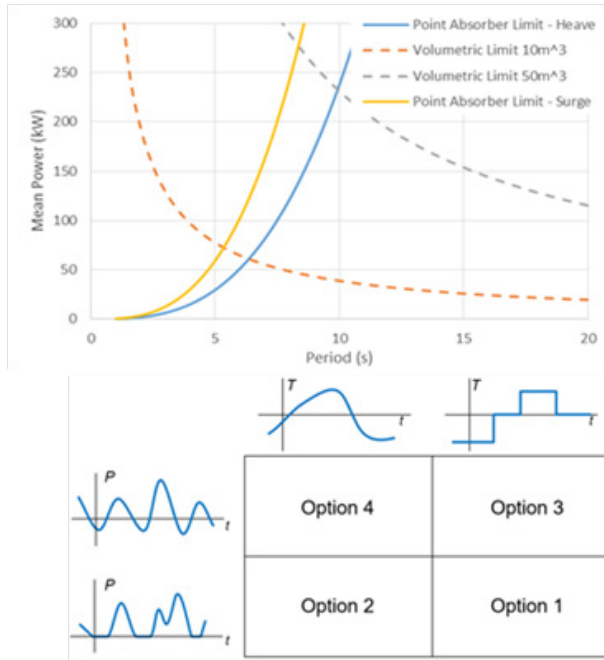


Controls Optimization

Final Technical Report



DOE Award Number: DE-EE0007173
 Project Period: 1/1/2016 to 12/31/2019
 Report Date: 11/12/19

Principal Investigator

Mirko Previsic – Re Vision Consulting
 Email: mirko@re-vision.net

Recipient Organization

Re Vision Consulting, LLC
 1104 Corporate Way
 Sacramento, CA 95831

Partners

Resolute Marine Energy
 CalWave
 Ocean Energy USA
 University of Michigan
 Integral Consulting
 HT Harvey and Associates

Acknowledgment: “This report is based upon work supported by the U. S. Department of Energy under Award No. DE-EE0007173“.

Disclaimer: “Any findings, opinions, and conclusions or recommendations expressed in this report are those of the author(s) and do not necessarily reflect the views of the Department of Energy”. This document was prepared by the organizations named below as an account of work sponsored or cosponsored by the U.S. Department of Energy (DoE). Neither DoE, RE vision consulting, LLC (RE vision), any cosponsor, the organization (s) below, nor any person acting on behalf of any of them:

(A) Makes any warranty or representation whatsoever, express or implied, (I) with respect to the use of any information, apparatus, method, process or similar item disclosed in this document, including merchantability and fitness for a particular purpose, or (II) that such use does not infringe on or interfere with privately owned rights, including any party’s intellectual property, or (III) that this document is suitable to any particular user’s circumstance; or

(B) Assumes responsibility for any damages or other liability whatsoever (including any consequential damages, even if RE Vision or any RE Vision representative has been advised of the possibility of such damages) resulting from your selection or use of this document or any other information, apparatus, method, process or similar item disclosed in this document.

The views and opinions of authors expressed herein do not necessarily state or reflect those of the United States Government or any agency thereof, or RE Vision Consulting, LLC.

Document by:
RE Vision Consulting, LLC
www.re-vision.net
Project Manager: Mirko Previsic
Email Address: mirko@re-vision.net

Table of Contents

Project Summary.....	5
Alignment with the Program.....	5
Project Objectives and Impacts.....	5
End-User Engagement and Dissemination Strategy	6
Management Approach	7
Technical Approach.....	8
Technical Accomplishments and Progress	8
Future Work (New and Ongoing Projects Only)	9
Wave Prediction System Development using Measurement Buoys as Sensing Elements	11
Linear and Non-Linear MPC Development and Application to Reference WEC Topologies	14
Causal Controls Development and Application to Reference WEC Topologies.....	15
PTO Modeling and Trade-Off Studies.....	15
Wave Tank Validation of 3 Reference Topologies.....	18
RT In-Ocean Control Testing and Validation.....	21
Techno-Economic Assessments.....	23

List of Figures

Figure 1 - Normalized performance as a function of the prediction horizon for a heaving point absorber and a surge WEC device.	12
Figure 2 - MPC sensitivity to amplitude and phase error in the wave prediction.....	12
Figure 3 - Wave Probe Layout.....	13
Figure 4 - Wave prediction from field campaign showing measured vs. predicted (propagated) wave surface elevation.....	13
Figure 5 - PTO Options 1-4	16
Figure 6 – Sample loss model used for controls-design purposes.	17
Figure 7 - Controls and force-tracking setup for testing a heaving buoy.....	19
Figure 8 - Physical setup of test in wave tank at the Oregon State University	19
Figure 9 - OE Buoy being tested at Oregon State University	20
Figure 10 - RME Device being tested at Oregon State University	20
Figure 11 - Controls Topology for In-Ocean Deployments.....	21
Figure 12 - LabView Controls Interface	21
Figure 13 - Demonstrator WEC Device: Scale (left), Build images (right).....	22

Figure 14 - Identification of Major Buoy Sub-Systems – Device in horizontal position 23

Figure 15 - Buoy deployed at sea (left) and on deck before installation (right) 23

List of Tables

Table 1 - Performance Effects of Wave-Prediction Error..... 14

Table 2 - Performance Comparison for Heaving Point Absorber..... 24

Table 3 – Baseline Cost Assessment..... 24

Table 4 - Cost Scaling Relationships..... 25

Table 5 - Cost and Economic Summary of Optimally Controlled WEC Device..... 25

Executive Summary

Project Summary

The over-arching project objective is to fully develop and validate optimal controls frameworks that can subsequently be applied widely to different WEC devices and concepts. Optimal controls of WEC devices represent a fundamental building block for WEC designers that must be considered as an integral part of every stage of device development. Using a building-blocks approach to optimal controls development, this effort will result in the full development of a feed-forward and feed-back control approach and a wave prediction system.

Phase I focused primarily on numerical offline optimization and validation using wave tank testing of three industry partners' WEC devices, including; CalWave, Ocean Energy, and Resolute Marine Energy. These industry partnerships allowed us to identify optimal control strategies for these different WEC topologies at different maturity levels. Phase II focused on demonstrating an integrated control system on an at-sea prototype that is to be custom-built and maturing the HW and SW required to successfully run our advanced controls code frameworks on at-sea systems. A secondary focus during phase II is to adapt our systems identification, controls and wave-prediction frameworks to become more robust and comprehensive in respect to RT capability, robustness, and reliability.

Alignment with the Program

This project contributes to the following MHK Program Approaches:

- **Foundational and Crosscutting R&D:**
 - Drive innovation in components, **controls**, manufacturing, materials and systems with early-stage R&D specific to MHK applications
 - Develop, improve, and validate numerical and experimental tools and methodologies needed to improve understanding of important fluid-structure interactions
 - Collaboratively develop and apply quantitative metrics to identify and advance technologies with high ultimate techno-economic potential for their market applications
- **Technology-Specific Design and Validation:**
 - Validate performance and reliability of systems by conducting in-water tests of industry-designed prototypes at multiple relevant scales

Project Objectives and Impacts

Control of WEC devices plays a critical role in improving power capture, decreasing structural loads, and reducing PTO requirements in WEC systems. Optimal controls leveraging Model Predictive control and causal (feed-back) control strategies have the potential to significantly improve the economic viability in most WEC devices under development.

The key objectives of this project are focused on developing “industry-ready” controls technology building blocks that can be applied to a wide range of different WEC topologies including:

- Development of optimal controls algorithm frameworks that can be applied to a wide range of different WEC topologies. Both causal and non-causal (requiring a prediction of excitation forces) are being evaluated and applied.

- Develop a wave prediction system that can be used to feed into Model Predictive Control (MPC) frameworks. Evaluate the use of wave radar and measurement buoys to provide wave measurements to feed into prediction algorithms.
- Develop and refine approaches by working with three different device developers and retiring technical issues through an incremental testing and validation process using: (1) numerical modeling, (2) wave tank testing, and (3) in-ocean validation on a small heaving point absorber.

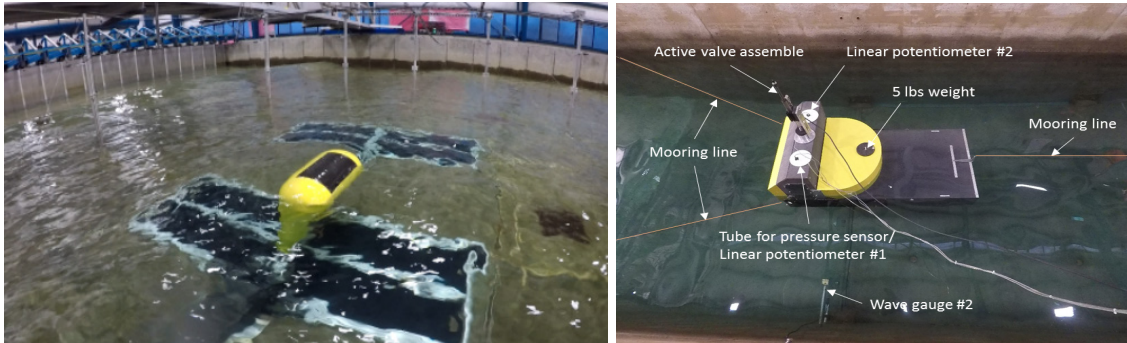


Illustration: Wave Tank Testing at OSU of RME Surge WEC (left), and OE Buoy (right)



Illustration: 8kW In-Ocean Control Testing WEC Unit

End-User Engagement and Dissemination Strategy

We focused on the optimizing four different WEC topologies. To do so, we engaged with three different device developers and optimized the control system of their devices including; (1) Resolute Marine Energy, (1) Ocean Energy USA, and (3) CalWave. These collaborations allowed us to focus on solving device-specific problems and bring these “lessons-learned” back to our algorithm frameworks. A fourth topology, a heaving point absorber tethered to the seabed was brought along to enable testing at sea on our own small controls unit at sea and fully integrate its controller with our wave prediction system.

Management Approach

Re Vision Consulting leads the project and established subcontracts with all project partners and consultants to execute on the scope. Quarterly reviews with the DoE project management were used to align project scope and adapt the project plan to most effectively achieve our core objectives. Most of the heavy lifting on controls development and validation was performed in-house. The co-location of the core technical team (4 FT Engineers), enabled a tight integration between technical disciplines and allowed for rapid resolution of issues. Communication with external team-members was done using weekly conference calls.

Key milestones revolved around the controls optimization and wave tank validation tasks during phase I and around the in-ocean testing and validation activities during phase II. The following provides a high level schedule and main milestones over the performance period.

Table 1: Schedule and Milestones

	2016	2017	2018	2019
Phase I Activities				
Detailed Implementation Planning				
RME - Controls Optimization				
RME - Wave Tank Testing				
OE - Controls Optimization				
OE - Wave Tank Testing				
CalWave - Controls Optimization				
Wave Prediction System Development				
Design of In-Ocean Demonstrator				
Phase II Activities				
Detailed Design				
Build of Demonstrator				
RT Testing of Wave Prediction System				
Testing of Demonstrator				
Milestones				
RME Device Optimized		●		
OE Buoy Optimized			●	
CalWave Controls Evaluated			●	
Wave-Prediction Buoys Built		●		
In-Ocean Validation of WP Accuracy			●	
Go/NoGo Review			●	
Demonstrator Ready for Deployment				●
Complete Demo In-Ocean Testing				●

Success in avoiding/reducing costs: Re Vision was able to take advantage of measurement hardware loaned from NREL reducing field-campaign costs. We also continuously re-aligned our scope to take advantage of technical opportunities and reducing cost. The result is that we were able to complete a broader scope than originally planned under our original budget umbrella.

Cost/time overruns: We underestimated the time and money required for building and testing our in-ocean demonstrator. We were able to largely mitigate cost overruns, but at the expense of a stretched out timeline. Specifically, the build process for our 8kW in-ocean demonstrator was delayed due to the long lead on PTO hardware components. This resulted in us missing the summer deployment window on the pacific coast during the summer of 2018, pushing it out by one year. We also underestimated the challenges associated with the in-ocean testing efforts.

Technical Approach

On the controls side, we leveraged linear and non-linear MPC methods, as well as causal methods developed by Jeff Scruggs at the University of Michigan. We then applied these methods to our target topologies and moved through a controls optimization process starting with a system with no constraints placed on them. This allowed us to identify and benchmark the theoretical upper limits of that topology and identify the potential level of improvements over the slow-tuned baseline. Subsequently we started to identify the design's sensitivity to PTO topology chosen, and constraints and losses imposed on the design. Trade-offs were evaluated using appropriate techno-economic benchmarking to identify optimality in the systems design. These trade-offs included all of the parameters affecting LCoE of the design such as average power capture, peak-to-average power, and structural loads on the device structure. This design-optimization approach is a significant change from other controls-optimization R&D, which is purely focused on power capture.

On the wave-prediction side, we started with the evaluation of methods that utilize wave-radar as well as wave measurement buoys but focused quickly on measurement buoys. This was largely because we felt that we could attain reasonable prediction accuracies with less complexity and relatively well defined technology development process. A subsequent project did focus on the utilization of wave radar in predicting ocean waves.

Validation during phase I was completed using wave tank testing. In the process we built physical models for the RME device (1:10 scale), the OE buoy (1:25 scale) and validated wave propagation models for the wave prediction work.

Our core objective was to insure that we can identify the techno-economic optimal controls strategy using causal and non-causal control laws, while retaining real-time capabilities. In the process, we had to solve a number of significant challenges, resulting in the development of novel systems identification techniques, better MPC solvers, and novel controls approaches. Together, these innovations enable solving most WEC controls challenges out there Today.

Phase II focused primarily on at-sea validation of our wave-prediction algorithms and the build/test of an at-sea 8kW controls demonstrator. To do so, we had to move our controls algorithms developed in Matlab onto robust RT hardware and develop a suitable front-end processing and fault handling. The end-product is a matured algorithm framework that can be widely applied to any WEC and PTO topology.

Technical Accomplishments and Progress

The project is almost complete and we were able to advance the state of the art in several key areas including:

- Demonstrated real-time wave prediction at sea. While academic papers have been presented on this topic, no-one to our knowledge has successfully demonstrated phase-resolved wave prediction with sufficient accuracy that would enable MPC in WEC technologies. This is a key building block to enable optimal control.
- Demonstrated real-time MPC at sea. To our knowledge MPC has only been demonstrated in wave tank environments. We are the first ones to demonstrate Model Predictive Control at sea. This effectively enables a new generation of controls on WEC devices deployed at sea.
- We introduced controls co-design into the wave energy space leveraging model predictive control. This will enable WEC design optimization while continuously insuring that controls optimality is enforced. This capability enables design for optimality from the concept stage and reduces significant uncertainties in the design optimization process.

- We developed a method to efficiently introduce loss models and PTO limitations in the controls design process. Bringing the PTO modeling capabilities into the controls design process and enabling trade-off studies while enforcing optimality is a critical capability for this sector and has not been systematically developed by this emerging industry.
- We made several advances in the areas of numerical methods including: (1) efficient numerical methods to represent the PTO in a controls model, (2) efficient development of sub-space models that significantly improve the computational efficiency to handle MPC-type problems, (3) integrated causal controls methods with MPC methods to significantly improve controls robustness and ability to handle errors in the wave prediction scheme, and (4) introduced several method extensions to handle constraints in causal controllers.

Our work with our device development partners has allowed them to establish critically needed trade-offs with confidence, which reflects in their device design today resulting in significant performance improvements and cost-reductions.

Future Work (New and Ongoing Projects Only)

While we have made significant progress in advancing state of the art optimal controls, significant challenges and advances need to be made to enable the widespread commercial adoption of optimal controls by device manufacturers. This includes the following core areas:

- Improvements in computational efficiency for non-linear MPC: To insure true optimality in many device types, non-linear MPC methods are required. Many of these solutions are not real-time capable and because MPC is a sequential optimization scheme, it cannot simply be improved by using parallel processing schemes typically employed in high-performance computing. Further work is needed to develop methods that are fully capable of handling these non-linearities in an efficient manner in real-time.
- Enabling commercialization: While we have demonstrated many of the controls and wave-prediction capabilities, continued funding will be required to turn these accomplishments in practical numerical tools that can be used across all stages of product development.

These challenges outlined above will require continued funding by US Department of Energy. We hope that we will be able to compete for such funding opportunities on a level playing field.

Award 8099, which will be presented separately is focused on extending the wave prediction efforts to leverage the synergies of measuring with in-situ buoys as well as wave radar and combining these approaches using sensor-fusion techniques. It builds directly onto this work and broadens the approaches leveraged to predict ocean waves.

Background

The current work builds on previous efforts in the areas of optimal controls for WEC devices by Re Vision Consulting and University of Michigan. These efforts include among others:

1. An NSF STTR award that allowed Re Vision Consulting to establish numerical approaches for linear and non-linear MPC as well as wave-prediction using radar and wave measurement buoys.
2. A SPA-I award from the US Department of Energy lead by Resolute Marine Energy (RME) aimed at studying optimal control trade-offs for its Surge WEC Device. Re Vision Consulting and University of Michigan were sub-recipients in this project.
3. The Wave Energy Prize Competition established by the US Department of Energy. Re Vision Consulting established MPC-based controls algorithms to explore upper performance limits for the Waveswing America Team, which won 3rd place out of 92 teams.
4. A parallel project was initiated in 2017 to look at sensor fusion methods to improve wave prediction accuracy leveraging wave radar measurements. This effort is being carried out in collaboration with the US Navy that previously developed wave prediction capabilities under its EMFS (Environmental Motion Forecasting System) program that leveraged radar hardware and algorithms to measure ocean waves using X-band radar.
5. Several engagements with device developers to assist in the WEC device optimization process including controls co-design.

The over-arching project objective for this project was to fully develop and validate an optimal controls framework that can subsequently be applied widely to different WEC devices and concepts. Optimal controls of WEC devices represent a fundamental building block for WEC designers that must be considered as an integral part of every stage of device development. Using a building-blocks approach to optimal controls development, this effort will result in the full development of a feed-forward and feed-back control approach and a wave prediction system.

The following elements formed a part of our scope of work:

1. Wave Prediction System Development using Measurement Buoys as Sensing Elements
2. Linear and Non-Linear MPC Development and Application to Reference WEC Topologies
3. Causal Controls Development and Application to Reference WEC Topologies
4. Systems ID and Reducing Model Order
5. PTO Modeling and Trade-Off Studies
6. Wave Tank Validation of 3 Reference Topologies
7. RT In-Ocean Control Testing and Validation
8. Techno-Economic Assessments

What follows is a brief descriptions of each one of these components. Details can be found in the enclosed appendices that provide more detailed background information on each one of these components. Where information is considered protected, it is identified as such. This includes device specific information (obtained from device developers) and data-sets that are of commercially sensitive nature.

Introduction to Work Packages

What follows, is a brief descriptions of each one of these components. Details can be found in the enclosed appendices that provide more detailed background information on each one of these components. Where information is considered protected, it is identified as such. This includes device specific information (obtained from device developers) and data-sets that are of commercially sensitive nature.

Wave Prediction System Development using Measurement Buoys as Sensing Elements

MPC relies on a prediction of the wave-excitation forces over a sufficiently long prediction horizon. Wave-prediction methods can be generally categorized as either auto-regressive or deterministic. Auto-regressive models extrapolate future wave excitation forces from a given measured history by fitting a model to it. This type of model tends to do well for a few seconds into the future, but these predictions are generally insufficient in length to meet the requirements of optimal feed-forward control for most WEC device topologies. For wave predictions to be “good enough” for controls, they need to be accurate enough and predict sufficiently far into the future to provide optimal results.

The required prediction horizon for MPC algorithms is a strong function of the device topology and configuration. In general, devices with a high inertia and weak coupling between the primary absorption mode and PTO require a longer prediction than devices with a low inertia and strong coupling between the primary absorption mode and PTO. Herein, we refer to this as a strongly coupled closed-loop response. The explanation for this observed phenomenon can be broken down into two distinct problems: (1) the non-causality of wave-excitation forces (Falnes 2002) and (2) the coupling between control action and motion response.

The more dominant prediction horizon driver appears to be how closely coupled the closed-loop response of the dynamic system is to the control input. This becomes apparent when evaluating the optimal prediction horizon for other topologies in this paper. Figure 14 shows the average normalized absorbed power as a function of the prediction horizon for two different topologies. It illustrates that the optimal prediction horizon for the RME Surge WEC device is longer than for the heaving point absorber. In some cases, that prediction horizon requirement is reduced to only about half a wave period, which opens up interesting alternatives to replace a deterministic wave forecast with an auto-regressive model and/or use causal controllers.

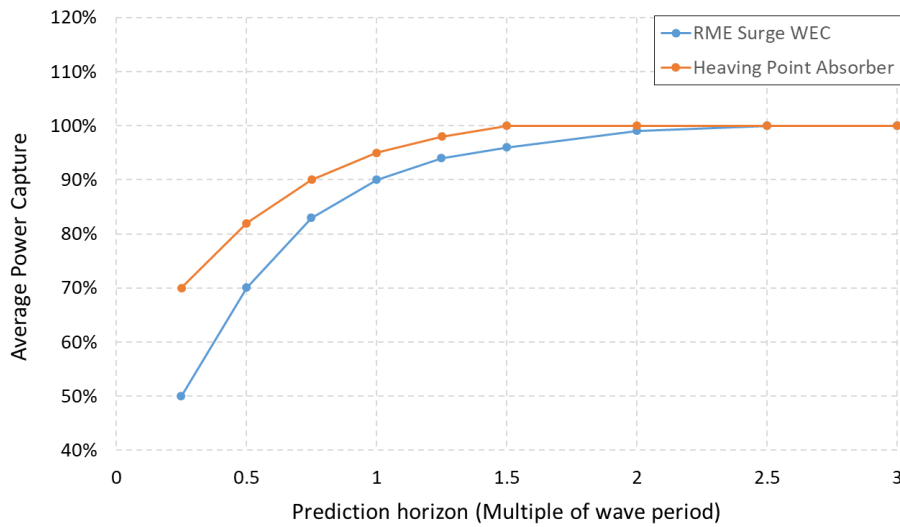


Figure 1 - Normalized performance as a function of the prediction horizon for a heaving point absorber and a surge WEC device.

A second issue to consider is the accuracy of the forecast. To better understand this issue, we carried out a sensitivity study to phase and amplitude errors of the forecast for a simple heaving point absorber. The study’s results, summarized in Figure 15, demonstrate that MPC is more robust against wave-amplitude prediction errors than phase prediction errors. It shows that a change in the phase error causes a bigger reduction in power than a change in the amplitude error.

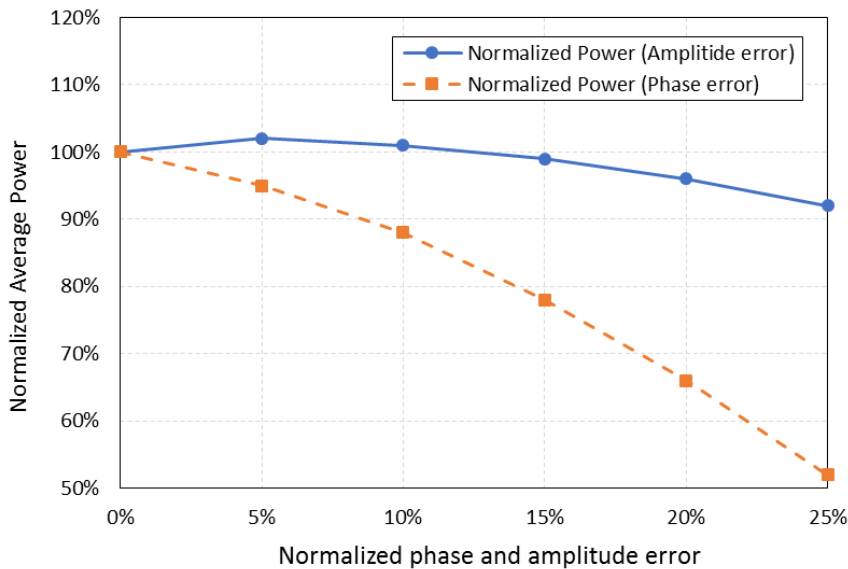


Figure 2 - MPC sensitivity to amplitude and phase error in the wave prediction

To understand how well waves can be forecasted in the open ocean, we carried out a field campaign in Santa Cruz, assimilated data from six custom-built wave-measurement buoys, and predicted the wave field to a down-wave location, where a seventh wave measurement buoy was located. The down-wave measurement buoy was then used to validate the wave prediction from the up-wave buoys. Various methods of identification, propagation and correction were applied and tested to minimize wave prediction errors. The final result showed that a mean absolute amplitude error of less than 15% is attainable for a forecasting

time horizon that is about twice as long as the dominant wave period. Figure 17 provides a snapshot of the actual and predicted wave surface elevation with a 20s forecasting horizon (roughly twice the wave period in this case).

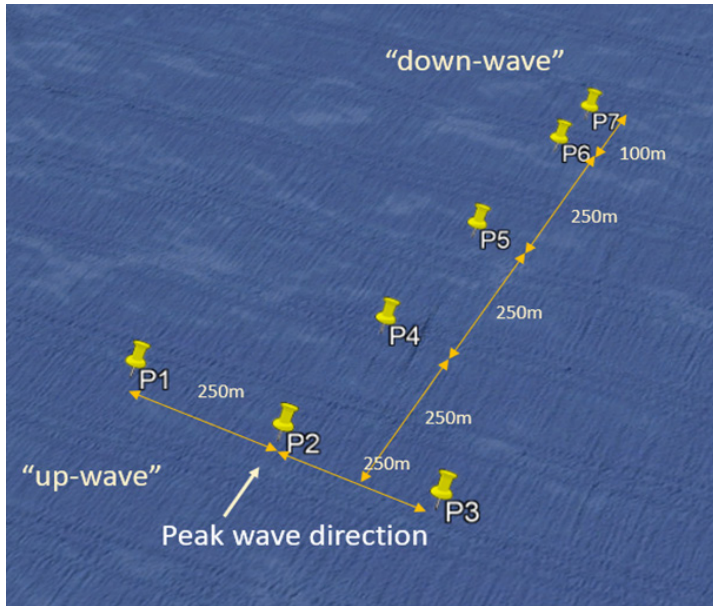


Figure 3 - Wave Probe Layout

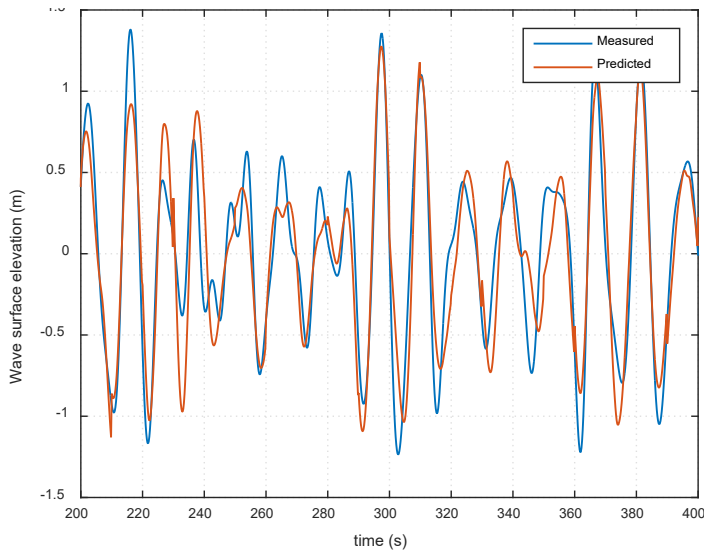


Figure 4 - Wave prediction from field campaign showing measured vs. predicted (propagated) wave surface elevation.

To understand the impact of this error on MPC, we used the predicted surface elevation values to compute a controls command with MPC and the actual values of the wave-surface elevation to drive the system dynamics model. This approach allowed us to understand the performance degradation due to the introduction of realistic prediction errors. The results for a simple heaving point absorber for a given sea state are shown in Table 2.

Table 1 - Performance Effects of Wave-Prediction Error

Controls Method	Absorbed Power	Normalized
Optimal Linear Damping	16.3 kW	100%
Optimal Causal Control	25.8 kW	153%
Linear MPC (No Prediction Error)	47.9 kW	293%
Linear MPC (Realistic Prediction Error)	39.6 kW	242%

Performance degradation is a function of the device topology and its sensitivity to the error as well as the control algorithm itself. However, a net improvement over the feed-back control system can be clearly demonstrated. Since this benchmark has been performed, we have been able to significantly improve the wave prediction accuracy from our systems using better instrumentation and improved algorithms and expect MPC performance to be very close to the idealized MPC version. We should also point out that the causal controller only used the PTO velocity as a feedback variable. The causal controller could be improved by assuming that either the wave surface elevation at the device or the wave pressure forces are known. Both of these assumptions would require additional instrumentation on the device.

This work-package included the following elements: (1) Wave Prediction modeling in the computational domain and trade-off studies, (2) Wave tank validation, (3) Build of 8 custom Gen1 wave measurement buoys, (4) In-Ocean data collection, and (5) Validation of Wave-Prediction Algorithms. The build and testing of a second generation wave measurement buoy system is being pursued under a separately funded project with the over-arching aim of improving wave prediction accuracy.

Datasets Collected

A total of 14 field measurement campaigns were carried out to benchmark and improve the wave prediction accuracy of the wave prediction system. Further data is being collected under a separately funded project and will be made available once that project completes.

Outcome

The key objective of this work package was to demonstrate wave prediction accuracy that is good-enough for controls purposes using Model Predictive Control. This objective has been fully met and present efforts focus on the development of a wave prediction system that can be used as a building block by device developers.

Additional Details & Publications

Appendix: A journal publication is forthcoming.

Linear and Non-Linear MPC Development and Application to Reference WEC Topologies

Controls optimization was carried out on 4 different WEC topologies, including (1) The OE buoy, (2) the Resolute Marine Energy Surge WEC device, (3) the Wave Carpet, and (4) a heaving point absorber that we moved along as a reference case design. Linear MPC, Non-Linear MPC control optimizations were carried out and refined on these devices. Method extensions were developed to enable the controls optimization using discreet PTO force control, improve the computational speed of MPC and NMPC algorithms, and represent PTO losses and dynamics in a universal way. Significant efforts were directed at systems identification methods and model order reduction using subspace techniques.

Outcome

Annual average power output improvements were attained for all WEC topologies and performance improvements were benchmarked against theoretical upper limits where possible. It showed that optimality can be guaranteed using MPC methods for any device type and considering any PTO topology. Controls studies using wave prediction time-series from at-sea testing showed that performance degradation due to realistic errors is less than 5%.

Additional Details & References

1. Appendix: Controls report describing methods used and application examples
2. Publication: A.Karthikeyan, M.Previsic, J.Scruggs, A.Chertok, “*Non-linear Model Predictive Control of Wave Energy Converters with Realistic Power Take-off Configuration and Loss Model*”, 2019 IEEE Conference on Control Technology and Applications, HongKong, China, August 2019
3. Conference Presentation: A.Karthikeyan, M.Previsic, A.Chertok, J.Scruggs, “*Constrained Optimal Control of a Flap-Type Wave Energy Converter with a Hydraulic Power Take-Off and Realistic Loss Model*”, Marine Energy Technology Symposium (METS), Washington, DC, USA, May 2018
4. Conference Presentation: M.Previsic, “*Towards the Practical Application of Optimal Controls in WECs*”, Marine Energy Technology Symposium (METS), Washington, DC, USA, May 2017

Causal Controls Development and Application to Reference WEC Topologies

Professor Jeff Scruggs at the University of Michigan developed several causal controls implementations and assisted with the development of loss models and subspace techniques. Most of his work has been published, so we suggest to review the publications directly.

In Scruggs et al (2013), a general technique for causal control of linear WEC systems is presented. In this technique, the wave-excitation force is modeled as a stochastic process with a known spectrum, and control decisions are made using only localized feedback information. In other words, deployed wave-forecasting sensors are not used, and feedback information is limited to dynamic phenomena in the immediate proximity of the WEC, as well as the WEC response itself. It is shown that, when the dynamic model of the WEC is linear and the PTO loss model is quadratic, the optimal causal controller developed in this framework can be represented as a linear transfer function and can be solved exactly as the solution to a LQG (Linear Quadratic Gaussian) problem. Such controllers can be broken into an observer subsystem (Kalman-Bucy filter), which estimates the full dynamic state of the WEC system, and a state feedback controller, which makes decisions on the basis of these estimates to maximize power in the absence of wave-prediction information.

Additional Details

Several papers were published as part of this and previous efforts. A list follows below:

1. J. Scruggs, Y. Lao, M. Previsic and A. Karthikeyan, “*Discrete-time causal control of WECs with finite stroke, in stochastic waves*”, in 13th European Wave and Tidal Energy Conference (EWTEC2019), Napoli, Italy, 2019.
2. R. Nie, J. Scruggs, A. Chertok, D. Clabby, M. Previsic and A. Karthikeyan, “*Optimal causal control of wave energy converters in stochastic waves - Accommodating nonlinear dynamic and loss models*,” International Journal of Marine Energy, vol. 15, pp. 41-55, 2016.
3. J. Scruggs, S. Lattanzio, A. Taflanidis and I. Cassidy, “*Optimal causal control of a wave energy converter in a random sea*,” Applied Ocean Research, vol. 42, pp. 1 - 15, 2013.

PTO Modeling and Trade-Off Studies

To better understand the trade-offs with different types of PTO capabilities, we have categorized all the PTOs into four different categories. This categorization allows us to establish fundamental trade-offs and

subsequently refine them based on the specifics of the physical system. These four options are illustrated below.

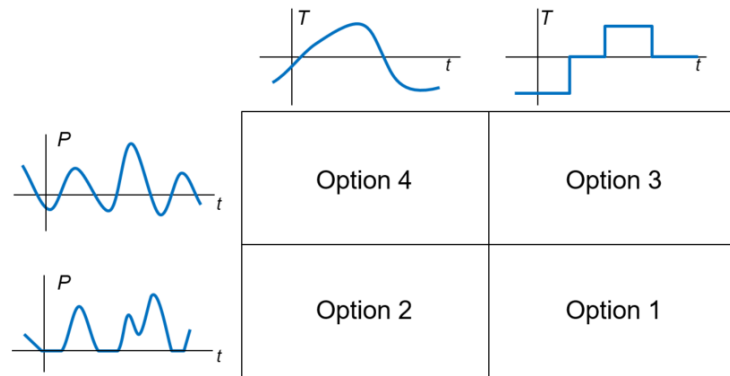


Figure 5 - PTO Options 1-4

Option 1 – Uni-directional power flow (damping only) with discrete force/torque values. This topology would be representative of a very simple hydraulic PTO, where the PTO force is given by a fixed system pressure. We still allow for that force to be switched between high and low and optimize the timing of these switching events.

Option 2 – Uni-directional power flow (damping only) with continuous force values. In this case, the force can be continuously varied, but only positive power flow is allowed. This uni-directional power flow constraint allows us to model PTOs that cannot act as an actuator (i.e., return power to the sea to maximize performance).

Option 3 – Same as Option 1, but allowing for bi-directional power flow.

Option 4 – Same as Option 2, but allowing for bi-directional power flow.

PTO capability and cost increase as PTO topology becomes progressively more complex from Option 1 to 4. This increased complexity can also be associated with higher failure rates. If properly weighted in a techno-economic model, these attributes can be translated into LCoE, allowing for an identification of the optimal topology for a given WEC design. While the complexity of the physical PTO increases with increasing capability, it is actually much easier to implement an optimal control algorithm for such an unconstrained system than for a heavily constrained one or one involving only discrete force levels.

Modeling the dissipation in the power train is essential when designing optimal control systems for WEC devices, because the objective is to maximize the *generated* power, not the *absorbed* power. However, it is often much more straightforward to control the absorbed power directly. Consequently, control decisions involving the absorbed power must anticipate the dissipation between absorbed and generated power. Such loss models can be as simple as a single efficiency number during conceptual design stages of a WEC device. However, as a WEC designer moves to a more realistic power train, the loss model must reflect this added complexity accurately.

In the course of this project, we developed an extremely detailed model of the hydraulic dynamics in the power train for the Surge WEC device for Resolute Marine Energy. This model is highly complex, involving nonlinear differential equations, high-frequency switching valves, and numerous saturation limits. Such a model, although essential for accurate simulation, is not conducive to control design, because its complexity makes it very difficult to analyze. As such, this highly accurate model was distilled to create a less accurate but still useful “control-oriented” PTO model.

This simplified model estimates the transmission dissipation in the power train as a nonlinear algebraic function of the flap torque, T , and angular velocity, ω . This model is physically meaningful, in the sense that it first approximates the high-pressure line flow Q_h and pump flow Q_p as

$$Q_h = G_0 + G_1 T + G_2 \omega T$$

$$Q_p = H_0 + H_1 \omega$$

and then approximates the dissipation from these as

$$\Phi = \Phi_{00} + \Phi_{01} Q_h + \Phi_{02} Q_h^2 + \Phi_{20} Q_p^2 + \Phi_{21} Q_p^2 Q_h + \Phi_{30} Q_p^3 + (1 - \eta_p) T \omega$$

where η_p is the static efficiency of the pump, and the parameters Φ_{ij} , G_i , and H_i are all algebraic functions of the physical parameters of the power train. (There are 24 distinct physical parameters, including pipe diameters, pre-charge pressures, and switching frequencies.)

This model, it should be remembered, is only an approximation of the true behavior. However, care was taken to be very explicit about what approximations were being made. These include the assumption that certain dynamics in the power train are “fast” in relation to the dynamics of the flap and waves and may be viewed (for the purpose of control decisions) as responding instantaneously. This eliminated the differential equations from the more accurate model. Additional simplifications were made by assuming that the pressure drops in the power train due to fluid flow were small in comparison to the accumulator pressures. For a given PTO configuration, PTO conversion efficiency becomes a simple function of velocity and torque. This type of model can be fitted easily and used effectively in the controls development process.

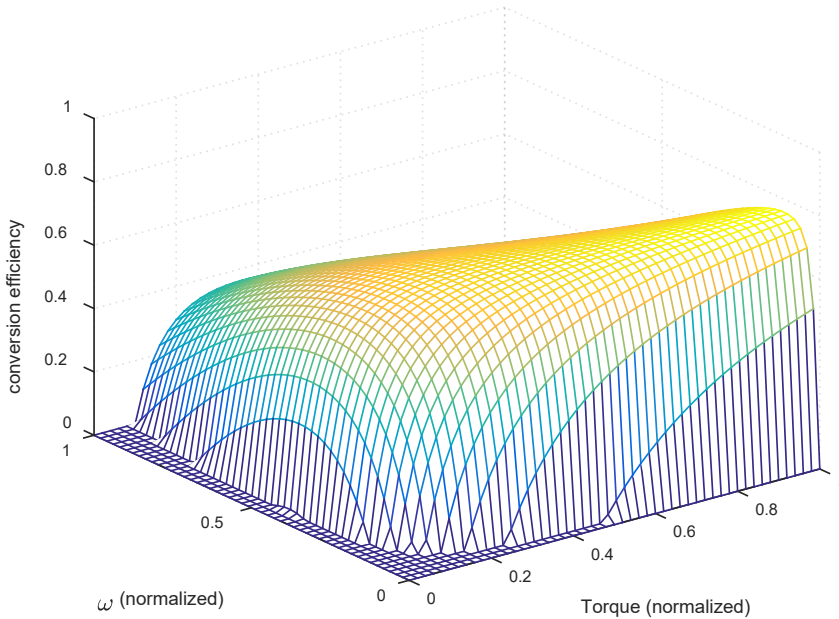


Figure 6 – Sample loss model used for controls-design purposes.

Because the approximate loss model is algebraically related to the parameters of the physical system, systematic parametric sensitivity studies can be conducted to determine how the performance of optimal control varies with these parameters. This provides an extremely useful and essential tool that can be leveraged in both the PTO and the controls optimization process. The final velocity/torque efficiency can be expressed easily as a polynomial function and used in the reduced-order plant model of the WEC device for controls purposes.

Additional Details

The controls report appendix contains a section that includes PTO modeling. Since most of the work was done on a device-specific PTO configuration with Resolute Marine Energy, this work will remain under a 5-year protection with the US Department of Energy:

1. Appendix: The Controls Methods Report includes a section on loss modelling

Wave Tank Validation of 3 Reference Topologies

The fluid-structure interaction effects can be scaled well from relatively small-scale models. In fact, some of the best research on fluid-structure interaction has been carried out in very small wave flumes. The core issue is often how the PTO can be modeled at a small scale to represent the behavior of the full-scale system. Building small-scale models of the PTO is usually unrealistic, because friction becomes dominant at smaller scales. As an example, consider a very large model that is tested at 1:10 scale. The Froude-scale for power is $\sim 10^{-3.5}$, so that we are producing $10^{3.5} = 3,162$ times less power in the model scale experiment than at full-scale. It is virtually impossible to retain Froude similarity for any electro-mechanical system over this scaling range.

Fortunately, off-the-shelf electronic actuators and controls can be effectively leveraged to mimic the behavior of a full-scale PTO. In our case, we leveraged servo-drives to provide the motion response and implemented closed-loop feedback controllers to track accurately the Froude-scaled force/torque behavior of the full-scale system. Specifically, we leveraged an off-the-shelf LinMot actuator/drive that was programmed to track a reference force value. A load cell and PID loop were used to separate any dynamic behavior of the actuator from the device dynamic. The following figure shows that setup for a heaving point absorber. Using a fast-tracking PI control loop was essential in allowing the system to track any demand torque provided by the real-time controller. In our case, we leveraged a SpeedGoat system that allowed us rapidly to design and implement control loops in a convenient Simulink environment.

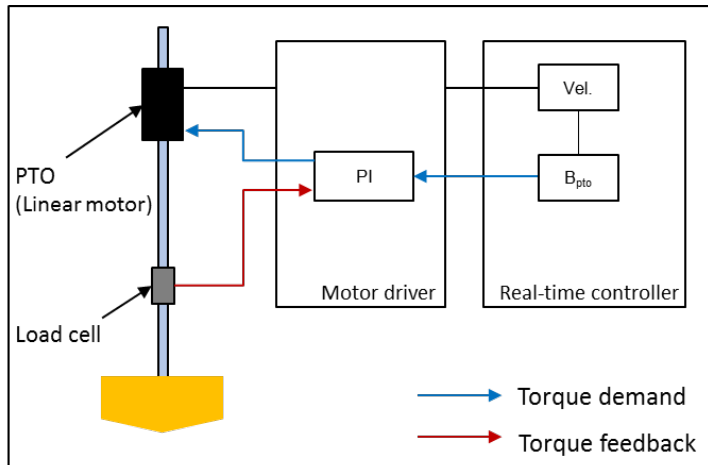


Figure 7 - Controls and force-tracking setup for testing a heaving buoy

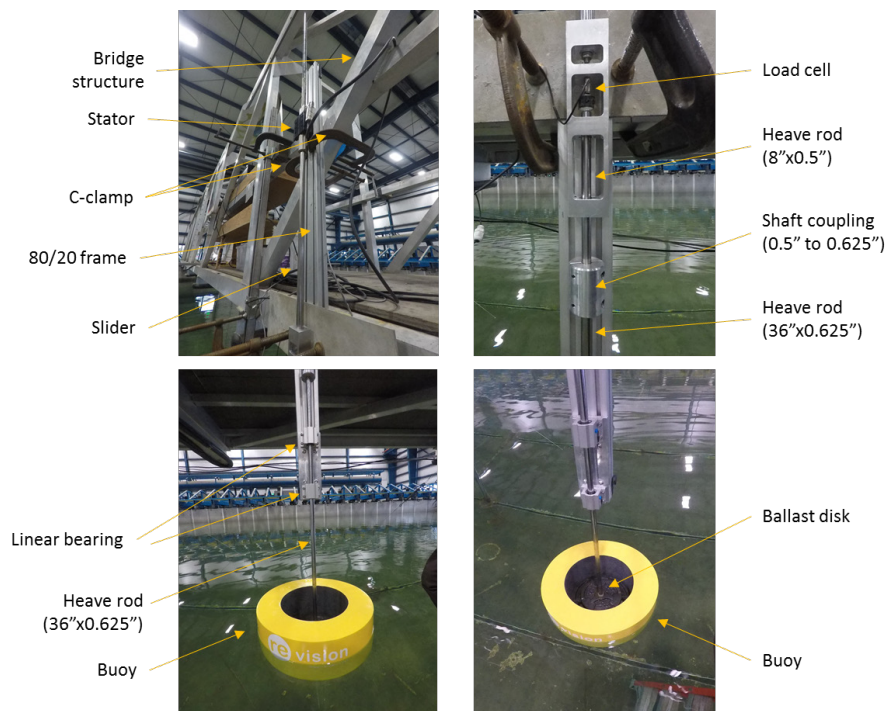


Figure 8 - Physical setup of test in wave tank at the Oregon State University

Issues encountered and resolved during our test campaign involved the PTO emulator and included (1) force-tracking Issues requiring fine-tuning of the PID loop, (2) measurement noise on the load cell, (3) bearing issues, and (4) an outdated driver on the SpeedGoat system that introduced delays into the control loop. While these issues were all resolvable, they illustrate the added complexity encountered with this type of setup compared with the more traditional, passive mechanical means of providing a viscous damping force that is possible when the control force is not dependent on time.

The causal controller was implemented directly on the SpeedGoat system because it is computationally very efficient. However, we were unable to test the MPC controller in real-time, because the algorithm is not real-time capable at model scale. Instead, with the knowledge of exactly which waves were pre-scribed, we pre-computed optimal PTO command values offline and synchronized the pre-computed PTO command

values with the wave-maker start signal. This allowed us to achieve our appropriate controls validation objective at this model scale.

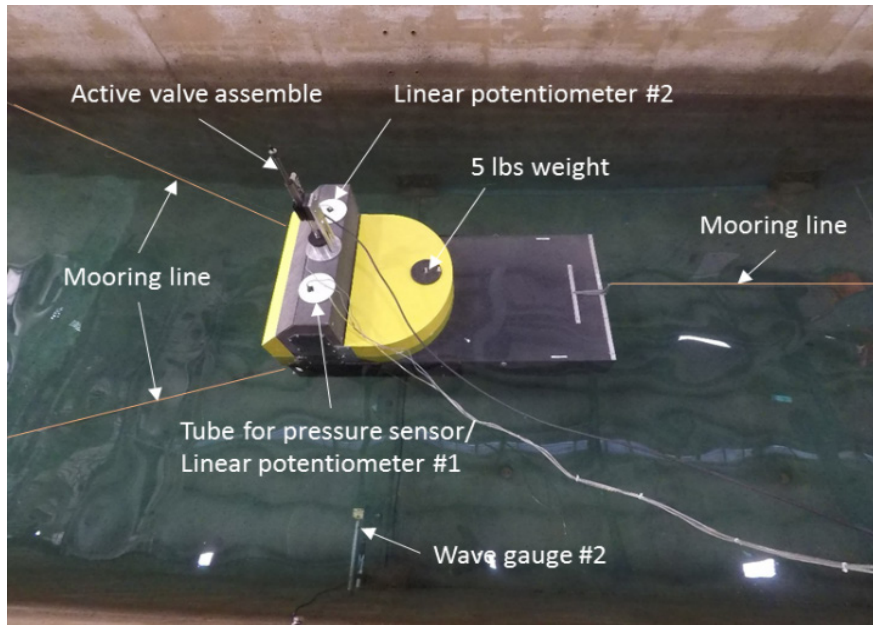


Figure 9 - OE Buoy being tested at Oregon State University



Figure 10 - RME Device being tested at Oregon State University

Wave tank testing was carried out on three different topologies, including: (1) the heaving point absorber, (2) the RME WEC device, and (3) the OE buoy. This effort allowed us to validate fluid-structure interaction models and validate controls strategies at model scale.

Datasets Collected

1. Appendix: Heaving Buoy Wave Tank Testing Report
2. Heaving Buoy Wave Tank Testing Dataset

RT In-Ocean Control Testing and Validation

In order to enable robust application of controls at sea, suitable HW and SW needs to be integrated. To do so, we built a small demonstrator WEC device and designed a controls architecture that allowed us to fully re-use controls algorithm codes developed and tested during earlier phases and therefore enable rapid prototyping and controls testing. While we initially tried to use a Speedgoat system, we found that the Simulink-based architecture was too constrained and did not allow us to execute many of computationally efficient codes written in Matlab and C. We also found that the Speedgoat HW system was not very robust encountering several driver related issues.

The overall controls topology is shown in the following figure and consists of: (1) a set of wave measurement buoys that transmit wave information in real-time to a wave-prediction algorithm, (2) a computer that runs the wave-prediction algorithms and provides a wave excitation force forecast, (3) a controls computer that uses the wave prediction and sensor feedback from the WEC device to compute an optimal response, and (4) a National Instruments cRio front end that provides robust industrial-grade I/O capabilities and incorporates low-level control to protect the hardware from overload and provides error handling capabilities. These systems communicate with each other over a low-latency ethernet-based communication link, called the Pacemaker that insures real-time communication.

The separation of these systems allowed for systems to be developed and tested concurrently so that the development of the different components would not interfere with each other. The same system was also used for hardware in the loop testing by running a WEC device emulator on the cRio device. Overall, this setup enabled a seamless development process, resulting in efficient project execution.

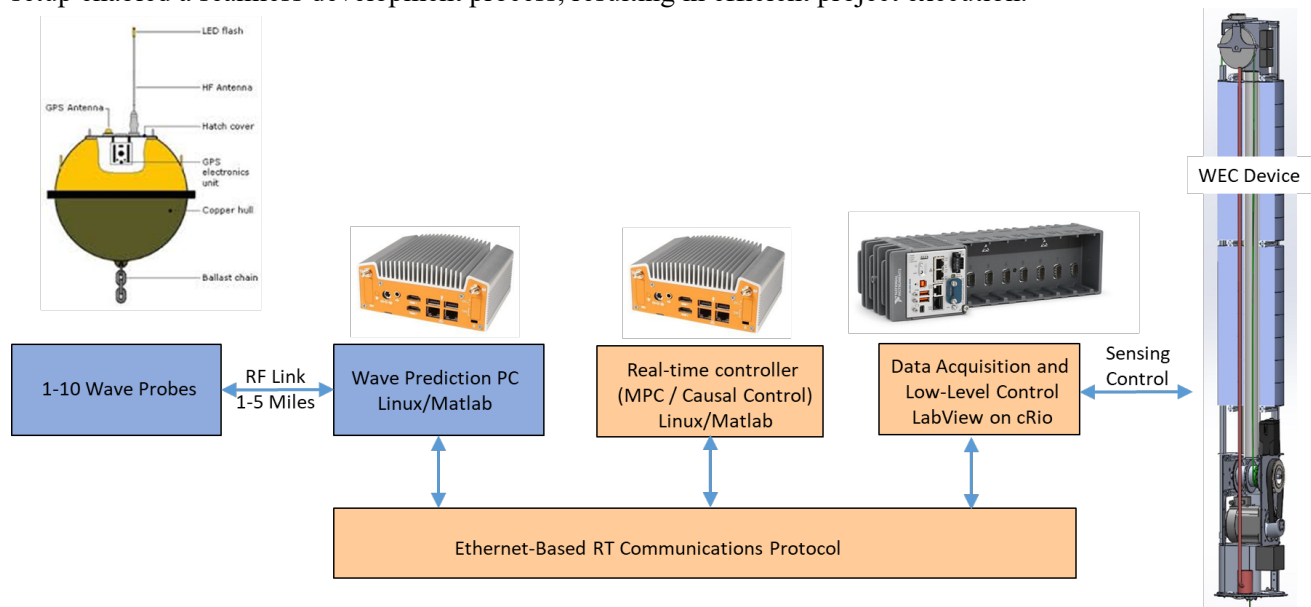


Figure 11 - Controls Topology for In-Ocean Deployments

The WEC device is a slender cylindrical buoy with a diameter of 0.5m and a height of 4m, and is connected to the seabed over a tensioned wire. The wire tension is controlled using a rotary winch that is driven by a commercial servo motor/drive system. Peak power output from the drive system is 8kW. To ease permitting requirements, the buoy was only deployed temporarily in about 20m of water depth in the Pacific Ocean off Santa Cruz, California, while being connected to a vessel for power.

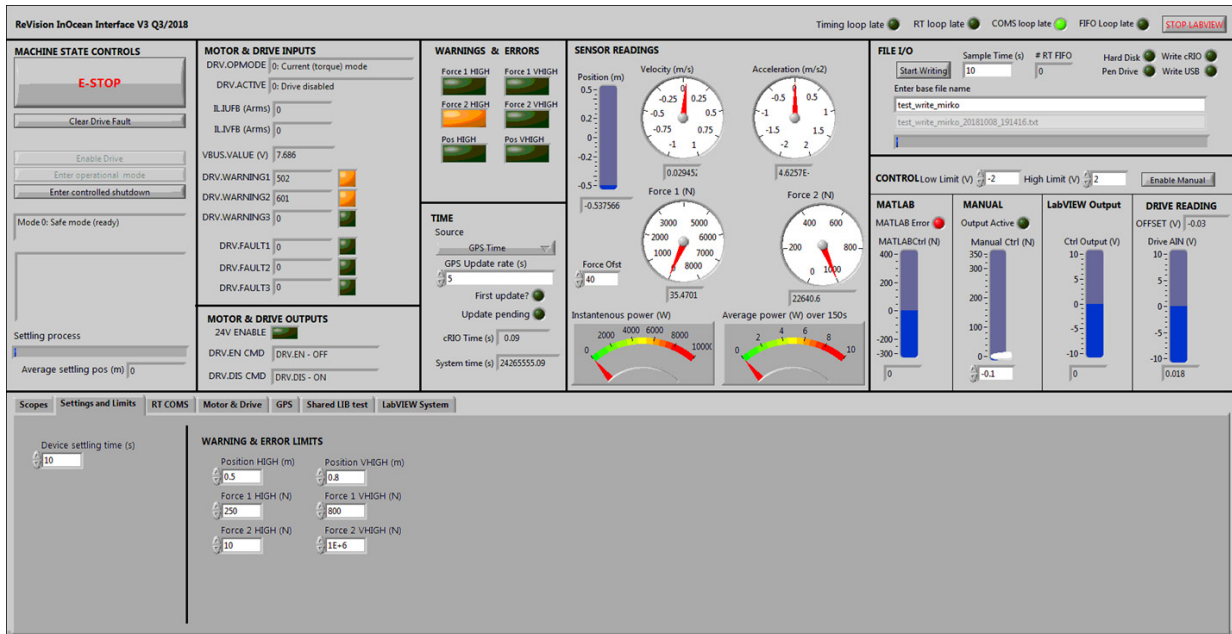


Figure 13 - Demonstrator WEC Device: Scale (left), Build images (right)

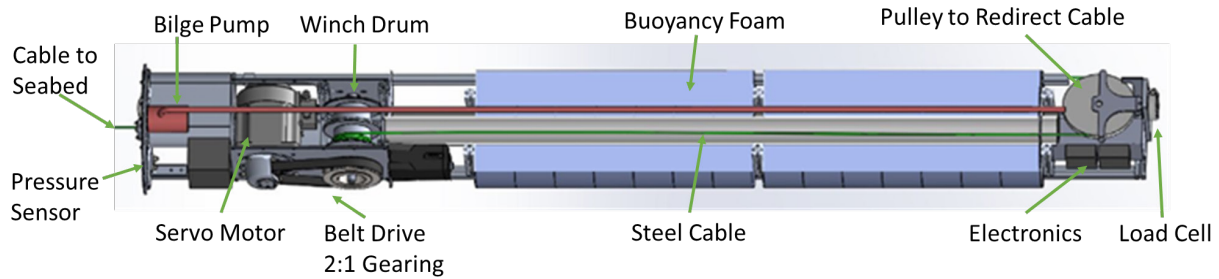


Figure 14 - Identification of Major Buoy Sub-Systems – Device in horizontal position

The deployment was carried out using a 52foot long research vessel with appropriate lift capabilities. The following images shows the deployment of the system and subsequent installed position off the coast in Santa Cruz in about 20m water depth.



Figure 15 - Buoy deployed at sea (left) and on deck before installation (right)

Outcomes

At-sea testing included initial validation using a velocity-dependent damping term and subsequent application of Model Predictive Control showed that the numerical simulations agree well with the at-sea time-domain execution showing that MPC control can be executed on devices at sea. Further testing will be required to fully validate a number of different controls strategies.

Techno-Economic Assessments

LCoE baseline assessments have been carried out during phase I of the project, which provides a detailed cost and economic assessment of the devices. Performance improvements have two fundamental effects: (1) they increase the capital cost of the powertrain because the increased power output will require a larger PTO to convert the mechanical power into electricity, and (2) power capture is increased. So on a very fundamental level, the LCoE improvements due to controls can be evaluated by scaling PTO costs linearly with average power capture. All other costs scale either at a \$/device level or \$/farm level. As mentioned above, various trade-offs were studied and these studies are device specific and protected by nondisclosure agreements. However, a brief example of the heaving point absorber working in heave against an

embedment anchor is given below to illustrate the effect of improved power capture due to controls. It should be acknowledged that such a simplified techno-economic assessment does not capture all the factors, but can be used to understand overall cost-drivers.

The heaving point absorber has the dimensions of Reference Model 3 (RM3), for which detailed cost and economic assessments have been completed. However, instead of reacting against a subsea reaction plate, it reacts against the seabed with a PTO configuration that is similar to the Aqua Harmonics WEC device or the Fred Olson device tested in Hawaii. This is a device archetype that has been identified as techno-economically promising.

As a first step the cost profile was identified by augmenting the RM3 cost profile. This involved primarily the removal of the subsea plate and replacing the anchor system with a structurally efficient embedment anchor. The baseline performance of this device is identified using viscous linear damping on a heaving point absorber. The upper performance limit is identified using MPC simulations on all sea-states within the scatter diagram. A simple 80% powertrain efficiency is assumed.

Table 2 - Performance Comparison for Heaving Point Absorber

Slow Tuning		
Rated Power (kW)		183
Annual Energy (MWh/yr)		481
Average Power (kW)		55
Capacity Factor		30%
MPC		
Rated Power (kW)		449
Annual Energy (MWh/yr)		1180
Average Power (kW)		135
Capacity Factor		30%
Relative Improvement		245%

A simplified assessment is used to establish cost-drivers on a system assuming that it is deployed at a scale of 100 Units and assuming that the technology features a similar O&M cost as land-based wind turbines Today. It is further assumed that financing of the technology has a fixed charge rate (FCR) of 7%, which is representative of a mature technology sector and is the standard assumption the US Department of Energy uses for its technology assessments.

Table 3 – Baseline Cost Assessment

	\$/kW	\$/1000/Unit	\$/1000/Farm	cents/kWh	in %
Development	\$590	\$108	\$10,774	1.6	5%
Infrastructure	\$1,180	\$215	\$21,549	3.1	9%
Mooring/Foundation	\$290	\$53	\$5,296	0.8	2%
Device Structural Components	\$1,210	\$221	\$22,097	3.2	9%
Power Take Off	\$1,690	\$309	\$30,862	4.5	13%
Subsystem Integration & Profit Margin	\$580	\$106	\$10,592	1.5	4%
Installation	\$3,600	\$657	\$65,743	9.6	28%
Contingency	\$910	\$166	\$16,618	2.4	7%
Total	\$ 10,050	\$1,835	\$183,531	26.8	78%
Fixed Charge Rate	7%				
O&M (Percent of Capex per Year)	2%				
LCoE	\$ 0.34				

Next some simple linear scaling relationships were established to identify the cost profile of a wave farm with the same WEC devices that have increased power output due to improvements in the control strategy.

Table 4 - Cost Scaling Relationships

Development	Fixed Cost per Farm		
Infrastructure	Fixed Cost per Farm		
Moorings/Foundation	Fixed Cost per Device		
Device Structural Components	Fixed Cost per Device		
Power Take Off	Fixed Cost per kW Rated		
Subsystem Integration & Profit Margin	10% X (Structural Components + Power Take Off + Moorings)		
Installation	Fixed Cost per Device		
Contingency	10% X Total Cost		

The big change driving economic improvements come from a larger amount of power capture per device, resulting in a lower shared costs for fixed per device costs (such as riser cables and moorings), and reduced structural cost per unit of energy output due to the improvements in the structural efficiency of the device.

Table 5 - Cost and Economic Summary of Optimally Controlled WEC Device

	\$/kW	\$1000/Unit	\$1000/Farm	cents/kWh	in %
Development	\$239.88	\$108	\$10,774	0.6	4%
Infrastructure	\$480	\$215	\$21,549	1.3	7%
Moorings/Foundation	\$118	\$53	\$5,296	0.3	2%
Device Structural Components	\$491.96	\$221	\$22,097	1.3	7%
Power Take Off	\$1,690	\$759	\$75,907	4.5	25%
Subsystem Integration & Profit Margin	\$230	\$103	\$10,330	0.6	3%
Installation	\$1,464	\$657	\$65,743	3.9	22%
Contingency	\$471	\$212	\$21,170	1.3	7%
Total	\$ 5,185	\$947	\$94,679	13.8	78%
Fixed Charge Rate	7%				
O&M (Percent of Capex per Year)	2%				
LCoE	\$ 0.18				

Additional Details

1. LCoE Assessment of Heaving Point Absorber (Excel)

Conclusions

In this project, we investigated causal and non-causal controls approaches and their application to WEC devices. Both controls frameworks are universal in nature and can be adapted and applied to most WEC topologies found within the literature. The key controls objective can be summarized as maximizing electrical power output while considering all losses in the system and respecting constraints. This type of constrained optimization is required to address successfully realistic WEC controls optimization problems.

During this project we were able to advance the state of the art in several key areas including:

- Demonstrated real-time wave prediction at sea. While academic papers have been presented on this topic, no-one to our knowledge has successfully demonstrated phase-resolved wave prediction with sufficient accuracy that would enable MPC in WEC technologies. This is a key building block to enable optimal control.
- Demonstrated real-time MPC at sea. To our knowledge MPC has only been demonstrated in wave tank environments. We are the first ones to demonstrate Model Predictive Control at sea. This effectively enables a new generation of controls on WEC devices deployed at sea.
- We introduced controls co-design into the wave energy space leveraging model predictive control. This will enable WEC design optimization while continuously insuring that controls optimality is enforced. This capability enables design for optimality from the concept stage and reduces significant uncertainties in the design optimization process.
- We developed a method to efficiently introduce loss models and PTO limitations in the controls design process. Bringing the PTO modeling capabilities into the controls design process and enabling trade-off studies while enforcing optimality is a critical capability for this sector and has not been systematically developed by this emerging industry.
- We made several advances in the areas of numerical methods including: (1) efficient numerical methods to represent the PTO in a controls model, (2) efficient development of sub-space models that significantly improve the computational efficiency to handle MPC-type problems, (3) integrated causal controls methods with MPC methods to significantly improve controls robustness and ability to handle errors in the wave prediction scheme, and (4) introduced several method extensions to handle constraints in causal controllers.

Our work with our device development partners has allowed them to establish critically needed trade-offs with confidence, which reflects in their device design today resulting in significant performance improvements and cost-reductions.

While we have made significant progress in advancing state of the art optimal controls, significant challenges and advances need to be made to enable the widespread commercial adoption of optimal controls by device manufacturers. This includes the following core areas:

- Improvements in computational efficiency for non-linear MPC: To insure true optimality in many device types, non-linear MPC methods are required. Many of these solutions are not real-time capable and because MPC is a sequential optimization scheme, it cannot simply be improved by using parallel processing schemes typically employed in high-performance computing. Further work is needed to develop methods that are fully capable of handling these non-linearities in an efficient manner in real-time.
- Enabling commercialization: While we have demonstrated many of the controls and wave-prediction capabilities, continued funding will be required to turn these accomplishments in practical numerical tools that can be used across all stages of product development.

These challenges outlined above will require continued funding by US Department of Energy. We hope that we will be able to compete for such funding opportunities on a level playing field. What follows are a few more thoughts related to optimal control of WEC devices.

The Need for Wave Prediction – While causal control with acceptable performance has been demonstrated on a limited set of device topologies, it remains to be explored to what extent causal control laws can approximate the performance of MPC with a wave-forecast. It is important that controls performance does not only relate to energy capture, but also the capabilities of the algorithm to accommodate realistic device-specific constraints such as PTO force, velocity, acceleration, and powerflow. It should be pointed out that the cost of predicting ocean waves (a requirement for effective MPC implementation) is very small compared to the cost of the device itself at commercial scales. A simple 1% improvement in power capture would pay for the cost of the wave prediction system many times over. Causal controls approaches however may be useful at smaller scales required for applications within the blue economy such as recharging unmanned vehicles at sea, where the economic calculus is driven by reliability and operational simplicity and not performance.

Controls Co-Design - Working with a number of different topologies at different TRL levels, we found that the performance improvements attainable for any given WEC are in general less than initially projected from theory and/or simplified models. This is because various constraints and losses in any realistic WEC system tend to reduce motion amplitudes that are required to improve power capture. In many cases, the PTO system's ability to modulate PTO forces/torques efficiently and cost effectively in real-time limits the performance upside potential of any WEC approach. It is therefore important that controls design be integrated into any WEC development effort, beginning with the conceptual design. Techno-economic models can become effective tools for evaluating trade-offs between performance and the incremental cost of additional PTO capabilities, leading to an optimized WEC design.

During the device development process it is important to understand the fundamental upper limits of a particular configuration and use sensitivity studies to understand the trade-offs and design-drivers involved in arriving at an economically optimal configuration. MPC can serve as an important tool to explore this trade-off space, because it allows us to establish upper limits of constrained systems, which is not easily done using analytical methods, or linearized frequency-domain methods. Once these trade-offs are fully understood, the designer can turn to the evaluation of simpler control strategies to further reduce complexity in the system.

Real-time Capabilities – The computational cost of control systems in WEC devices span about 2 orders of magnitude - anywhere from 10X slower than real time to 10X faster than real-time. This means that some of the more complex, non-linear MPC approaches cannot yet be used in realistic applications. However, we have to remember that computational capabilities are rapidly advancing and according to Moores law, which predicts a doubling a computational power every 18 months, a 10X improvement will require less than 6 years to materialize.

Robustness – While we demonstrated that causal and non-causal controllers can be implemented on at-sea WEC devices, our work also shows that these controls and wave prediction building blocks need to be incredibly robust and fault tolerant to be useful on at-sea devices. Further work will be required to turn these controls capabilities into building blocks to enable at-sea optimal control.

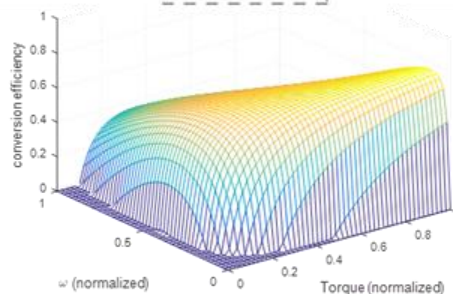
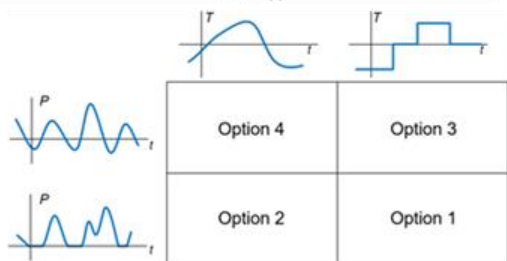
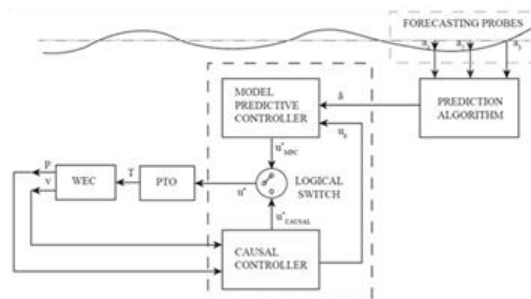
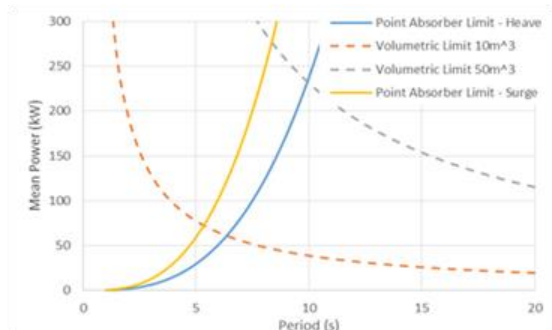
As optimal controls in WEC devices continues to evolve, it is shaping what type of systems will become cost-competitive in the future, and is impacting how we fundamentally think about wave energy extraction.

References

1. Publication: A.Karthikeyan, M.Previsic, J.Scruggs, A.Chertok, "Non-linear Model Predictive Control of Wave Energy Converters with Realistic Power Take-off Configuration and Loss Model", 3rd IEEE Conference on Control Technology and Applications, HongKong, China, August 2019
2. Conference Presentation: A.Karthikeyan, M.Previsic, A.Chertok, J.Scruggs, "Constrained Optimal Control of a Flap-Type Wave Energy Converter with a Hydraulic Power Take-Off and Realistic Loss Model", Marine Energy Technology Symposium (METS), Washington, DC, USA, May 2018
3. Conference Presentation: M.Previsic, "Towards the Practical Application of Optimal Controls in WECs", Marine Energy Technology Symposium (METS), Washington, DC, USA, May 2017
4. Publication: J. Scruggs, Y. Lao, M. Previsic and A. Karthikeyan, "Discrete-time causal control of WECs with finite stroke, in stochastic waves", in 13th European Wave and Tidal Energy Conference (EWTEC2019), Napoli, Italy, 2019.
5. Publication: R. Nie, J. Scruggs, A. Chertok, D. Clabby, M. Previsic and A. Karthikeyan, "Optimal causal control of wave energy converters in stochastic waves - Accommodating nonlinear dynamic and loss models," International Journal of Marine Energy, vol. 15, pp. 41-55, 2016.
6. Publication: J. Scruggs, S. Lattanzio, A. Taflanidis and I. Cassidy, "Optimal causal control of a wave energy converter in a random sea," Applied Ocean Research, vol. 42, pp. 1 - 15, 2013.
7. Appendix: Controls report describing methods used and application examples
8. Appendix: Heaving Buoy Wave Tank Testing Report
9. Heaving Buoy Wave Tank Testing Dataset
10. LCoE Assessment of Heaving Point Absorber (Excel)

Appendices

Controls Algorithms Report



DOE Award Number: DE-EE0007173
 Project Period: 1/1/2016 to 12/31/2019
 Report Date: 11/12/19

Author

Anantha Karthikeyan

Principal Investigator

Mirko Previsic – Re Vision Consulting

Email: mirko@re-vision.net

Recipient Organization

Re Vision Consulting, LLC
 1104 Corporate Way
 Sacramento, CA 95831

Partners

Resolute Marine Energy
 CalWave
 Ocean Energy USA
 University of Michigan
 Integral Consulting
 HT Harvey and Associates

Acknowledgment: “This report is based upon work supported by the U. S. Department of Energy under Award No. DE-EE0007173”.

Disclaimer: “Any findings, opinions, and conclusions or recommendations expressed in this report are those of the author(s) and do not necessarily reflect the views of the Department of Energy”. This document was prepared by the organizations named below as an account of work sponsored or cosponsored by the U.S. Department of Energy (DoE). Neither DoE, RE vision consulting, LLC (RE vision), any cosponsor, the organization (s) below, nor any person acting on behalf of any of them:

(A) Makes any warranty or representation whatsoever, express or implied, (I) with respect to the use of any information, apparatus, method, process or similar item disclosed in this document, including merchantability and fitness for a particular purpose, or (II) that such use does not infringe on or interfere with privately owned rights, including any party’s intellectual property, or (III) that this document is suitable to any particular user’s circumstance; or

(B) Assumes responsibility for any damages or other liability whatsoever (including any consequential damages, even if RE Vision or any RE Vision representative has been advised of the possibility of such damages) resulting from your selection or use of this document or any other information, apparatus, method, process or similar item disclosed in this document.

The views and opinions of authors expressed herein do not necessarily state or reflect those of the United States Government or any agency thereof, or RE Vision Consulting, LLC.

Proprietary Data Notice: If there is any patentable material or protected data in the report, the recipient, consistent with the data protection provisions of the award, must mark the appropriate block in Section K of the DOE F 241.3, clearly specify it here, and identify them on appropriate pages of the report. Other than patentable material or protected data, reports must not contain any proprietary data (limited rights data), classified information, information subject to export control classification, or other information not subject to release. Protected data is specific technical data, first produced in the performance of the award, which is protected from public release for a period of time by the terms of the award agreement. Reports delivered without such notice may be deemed to have been furnished with unlimited rights, and the Government assumes no liability for the disclosure, reproduction or use of such reports.

Document by:
RE Vision Consulting, LLC
www.re-vision.net
Project Manager: Mirko Previsic
Email Address: mirko@re-vision.net

Table of Contents

Table of Contents	3
1 Introduction	7
2 Overview	7
3 Example of a Heaving Point Absorber	9
4 Dimensions of the Heaving Buoy	11
5 Theoretical Limits on the Average Absorbed Power	12
5.1 Point Absorber Limit.....	12
5.2 Volumetric Limit.....	13
6 Optimal Linear Damping.....	13
6.1 Results of Optimal Linear Damping Control	14
7 Linear Model Predictive Control	16
7.1 Results of Linear Model Predictive Control	19
8 Performance Benchmarking for a Deep-Water Reference Site	21
9 MPC Performance with Realistic Errors in Wave Prediction.....	23
9.1 Optimal Linear Damping (Baseline)	24
9.2 Linear MPC with Perfect Wave Prediction	26
9.3 Linear MPC with Realistic Errors in Wave Prediction	28
10 Nonlinear Model Predictive Control	29
10.1 Example Flap-Type WEC Device.....	30
10.2 Nonlinear MPC Problem Setup.....	32
10.3 Nonlinear MPC Algorithm and the Loss Model	33
10.4 Results of Nonlinear Model Predictive Control.....	34
11 Causal Control	36
11.1 Discrete-Time Causal Control with Nonlinear Stroke Protection	36
11.2 Optimal Causal Control with Nonlinear Dynamics and Loss Model	36
12 Power Take-Off Configurations.....	36
13 System Identification Methods	39
14 References	41

List of Figures

Figure 1 - Control configurations used in Wave Energy Conversion	8
Figure 2 - Model of a one-body point absorber WEC device	9
Figure 3 - Heaving buoy with dimensions	11
Figure 4 - Block diagram of Optimal linear damping control.....	13
Figure 5 - Comparison of optimal linear damping vs theoretical limits	14
Figure 6 - Optimal linear damping time domain response with wave input of $H = 1m$, $T = 15s$	15
Figure 7 - Optimal linear damping normalized time domain response with wave input of $H = 1m$, $T = 15s$	15
Figure 8 - Block diagram of Model Predictive Control	19
Figure 9 - Linear MPC performance vs linear damping (baseline) and theoretical limits	20
Figure 10 - Linear MPC time domain response with wave input of $H = 1m$, $T = 15s$	20
Figure 11 - Linear MPC normalized time domain response with wave input of $H = 1m$, $T = 15s$	21
Figure 12 - A 480s time window of wave elevation measurement data collected at Santa Cruz.....	24
Figure 13 - Mean absorbed power vs damping for given wave measurement time series. * indicates the optimum value of damping and maximum value of mean absorbed power	25
Figure 14 - Device response with optimal linear damping	25
Figure 15 - (a) top: Wave elevation measurement and prediction (b) bottom: wave excitation force measurement and prediction for the case of perfect prediction	26
Figure 16 - Linear MPC with perfect wave prediction	27
Figure 17(a) top: wave elevation (predicted vs measured) (b) bottom: wave excitation force (predicted vs measured).....	27
Figure 18 - Comparison between the predicted and measured wave excitation force for a select time window.....	28
Figure 19 - Device response using Linear MPC with a 15% mean absolute error in wave prediction.....	29
Figure 20 - Block diagram of feed-forward control of flap-type WEC.....	30
Figure 21- Yakutat scatter diagram	34
Figure 22 - PTO Options 1-4.....	37
Figure 23 - Normalized response of surge WEC under control option 4 (Note: negative power flow)	38
Figure 24 - Normalized Response of Surge WEC under Control Option 2 (Note: no negative power flow)	38
Figure 25 - Normalized Response of Surge WEC under Control Option 3 (Note: negative power flow allowed.....	39

Figure 26 - Normalized Response of Surge WEC under Control Option 1 (Note: no negative power flow allowed) 39

Figure 27 - Comparison of truth model vs identified model for different states 41

List of Tables

Table 1 - Dimensions of Heaving Buoy 11

Table 2 - Scatter diagram for DOE reference site in Humboldt Bay, CA 22

Table 3 - Constrained Performance Matrix (Optimal linear damping) 22

Table 4 - Constrained Performance Matrix (Linear MPC)..... 23

Table 5 - Performance benchmarking of Optimal linear damping and Linear MPC at DOE reference site 23

Table 6 - Absorbed and normalized power for optimal linear damping (baseline), MPC with perfect prediction and MPC with error in prediction 29

Table 7 - Performance of Coulomb damping (baseline) and Non-linear MPC (continuous control, two-way power flow) for an example flap-type WEC..... 35

1 Introduction

Advanced control optimization is well recognized as a major pathway for cost reduction in wave energy conversion applications. Intelligent real-time control has shown significant improvements in power capture for various device topologies and power take-off mechanisms. For some devices the relative improvement in power capture using advanced control is on the order of two to three-fold over baseline “slow-tuning” method of viscous damping. This makes advanced control an exciting avenue for research and development that has the potential to improve the economics of wave energy conversion systems.

The control system affects power capture, structural loads, and power take off (PTO) design. To achieve true economic optimality in a WEC system, optimal control needs to be considered as part of the design trade-off space. Simply adding controls to an existing WEC device topology will often not yield significant performance improvements, because the PTO may not be able to provide the capabilities needed to improve performance or the device envelope is not optimized to take advantage of advanced controls. Device and PTO attributes can only be optimized if their cost-drivers and their performance impacts are quantified. Constrained optimal control is a key tool in this optimization process.

This paper reviews the controls approaches utilized in our controls optimization project and shows the main formulations to provide the reader with background on the methods used. The main sections include:

- Optimal linear damping control formulation and performance benchmarking for a heaving point absorber
- Linear MPC formulation and performance benchmarking for a heaving point absorber
- Linear MPC performance with realistic errors in wave prediction
- Non-linear MPC formulation and performance benchmarking for a flap-type WEC
- Optimal Causal Control
- Power Take-off configurations used in wave energy conversion
- System identification methods for numerical modeling and model order reduction

2 Overview

Control systems are broadly classified on as either (a) feedback or (b) feed-forward controllers. A feedback controller uses information from sensors that monitor the states or outputs of a dynamical system, in our case the Wave Energy Converter (WEC). The sensor information is used as feedback by the controller to follow a desired command signal. Whereas, feed-forward controllers act solely on the command signal without feedback from sensors that measure system output variables. Combination of feed-forward and

feedback control is also possible in a hybrid manner as shown in Figure 1. In general, for wave energy conversion applications, the controller issues command signals based on measurements of output quantities such as position, velocity and input variables such as pressure or wave excitation force.

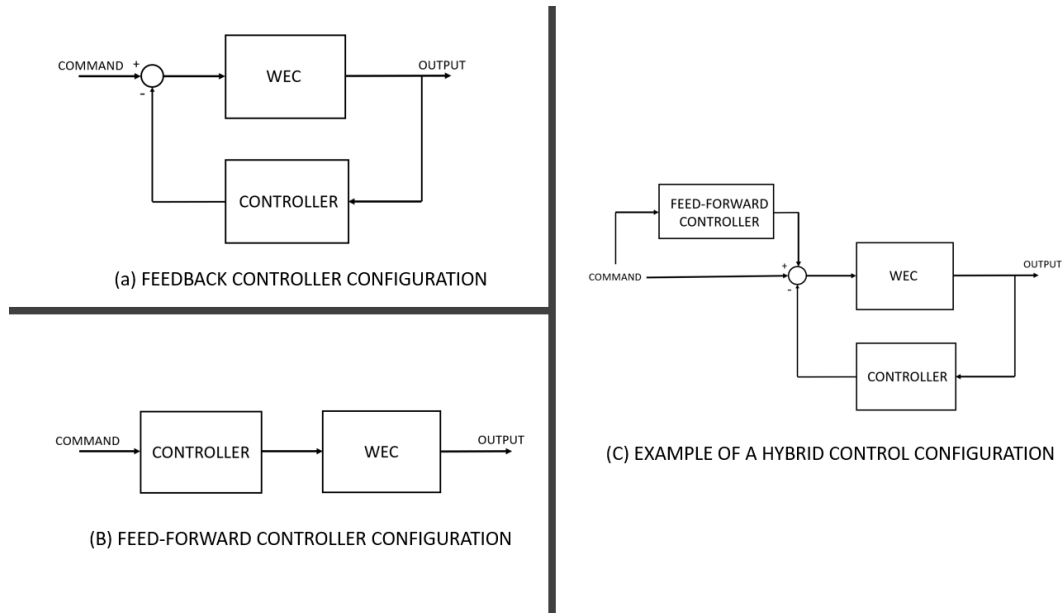


Figure 1 - Control configurations used in Wave Energy Conversion

Control laws used in wave energy conversion are also classified as either causal or non-causal depending on the use of wave prediction data using up-wave sensor measurements. Feedback controllers have a causal relationship between the control command signal and input/measurement signals. Whereas, controllers such as Model Predictive Control (MPC) require anticipatory information of future waves to plan control commands using a non-causal optimization method.

In this report we will discuss the following control algorithms in detail

- Optimal linear damping
- Linear MPC
- Nonlinear MPC
- Optimal Causal Control

Optimal linear damping will be considered as a baseline for evaluating the performance of Linear MPC and Causal Control. We will use a cylindrical heaving point absorber as an example for the first two cases. This point absorber WEC is described in the next section.

3 Example of a Heaving Point Absorber

Many WEC topologies have appeared in literature, a few of them allowing the possibility of an active controller. Among these, the linear one-body point-absorber, has received the greatest attention in literature. This converter is composed of a semi-submerged floating body, which is fixed to the seabed through a connection containing a linear actuator. This device is subject to: (1) an inertial force, (2) a viscous force due to hydrodynamic dissipation, (3) a buoyancy force, proportional to the device displacement according to Archimedes' principle, (4) a radiation force $f_r(t)$ capturing the wave radiation effect of the device, and (5) an excitation force $f_e(t)$ which represents the effect that the wavefield has on the device. In addition, a control force $u(t)$ is applied to the device. Denoting with $z(t)$ the WEC heaving displacement, the balance of forces on the device is given by

$$m\ddot{z}(t) + r \dot{z}(t) + k z(t) = f_r(t) + u(t) + f_e(t)$$

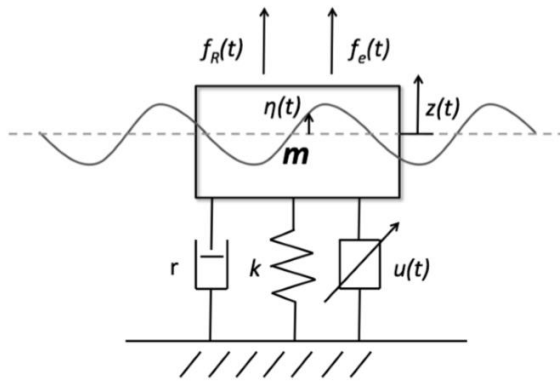


Figure 2 - Model of a one-body point absorber WEC device

where m is the device mass, r is the viscous damping, and k is the buoyancy stiffness, defined as $k = \rho g S$, where ρ is the water density, g the gravitational constant, and S the water-plane area. The radiation force $f_R(t)$, can be expressed as

$$f_R(t) = -m_\infty \ddot{z}(t) - f_r(t)$$

$$f_r(t) = -m_\infty \ddot{z}(t) - \int_{-\infty}^t h_r(t - \tau) \dot{z}(\tau) d\tau$$

where m_∞ is the added mass, $f_r(t)$ is the radiation force, and $h_r(t)$ is the impulse response function of the radiation force. For simplicity, in the rest of the paper we will refer to the term $f_r(t)$ as the radiation force. The excitation force $f_e(t)$ is expressed as

$$f_e(t) = \int_{-\infty}^{+\infty} h_e(t - \tau) \bar{\eta}(\tau) d\tau$$

Where $h_e(t)$ is the excitation force impulse response function and $\bar{\eta}(t)$ is the wave elevation at the device location. The impulse response function relating the wave elevation to the excitation force affecting the device is non-causal. The main reason is that the chosen input, i.e. the wave elevation at the device location, is not the direct cause of the output, i.e. the interaction force between the wavefield and the device. The actual cause of the output may be a storm far away, and the resulting wavefield is only a means through which such input propagates, hence the loss of causality.

In order to recast the system dynamics into state-space form, the radiation force $f_r(t)$ can be discretized through the following state-space realization:

$$\begin{aligned} \dot{X}_r(t) &= A_r X_r(t) + B_r \dot{z}(t) \\ f_r(t) &= C_r X_r(t) + D_r \dot{z}(t) \end{aligned}$$

This leads to the following state-space model

$$\begin{aligned} \dot{x}(t) &= Ax(t) + Bu(t) + Bf_e(t) \\ y(t) &= Cx(t) + Du(t) \end{aligned}$$

with

$$\begin{aligned} A &= \begin{bmatrix} A_r & 0 & B_r \\ 0 & 0 & I \\ -\frac{C_r}{m+m_\infty} & -\frac{k}{m+m_\infty} & -\frac{r+D_r}{m+m_\infty} \end{bmatrix} \\ B &= \begin{bmatrix} 0 \\ 0 \\ 1 \\ m+m_\infty \end{bmatrix} \\ C &= \begin{bmatrix} 0_r & 1 & 0 \\ 0_r & 0 & 1 \end{bmatrix} \\ D &= \begin{bmatrix} 0 \\ 0 \end{bmatrix} \end{aligned}$$

where $x(t) = [X_r(t) \quad p(t) \quad v(t)]^T$ is the state-space vector containing the variables X_r used to discretize the radiation force, the position $p(t)$ and the velocity $v(t)$ of the device. 0_r is a matrix of zeros with appropriate dimension. Similarly, I is an identity matrix of appropriate dimensions.

4 Dimensions of the Heaving Buoy

To analyze the performance of optimal linear damping and Linear, we consider a cylindrical heaving buoy (see Figure 3) with dimensions given in Table 1.

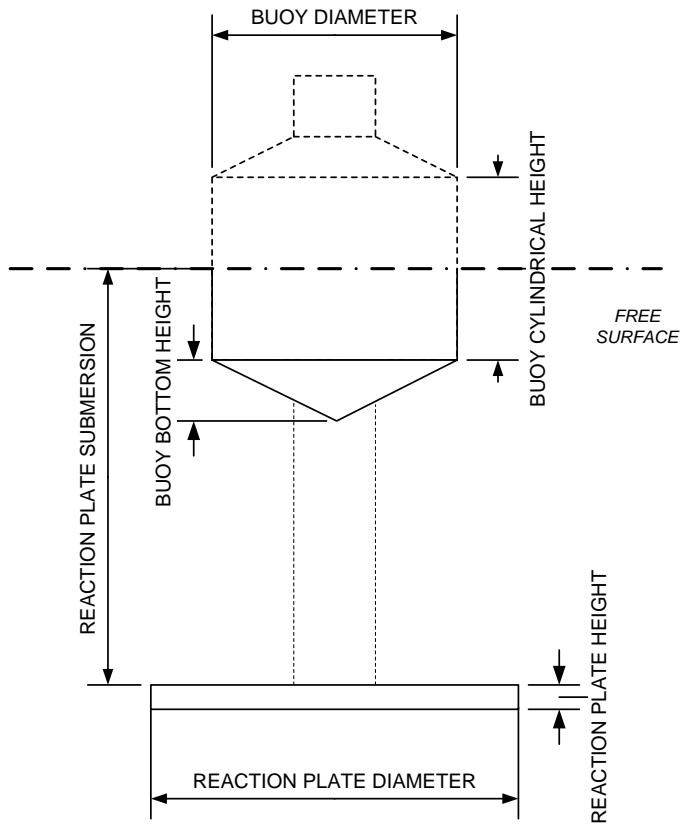


Figure 3 - Heaving buoy with dimensions

Table 1 - Dimensions of Heaving Buoy

Quantity	Value	units
Buoy diameter	11	m
Buoy cylinder height	4	m
Reaction diameter ratio	1	-
Reaction diameter	11	m
Buoy conical height	1.2	m

Buoy displaced volume	228	m ³
Total displacement	2	m
Motion displaced volume	190	m ³
Buoy mass	228080	kg
Area	95	m ²
Coefficient of drag (CD)	0.5	-

5 Theoretical Limits on the Average Absorbed Power

5.1 Point Absorber Limit

Point-absorber effect in wave-energy extraction was first described by [1], and shortly after theoretical limits for the ocean-wave absorption by oscillating bodies were derived by several authors, independently [2] [3] [4]. As described in [5], for a heaving axisymmetric body oscillating without constraints in resonance with an incoming regular wave of period T and wave height H the average absorbed power \bar{P}_a is limited by the expression

$$d_a \leq \frac{1}{k} = \frac{\lambda}{2\pi}$$

Or equivalently

$$\bar{P}_a \leq \frac{1}{k} J_E = \frac{\rho}{128} \left(\frac{g}{\pi}\right)^3 T^3 H^2$$

Where $d_a = \bar{P}_a / J_E$ (m) is the absorption width, J_E (W/m) is the wave-power level, and k ($1/m$) is the wave number. The last equality is only valid for deep water conditions and is referred to as the point absorber limit. If we define the excitation power \bar{P}_e as the averaged product of the excitation force and the body velocity $\bar{P}_e = \overline{F_e(t)u(t)}$ and the average radiation power as $\bar{P}_r = \overline{F_r(t)u(t)}$, the absorbed power is $\bar{P}_a = P_e - P_r$. The theoretical limit may be reached provided the average absorbed power equals half the average excitation power, which happens when the radiated power equals the absorbed power, $\bar{P}_a = \bar{P}_r$.

It is known that the point absorber limit can only be reached up to a certain wave height and period, depending on the constraint set for the motion amplitudes. Beyond, only a lower relative power absorption can be realized, which is defined by a devices volumetric limit.

5.2 Volumetric Limit

This second limit is due to the finite volume swept by the body during its oscillation cycle. It was theoretically described by [4]. Their starting point was that the absorbed power must be less than the excitation power, and that equality can be approached only if the radiated power becomes negligible in comparison. By arguing further that the total volume V of the body sets limits for the maximum excursion, velocity, and excitation force in heave, they arrived at an upper theoretical bound for the power P_a that can be absorbed by a heaving body. This is called the volumetric limit which is given by

$$\bar{P}_a < (\pi\rho gHV/4T)$$

The point absorber limit and the volumetric limit tell us that no matter how well we control the motion of our device we will not be able to reach the region above any of them.

6 Optimal Linear Damping

Optimal linear damping is a control strategy that involves the application of a damping force proportional to the velocity of the WEC. The power take-off (PTO) applies this damping force against the velocity, consequently extracting power from the ocean waves. Typically, the damping force is defined as follows

$$F_{PTO}(t) = -B v(t)$$

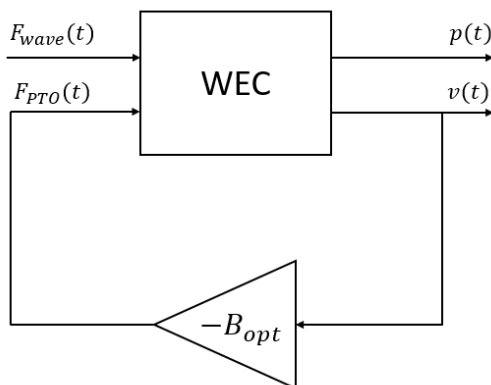


Figure 4 - Block diagram of Optimal linear damping control

Where, B is the damping coefficient and $v(t)$ is the device velocity. An optimal value of damping (B_{opt}) can be pre-calculated from offline simulations for different sea states. The damping value which maximizes

the average absorbed power is identified as the optimal damping coefficient (B_{opt}) for that sea state. The PTO force $F_{PTO}(t)$ and absorbed power $P_{abs}(t)$ in the case of optimal linear damping are given by

$$F_{PTO}(t) = -B_{opt}v(t)$$

$$P_{abs}(t) = -F_{PTO}(t)v(t)$$

Figure 4 shows a block diagram of optimal linear damping control. Here $F_{wave}(t)$ is the wave excitation force, $p(t)$ is the device position, $v(t)$ is the velocity and $F_{PTO}(t)$ is the PTO control force that is calculated using the velocity feedback signal.

6.1 Results of Optimal Linear Damping Control

Optimal linear damping was applied to a set of sinusoidal wave inputs of height $H=1\text{m}$ and period in the range of 3s to 18s. Figure 5 shows a comparison of optimal linear damping performance vs the theoretical limits. It is clear from these results that a “slow-tuning” method such as optimal linear damping is not an effective control strategy to maximize power absorption. Figure 6 and Figure 7 show an example of the device response with MPC for an input wave of $H=1\text{m}$, $T=15\text{s}$.

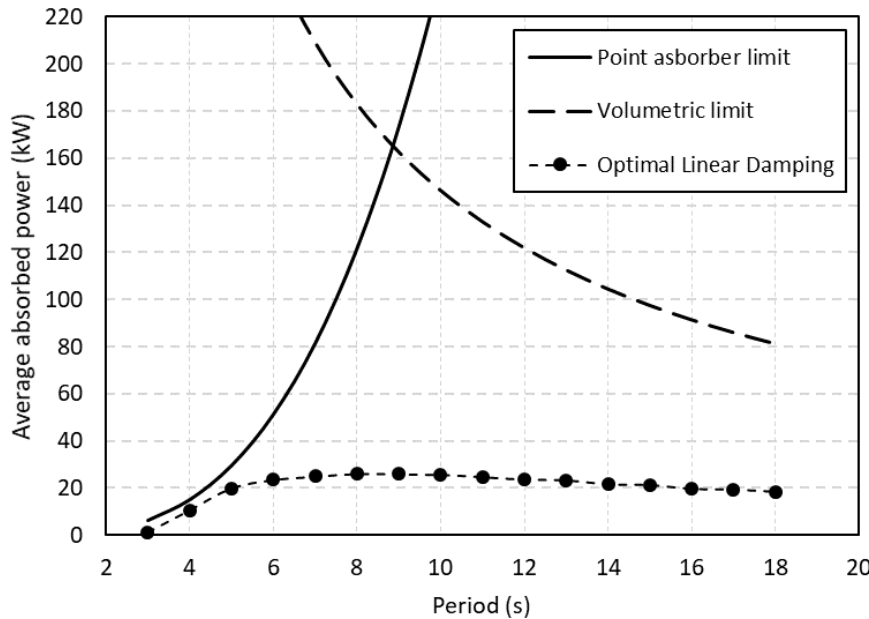


Figure 5 - Comparison of optimal linear damping vs theoretical limits

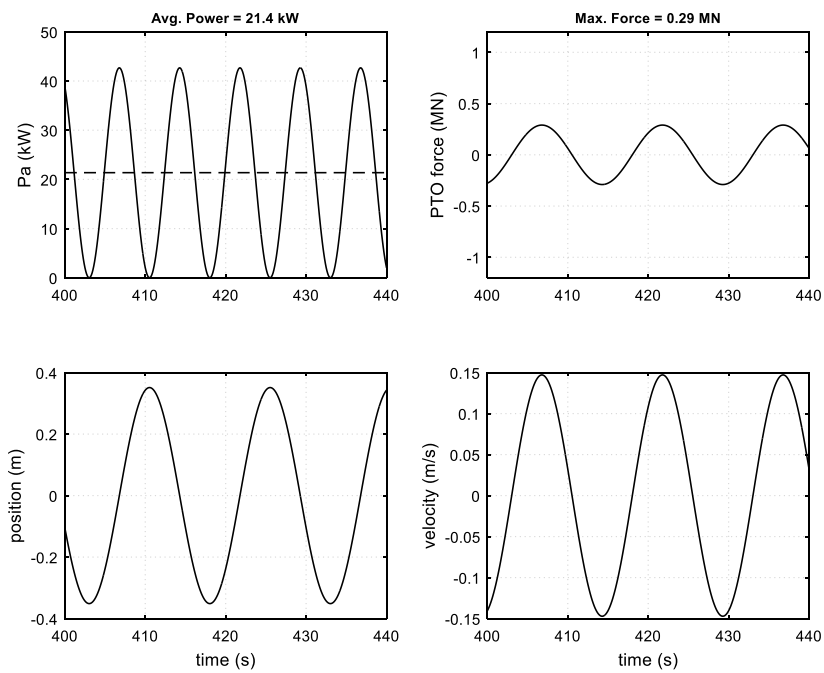


Figure 6 - Optimal linear damping time domain response with wave input of $H = 1m$, $T = 15s$

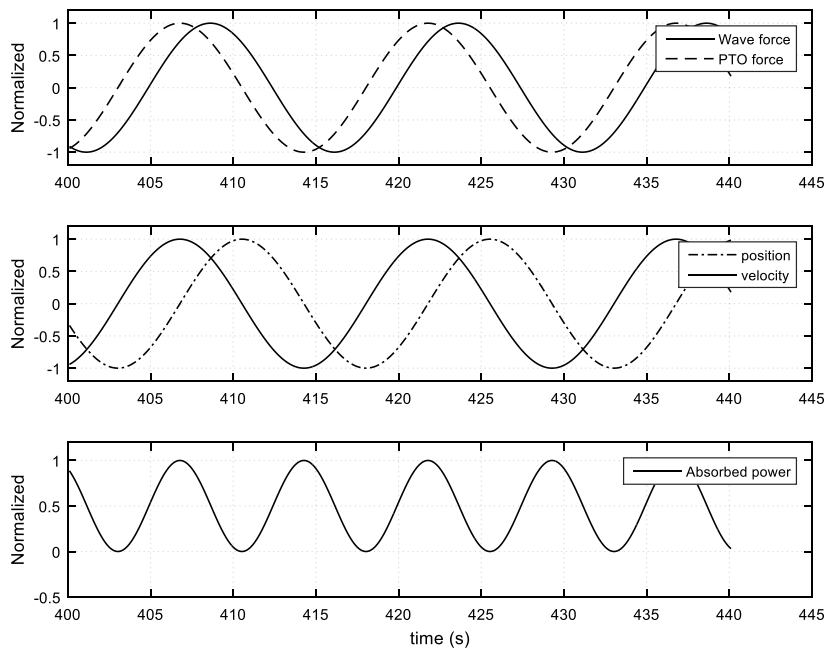


Figure 7 - Optimal linear damping normalized time domain response with wave input of $H = 1m$, $T = 15s$

7 Linear Model Predictive Control

Linear Model Predictive Control (MPC) is used for optimizing the performance of a Wave Energy Converter (WEC) with a linear device model. In this type of problem, the device dynamics is linearized and non-linearities such as viscous drag are approximated using linear relationships. Under the assumption of no loss in the power generation process, optimizing the device average power absorbed \bar{P}_a at a given instant t_0 over a defined control horizon T_h can be achieved by determining the optimal control sequence $u(t)$ maximizing the following cost function:

$$\bar{P}_a = -\frac{1}{T_h} \int_{t_0}^{t_0+T_h} v(t)u(t)dt$$

Where, $v(t)$ is the device velocity. The minus sign is due to the convention of considering absorbed energy with a negative sign. After discretizing the integral and changing sign, the optimization problem now requires the minimization of

$$J = \frac{1}{N} \sum_{k=0}^{N-1} x_{k+1}^T S_v^T u_k$$

in which N is the number of time intervals over the control horizon T_h , and S_v is a linear operator extracting the WEC velocity from the state-space vector. The control force and state vector, however, are not independent variables, and they are constrained by the dynamics equation of the WEC, which in discrete time is defined as

$$x_{k+1} = A_d x_k + B_d u_k + B_d f_{e_k}, \quad k = 0, \dots, N-1$$

with assigned initial condition $x_0 = \bar{x}_0$. In order to preserve mechanical and structural integrity, motion and machinery constraints are imposed, which limit the maximum actuation force and the WEC device velocity and vertical displacement for structural safety, i.e.

$$u_{min} \leq u_k \leq u_{max}, \quad k = 0, \dots, N-1$$

$$p_{min} \leq S_p x_k \leq p_{max}, \quad k = 0, \dots, N$$

$$v_{min} \leq S_v x_k \leq v_{max}, \quad k = 0, \dots, N$$

where S_p is a linear operator extracting the WEC displacement from the state vector. The cost function, together with the constraints represents a linear MPC problem in its standard formulation. A more compact formulation can be obtained by defining the following vectors

$$X = [x_1^T \quad x_2^T \quad \dots \quad x_N^T]^T$$

$$U = [u_1^T \quad u_2^T \quad \dots \quad u_N^T]^T$$

In this way, the cost function can then be expressed as

$$J = \frac{1}{N} X^T S_v^T U$$

The inequality constraints become

$$D_u U \leq d_u$$

$$D_x X \leq d_x$$

With

$$D_u = \begin{bmatrix} I \\ -I \end{bmatrix} \quad d_u = \begin{bmatrix} u_{max} \\ -u_{min} \end{bmatrix}$$

$$D_x = \begin{bmatrix} S_p \\ -S_p \\ S_v \\ -S_v \end{bmatrix} \quad d_x = \begin{bmatrix} p_{max} \\ -p_{min} \\ v_{max} \\ -v_{min} \end{bmatrix}$$

in which S_v and S_p are block-diagonal matrices having the velocity extraction matrix S_v and the position extraction matrix S_p , respectively, on the main block-diagonal. By recursively applying the discrete-time dynamics equations, it is possible to express X as a function of the control vector U , the excitation force vector F_e , and the initial condition \bar{x}_0 :

$$X = A_d \bar{x}_0 + B_d U + B_d F_e$$

where

$$A_d = \begin{bmatrix} A_d \\ A_d^2 \\ \vdots \\ A_d^N \end{bmatrix}$$

$$B_d = \begin{bmatrix} B_d & 0 & 0 & 0 \\ A_d B_d & B_d & 0 & 0 \\ \vdots & \vdots & \ddots & 0 \\ A_d^{N-1} B_d & A_d^{N-2} B_d & \dots & B_d \end{bmatrix}$$

$$F_e = [f_{e_0}^T \quad f_{e_1}^T \quad \dots \quad f_{e_{N-1}}^T]^T$$

This allows us to rewrite the MPC problem as the following cost function and constraint equations

$$\min_U U^T B_d^T S_v^T U + (S_v A_d \bar{x}_0 + S_v B_d F_e)^T U$$

$$\begin{bmatrix} D_u \\ D_x J_u \end{bmatrix} U \leq \begin{bmatrix} d_u \\ d_x - D_x A_d \bar{x}_0 - D_x B_d F_e \end{bmatrix}$$

Provided the Hessian of the cost function is positive definite, the maximization of power take-off requires the solution of a constrained convex optimization problem, for which well-consolidated routines, such as interior-point or active-set methods are available in literature. Positive definiteness of the Hessian is in general always guaranteed for the optimization of a point-absorber device, unless the time step chosen for the conversion of the continuous time model into discrete time turns out to be too large to represent the actual dynamic behavior of the WEC device. At each timestep, an MPC problem needs to be solved, and the first value of the optimal solution vector U^* is applied to the system. In this way, it is possible to achieve a real-time instantaneous optimization of the WEC device average power take-off. It has to be noticed, however, that, since the state vector x also contains the dummy variables used for the state space realization of the radiation force, the whole state is in general not available, and the initial condition \bar{x}_0 in the MPC optimization is not known and needs to be reconstructed through a state observer based on sensors placed on the device. Furthermore, an excitation force prediction must be calculated 20 to 30s into the future using up-wave measurement probes.

Figure 8 shows a block diagram of Linear MPC. $F_w(t)$ is the wave excitation force at time t . $\hat{F}_w(\tau)$ is the wave excitation force prediction for all $\tau > t$. $p(t)$ is the device position, $v(t)$ is the velocity and $U(t)$ is the PTO control force that is calculated using the wave force prediction by MPC.

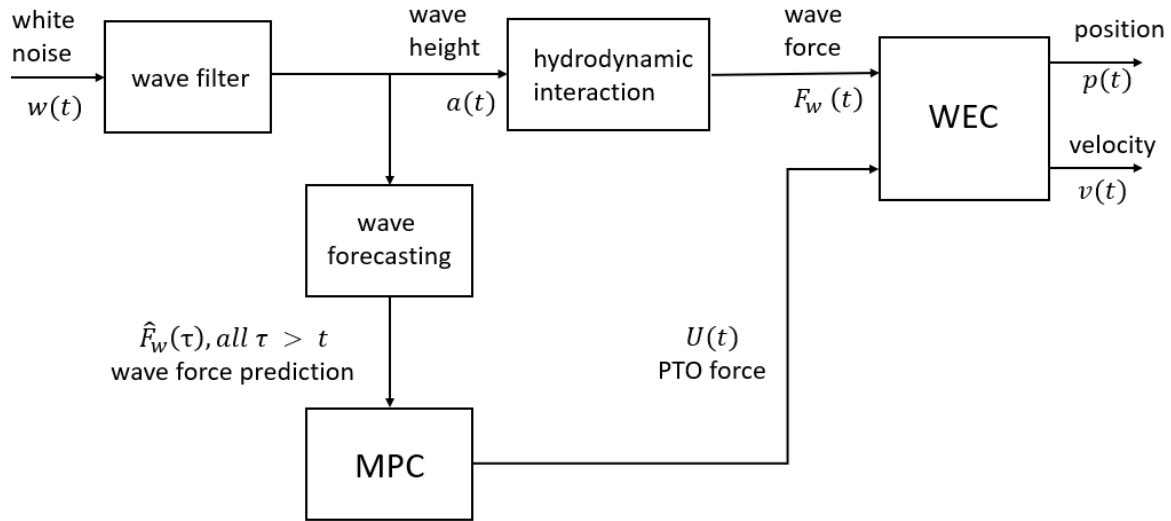


Figure 8 - Block diagram of Model Predictive Control

7.1 Results of Linear Model Predictive Control

Linear MPC was applied to a set of sinusoidal wave inputs of height $H=1\text{m}$ and period in the range of 3s to 18s. Motion constraint of $\pm 1\text{m}$ was enforced during these simulations. shows a comparison of Linear MPC performance vs optimal linear damping and the theoretical limits. It is evident that Linear MPC can maximize the average power captured, bringing it close to the theoretical limits. It is also clear from this plot that MPC can provide significant improvement in performance over baseline optimal damping control. Figure 10 shows an example of the device response with MPC for an input wave of $H=1\text{m}$, $T=15\text{s}$. Notice that the position constraint of $\pm 1\text{m}$ is effectively met during this simulation. MPC also exhibits a “latching” behavior where the buoy is held stationary for a period before extracting power in the next stroke cycle.

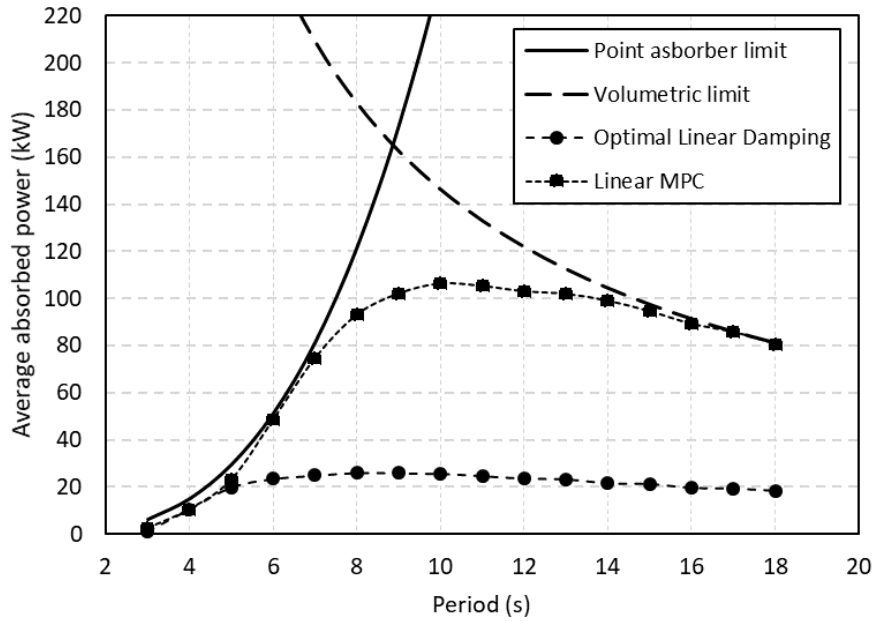


Figure 9 - Linear MPC performance vs linear damping (baseline) and theoretical limits

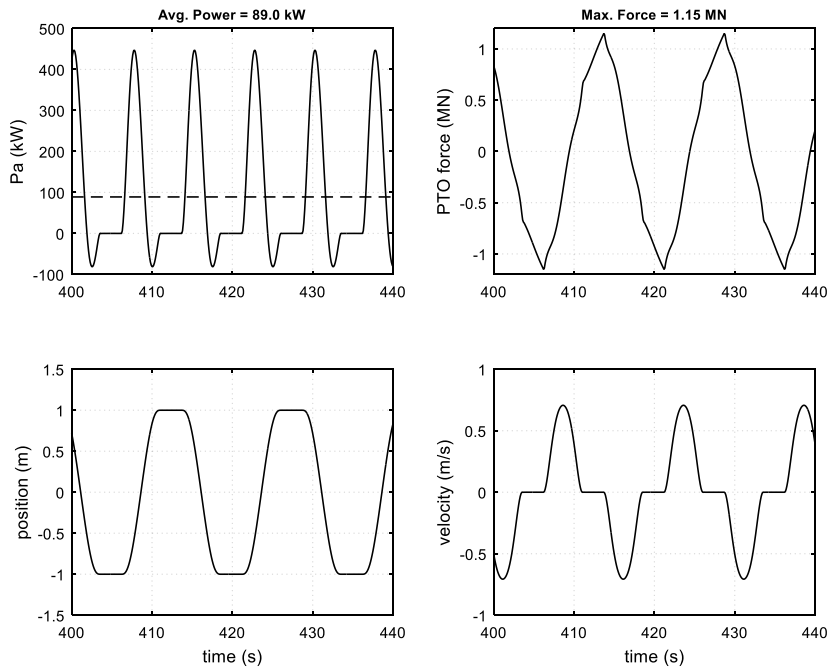


Figure 10 - Linear MPC time domain response with wave input of $H = 1m$, $T = 15s$

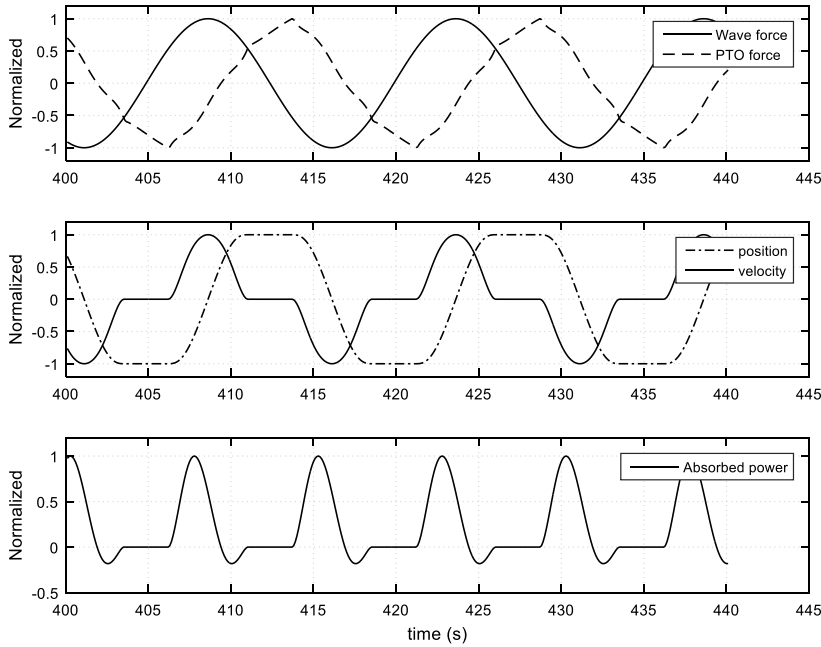


Figure 11 - Linear MPC normalized time domain response with wave input of $H = 1m$, $T = 15s$

8 Performance Benchmarking for a Deep-Water Reference Site

Simulation studies were carried out with optimal linear damping and Linear MPC to estimate the annual energy captured at the DOE deep water reference site in Humboldt Bay, CA. Motion constraints of $\pm 1m$ were applied for each simulation. Table 2 shows the scatter diagram for this reference site. Table 3 and Table 4 show the constrained performance matrix for optimal linear damping and Linear MPC respectively. For performance benchmarking the annual energy and capacity factor are defined as follows

$$\text{Annual energy} \left(\frac{\text{MWh}}{\text{yr}} \right) = \text{Average Power (kW)} * 24 * 365 / 1000$$

$$\text{Capacity factor} = \text{Average Power} / \text{Rated Power}$$

Assuming a capacity factor of 30% for our analysis revealed a 245% relative improvement in performance with MPC (see Table 5).

Table 2 - Scatter diagram for DOE reference site in Humboldt Bay, CA

% of Total Occurance		Energy Period - Te (s), center of bin																				
		0.5	1.5	2.5	3.5	4.5	5.5	6.5	7.5	8.5	9.5	10.5	11.5	12.5	13.5	14.5	15.5	16.5	17.5	18.5	19.5	20.5
Hm0 (m), center of bin	0.25	0.0	0.0	0.0	0.0	0.0	0.0	0.0	0.0	0.0	0.0	0.0	0.0	0.0	0.0	0.0	0.0	0.0	0.0	0.0	0.0	0.0
	0.75	0.0	0.0	0.0	0.0	0.0	0.5	1.5	2.7	1.9	1.1	0.5	0.2	0.0	0.0	0.0	0.0	0.0	0.0	0.0	0.0	0.0
	1.25	0.0	0.0	0.0	0.0	0.0	0.6	4.1	5.6	4.5	2.7	1.3	0.7	0.3	0.1	0.0	0.0	0.0	0.0	0.0	0.0	0.0
	1.75	0.0	0.0	0.0	0.0	0.0	0.1	3.3	5.1	4.6	3.9	2.1	1.2	0.8	0.3	0.1	0.0	0.0	0.0	0.0	0.0	0.0
	2.25	0.0	0.0	0.0	0.0	0.0	0.0	0.9	5.3	3.7	4.1	2.9	1.3	0.8	0.4	0.2	0.1	0.0	0.0	0.0	0.0	0.0
	2.75	0.0	0.0	0.0	0.0	0.0	0.0	0.1	2.4	2.6	2.8	2.8	1.6	0.8	0.3	0.1	0.1	0.0	0.0	0.0	0.0	0.0
	3.25	0.0	0.0	0.0	0.0	0.0	0.0	0.4	1.5	1.5	2.0	1.4	0.8	0.3	0.1	0.0	0.0	0.0	0.0	0.0	0.0	0.0
	3.75	0.0	0.0	0.0	0.0	0.0	0.0	0.0	0.5	0.6	1.1	1.0	0.6	0.3	0.1	0.0	0.0	0.0	0.0	0.0	0.0	0.0
	4.25	0.0	0.0	0.0	0.0	0.0	0.0	0.0	0.1	0.2	0.4	0.6	0.4	0.2	0.1	0.0	0.0	0.0	0.0	0.0	0.0	0.0
	4.75	0.0	0.0	0.0	0.0	0.0	0.0	0.0	0.0	0.1	0.1	0.3	0.3	0.2	0.1	0.0	0.0	0.0	0.0	0.0	0.0	0.0
	5.25	0.0	0.0	0.0	0.0	0.0	0.0	0.0	0.0	0.0	0.0	0.0	0.1	0.2	0.1	0.1	0.0	0.0	0.0	0.0	0.0	0.0
	5.75	0.0	0.0	0.0	0.0	0.0	0.0	0.0	0.0	0.0	0.0	0.0	0.0	0.0	0.1	0.1	0.0	0.0	0.0	0.0	0.0	0.0
	6.25	0.0	0.0	0.0	0.0	0.0	0.0	0.0	0.0	0.0	0.0	0.0	0.0	0.0	0.0	0.0	0.0	0.0	0.0	0.0	0.0	0.0
	6.75	0.0	0.0	0.0	0.0	0.0	0.0	0.0	0.0	0.0	0.0	0.0	0.0	0.0	0.0	0.0	0.0	0.0	0.0	0.0	0.0	0.0
	7.25	0.0	0.0	0.0	0.0	0.0	0.0	0.0	0.0	0.0	0.0	0.0	0.0	0.0	0.0	0.0	0.0	0.0	0.0	0.0	0.0	0.0
	7.75	0.0	0.0	0.0	0.0	0.0	0.0	0.0	0.0	0.0	0.0	0.0	0.0	0.0	0.0	0.0	0.0	0.0	0.0	0.0	0.0	0.0
	8.25	0.0	0.0	0.0	0.0	0.0	0.0	0.0	0.0	0.0	0.0	0.0	0.0	0.0	0.0	0.0	0.0	0.0	0.0	0.0	0.0	0.0
8.75	0.0	0.0	0.0	0.0	0.0	0.0	0.0	0.0	0.0	0.0	0.0	0.0	0.0	0.0	0.0	0.0	0.0	0.0	0.0	0.0	0.0	
9.25	0.0	0.0	0.0	0.0	0.0	0.0	0.0	0.0	0.0	0.0	0.0	0.0	0.0	0.0	0.0	0.0	0.0	0.0	0.0	0.0	0.0	
9.75	0.0	0.0	0.0	0.0	0.0	0.0	0.0	0.0	0.0	0.0	0.0	0.0	0.0	0.0	0.0	0.0	0.0	0.0	0.0	0.0	0.0	
		0.6	1.7	2.9	4.1	5.2	6.4	7.5	8.7	9.9	11.0	12.2	13.3	14.5	15.7	16.8	18.0	19.1	20.3	21.5	22.6	23.8
		Peak Period - Tp (s), center of bin																				

Table 3 - Constrained Performance Matrix (Optimal linear damping)

		Energy Period - Te (s), center of bin																				
		0.5	1.5	2.5	3.5	4.5	5.5	6.5	7.5	8.5	9.5	10.5	11.5	12.5	13.5	14.5	15.5	16.5	17.5	18.5	19.5	20.5
Hm0 (m), center of bin	0.25	0	0	0	0	0	0	0	1	1	0	0	0	0	0	0	0	0	0	0	0	
	0.75	0	0	0	0	4	5	5	6	6	6	6	6	6	6	0	0	0	0	0	0	
	1.25	0	0	0	0	10	13	14	16	17	17	17	16	16	15	15	14	0	0	0	0	
	1.75	0	0	0	0	25	28	32	33	33	33	32	31	30	29	28	0	0	0	0	0	
	2.25	0	0	0	0	0	47	53	55	55	54	53	51	49	48	46	45	0	0	0	0	
	2.75	0	0	0	0	0	70	79	82	82	81	79	77	74	72	69	67	0	0	0	0	
	3.25	0	0	0	0	0	110	115	115	114	111	107	103	101	96	94	77	65	0	0	0	
	3.75	0	0	0	0	0	146	152	153	151	147	143	137	135	128	125	0	0	0	0	0	
	4.25	0	0	0	0	0	0	183	183	183	183	183	183	176	174	165	160	0	0	0	0	
	4.75	0	0	0	0	0	0	183	183	183	183	183	183	183	183	183	183	0	0	0	0	
	5.25	0	0	0	0	0	0	0	183	183	183	183	183	183	183	183	0	0	0	0	0	
	5.75	0	0	0	0	0	0	0	0	183	183	183	183	183	183	0	0	0	0	0	0	
	6.25	0	0	0	0	0	0	0	0	0	183	183	183	183	0	0	0	0	0	0	0	
	6.75	0	0	0	0	0	0	0	0	0	0	183	183	0	0	0	0	0	0	0	0	
	7.25	0	0	0	0	0	0	0	0	0	0	0	0	0	0	0	0	0	0	0	0	
	7.75	0	0	0	0	0	0	0	0	0	0	0	0	0	0	0	0	0	0	0	0	
	8.25	0	0	0	0	0	0	0	0	0	0	0	0	0	0	0	0	0	0	0	0	
8.75	0	0	0	0	0	0	0	0	0	0	0	0	0	0	0	0	0	0	0	0		
9.25	0	0	0	0	0	0	0	0	0	0	0	0	0	0	0	0	0	0	0	0		
9.75	0	0	0	0	0	0	0	0	0	0	0	0	0	0	0	0	0	0	0	0		
		0.6	1.7	2.9	4.1	5.2	6.4	7.5	8.7	9.9	11.0	12.2	13.3	14.5	15.7	16.8	18.0	19.1	20.3	21.5	22.6	23.8
		Peak Period - Tp (s), center of bin																				

Table 4 - Constrained Performance Matrix (Linear MPC)

		Energy Period - Te (s), center of bin																				
		0.5	1.5	2.5	3.5	4.5	5.5	6.5	7.5	8.5	9.5	10.5	11.5	12.5	13.5	14.5	15.5	16.5	17.5	18.5	19.5	20.5
Hm0 (m), center of bin	0.25	0	0	0	0	0	0	0	7	11	0	0	0	0	0	0	0	0	0	0	0	0
	0.75	0	0	0	0	5	13	27	37	42	44	45	45	45	0	0	0	0	0	0	0	0
	1.25	0	0	0	0	16	37	56	69	75	78	79	79	78	77	76	74	0	0	0	0	0
	1.75	0	0	0	0	0	64	89	103	110	113	114	113	112	110	108	105	0	0	0	0	0
	2.25	0	0	0	0	0	122	138	146	148	150	148	146	144	141	136	132	0	0	0	0	0
	2.75	0	0	0	0	0	156	174	183	184	186	184	180	177	174	168	162	0	0	0	0	0
	3.25	0	0	0	0	0	211	219	221	222	220	215	211	207	200	193	185	178	0	0	0	0
	3.75	0	0	0	0	0	248	257	258	259	256	251	246	240	232	224	0	0	0	0	0	0
	4.25	0	0	0	0	0	294	295	296	292	286	280	274	265	255	0	0	0	0	0	0	0
	4.75	0	0	0	0	0	332	332	333	329	322	314	307	297	287	0	0	0	0	0	0	0
	5.25	0	0	0	0	0	369	370	365	357	349	341	330	0	0	0	0	0	0	0	0	0
	5.75	0	0	0	0	0	402	393	384	375	362	0	0	0	0	0	0	0	0	0	0	0
	6.25	0	0	0	0	0	429	419	409	395	0	0	0	0	0	0	0	0	0	0	0	0
	6.75	0	0	0	0	0	449	443	0	0	0	0	0	0	0	0	0	0	0	0	0	0
	7.25	0	0	0	0	0	0	0	0	0	0	0	0	0	0	0	0	0	0	0	0	0
	7.75	0	0	0	0	0	0	0	0	0	0	0	0	0	0	0	0	0	0	0	0	0
8.25	0	0	0	0	0	0	0	0	0	0	0	0	0	0	0	0	0	0	0	0	0	
8.75	0	0	0	0	0	0	0	0	0	0	0	0	0	0	0	0	0	0	0	0	0	
9.25	0	0	0	0	0	0	0	0	0	0	0	0	0	0	0	0	0	0	0	0	0	
9.75	0	0	0	0	0	0	0	0	0	0	0	0	0	0	0	0	0	0	0	0	0	
		0.6	1.7	2.9	4.1	5.2	6.4	7.5	8.7	9.9	11.0	12.2	13.3	14.5	15.7	16.8	18.0	19.1	20.3	21.5	22.6	23.8
		Peak Period - Tp (s), center of bin																				

Table 5 - Performance benchmarking of Optimal linear damping and Linear MPC at DOE reference site

Optimal linear damping		
	Rated Power (kW)	183
	Annual Energy (MWh/yr.)	481
	Average Power (kW)	55
	Capacity Factor	30%
MPC		
	Rated Power (kW)	449
	Annual Energy (MWh/yr.)	1180
	Average Power (kW)	135
	Capacity Factor	30%
Relative Improvement		245%

9 MPC Performance with Realistic Errors in Wave Prediction

To study the effect of errors in wave prediction on MPC performance we simulated MPC with real measurement data collected during a field campaign at Santa Cruz and wave predictions obtained from up-

wave measurements. This wave elevation measurement data has a significant wave height $H_s = 2.03\text{m}$ and peak period $T_p = 13.7\text{s}$. A 480s measurement time window was selected for evaluating the performance of (a) optimal linear damping (baseline) (b) Linear MPC with perfect prediction (ideal case) and (c) Linear MPC with errors in wave prediction (realistic case). The point absorber WEC described earlier was used as the target WEC for numerical simulation and performance assessment for the three cases. The wave elevation measurement input for all three simulations is shown below:

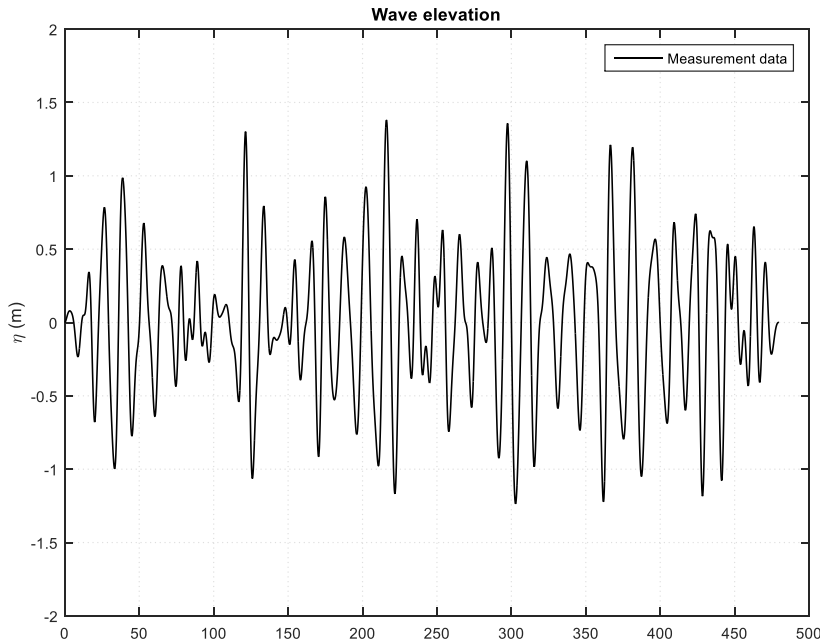


Figure 12 - A 480s time window of wave elevation measurement data collected at Santa Cruz

9.1 Optimal Linear Damping (Baseline)

The optimal damping value for this sea state was found by simulating the numerical model of the heaving buoy for different damping values. A series of simulations were carried out, starting with a low damping value of 1KN-s/m, followed by increasing values of damping in successive simulations until an optimum value was achieved. Figure 13 shows the mean absorbed power as a function of the simulated damping value. The maximum value of mean absorbed power (45.9 kW) corresponds to the optimum damping value (1515 k N-s/m). This is indicated by a * in Figure 13.

Figure 14 shows the device response with optimal linear damping. The device motion is well within the motion constraint of $\pm 1\text{m}$. The max. PTO force is 0.7MN and the average power value 45.9kW.

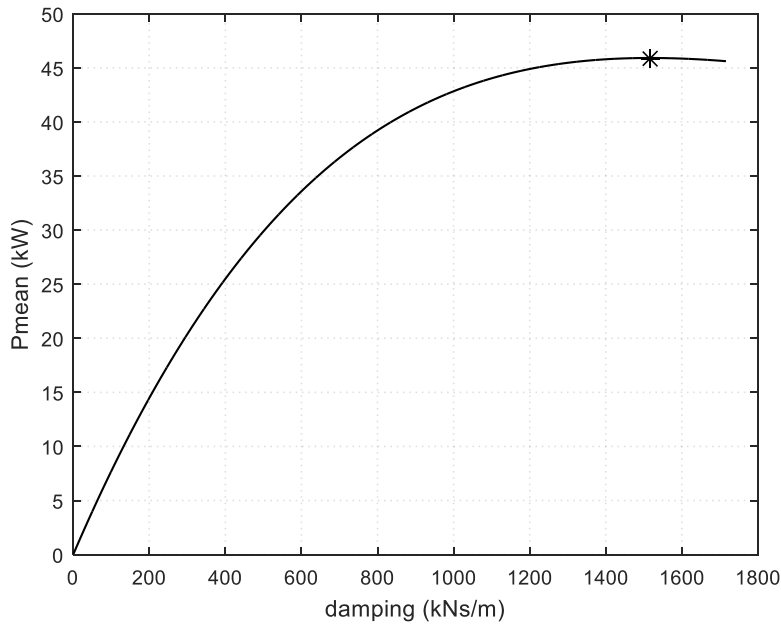


Figure 13 - Mean absorbed power vs damping for given wave measurement time series. * indicates the optimum value of damping and maximum value of mean absorbed power

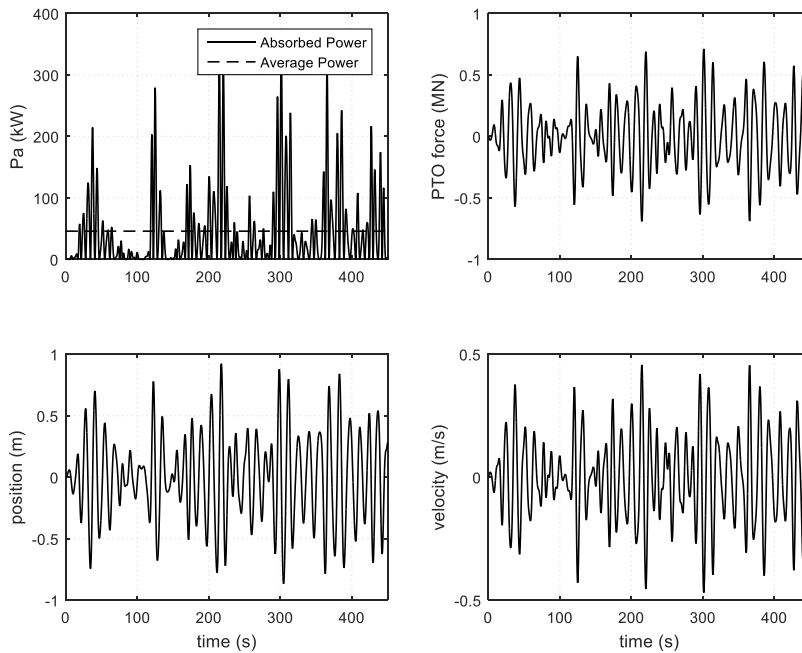


Figure 14 - Device response with optimal linear damping

9.2 Linear MPC with Perfect Wave Prediction

We simulated the Linear MPC algorithm assuming a perfect wave forecast at every update interval of the algorithm. A prediction horizon of 15s was chosen and motion constraints of $\pm 1\text{m}$ were imposed. The wave elevation measurement data and device response with MPC are shown in Figure 15 and Figure 16 respectively. Notice that MPC meets the motion constraints effectively during this simulation. The average absorbed power for this simulation was 108.9kW. In this ideal scenario where perfect wave forecast is assumed, MPC provides a relative improvement of 237% over the baseline.

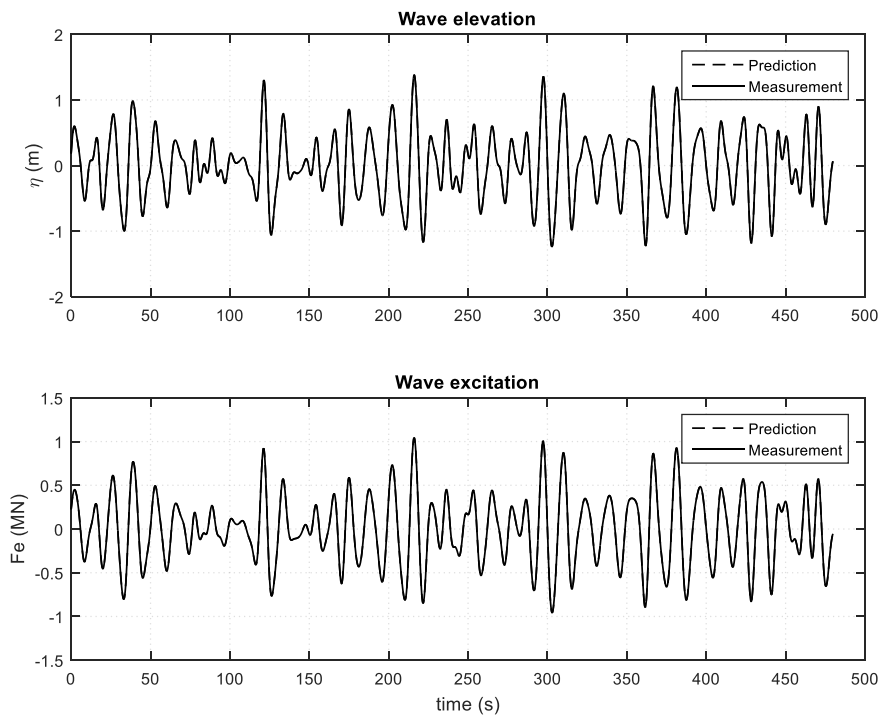


Figure 15 - (a) top: Wave elevation measurement and prediction (b) bottom: wave excitation force measurement and prediction for the case of perfect prediction

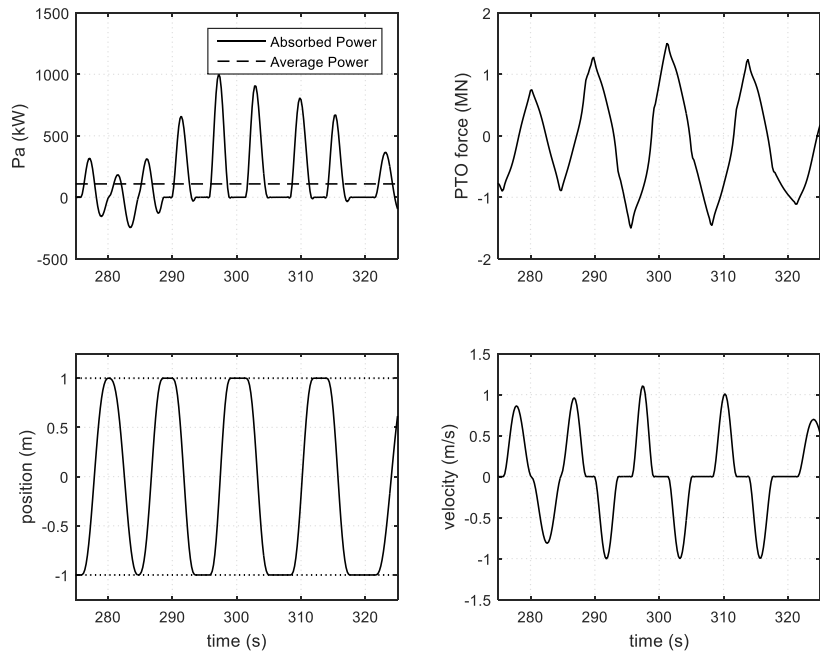


Figure 16 - Linear MPC with perfect wave prediction

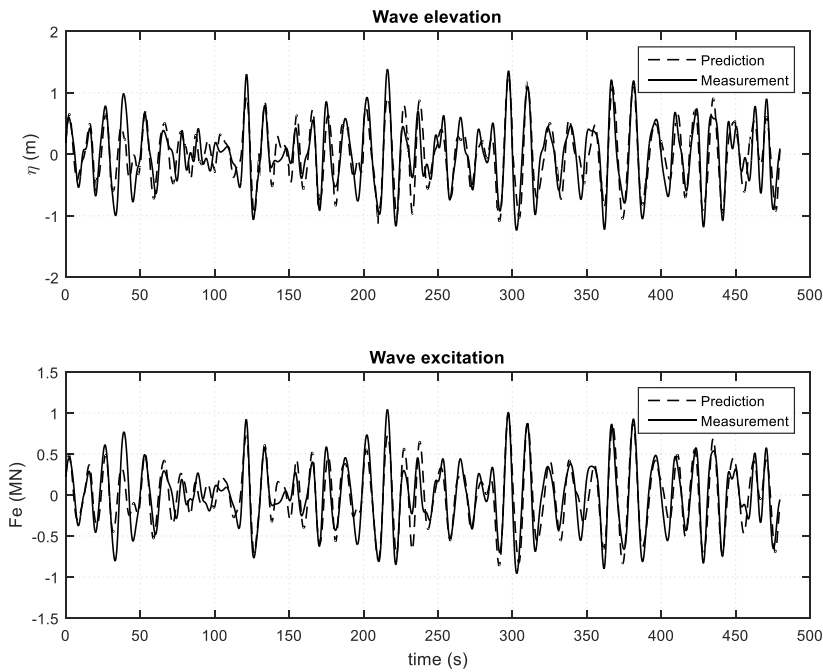


Figure 17(a) top: wave elevation (predicted vs measured) (b) bottom: wave excitation force (predicted vs measured)

9.3 Linear MPC with Realistic Errors in Wave Prediction

Figure 17 shows a visualization of the wave elevation and wave excitation force time series for the measured and predicted signals. The mean absolute error in prediction ($\tilde{\eta}_{error}$) for this case is 15.3%. This error metric is calculated according to the formula

$$\tilde{\eta}_{error} = \langle |\eta_{meas} - \hat{\eta}_{pred}| \rangle / \max(|\eta_{meas} - \hat{\eta}_{pred}|)$$

Where the operation $\langle \eta \rangle$ calculates the mean value of a given time series η . When compared to the idealized case with perfect wave prediction, the reduction in MPC performance due to a 15.3% mean absolute error was 5.6%. Whereas, the relative improvement with respect to the baseline was still as high as 224%.

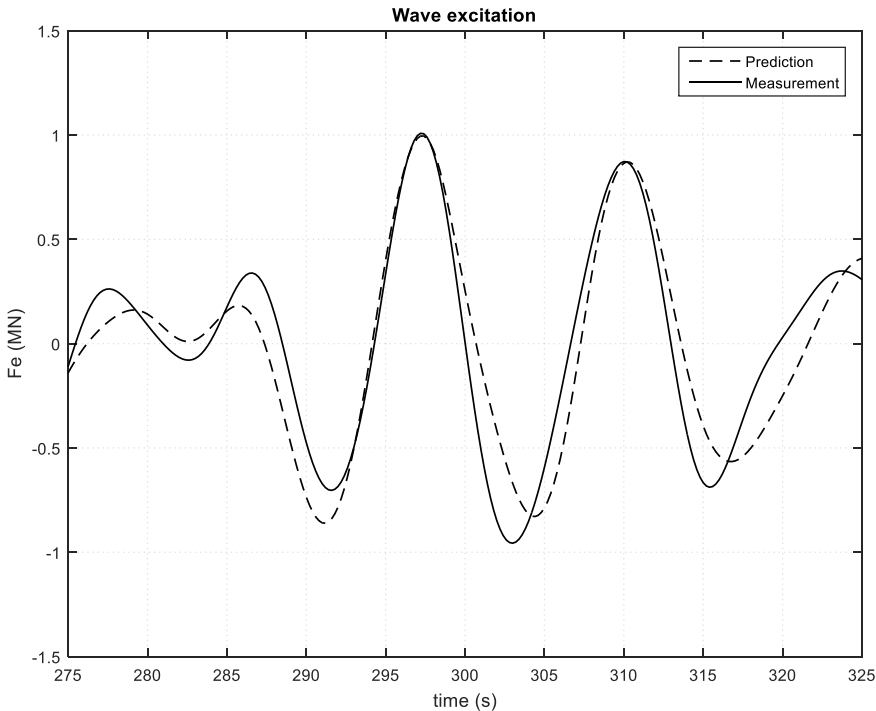


Figure 18 - Comparison between the predicted and measured wave excitation force for a select time window

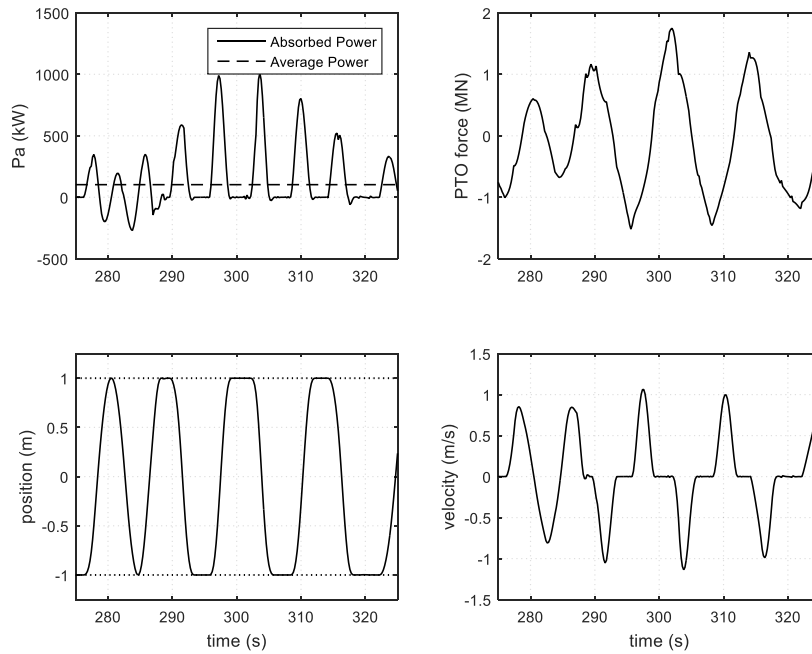


Figure 19 - Device response using Linear MPC with a 15% mean absolute error in wave prediction

The results of this study are summarized below in Table 6. For this example, the results show that MPC can provide significant improvement in performance with a realistic 15% mean absolute error in wave prediction.

Table 6 - Absorbed and normalized power for optimal linear damping (baseline), MPC with perfect prediction and MPC with error in prediction

Control Method	Absorbed Power (kW)	Normalized (%)
Optimal linear damping (baseline)	45.9	100%
Linear MPC (perfect prediction)	108.9	237%
Linear MPC (prediction with errors)	102.8	224%

10 Nonlinear Model Predictive Control

Non-linear Model Predictive Control (NMPC) is applied in cases where the device dynamics features significant nonlinearities that cannot be linearized. Common examples of nonlinearity in wave energy conversion are viscous drag, hysteresis, stiction in the mechanical parts and losses occurring in the powertrain.

10.1 Example Flap-Type WEC Device

We take the example of a flap-type WEC device to describe our NMPC algorithm. The WEC is bottom-mounted and comprises a hinged flap that drives a PTO system. A buoyancy chamber at the top of the WEC provides restoring force to the flap and, as waves pass overhead, the flap oscillates and drives one or more hydraulic PTO pumps. A high-level illustration of the control algorithm setup for this WEC is provided in Figure 20. The theory developed for this flap-type WEC can be easily extended to other WEC topologies, however, each device may show a different behavior based on its geometry, mode of operation and control method.

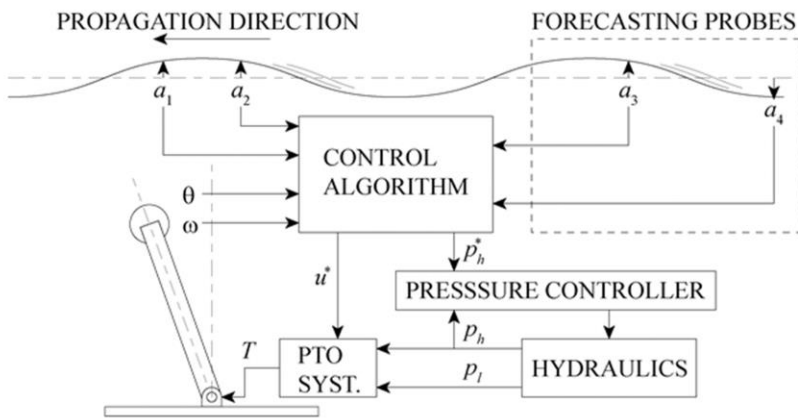


Figure 20 - Block diagram of feed-forward control of flap-type WEC

The linear dynamics of the flap (referred to as the plant) is modelled in state space, while non-linearity (viscous drag force) is modelled separately within the system. The overall system dynamics is computed by adding the output of the linear and non-linear blocks. The time integration of the system dynamics is carried out using a suitable Runge-Kutta scheme. Using Newton's laws of motion, the dynamics of the flap can be modelled according to the following force balance equation.

$$I_{total}\ddot{\theta} = T_{wave} + T_{PTO} - T_{rad} - T_{hydro} - T_{visc}$$

$$I_{total} = I + I_a$$

$$T_{hydro} = k_p\theta$$

$$T_{visc} = C_d|v_d|v_d$$

where I_{total} , is the sum of the moment of inertia of the flap and the infinite frequency added inertia. T_{hydro} denotes the hydrostatic restoring torque. T_{visc} denotes the nonlinear viscous drag force caused by flow

separation at the edges of the flap. The viscous drag force is approximated using the hyperbolic tangent function, as

$$T_{visc} = C_d \tanh(K v_d) v_d$$

Setting $K = 10$ in the above expression gives a good approximation to the value of viscous drag. This is done in order to use smooth analytical gradients and to aid in convergence. For numerical simulation and controls optimization, the force balance equation is modelled in state-space form as follows

$$\begin{aligned} \dot{x}(t) &= f_1(x(t), u(t), T_{wave}, T_{visc}) \\ &= Ax(t) + Bu(t) + ET_{visc}(t) + ET_{wave}(t) \end{aligned}$$

With

$$A = \begin{bmatrix} A_r & 0 & B_r \\ 0 & 0 & I \\ -\frac{C_r}{I_{total}} & -\frac{k_p}{I_{total}} & -\frac{D_r}{I_{total}} \end{bmatrix} \quad B = \begin{bmatrix} 0 \\ 0 \\ 1 \end{bmatrix} \quad E = \begin{bmatrix} 0 \\ 0 \\ 1 \end{bmatrix}$$

and where $\{A_r \ B_r \ C_r \ D_r\}$ represent the state-space matrices of the radiation-damping sub-system. Torque $u(t) = T_{PTO}(t)$ is treated as the control input, and the state vector $x = [x_r^T \ \theta \ \dot{\theta}]^T$ includes the radiation-damping states, angular position and angular velocity, respectively. For simplicity of notation we write $f_1(x(t), u(t), T_{wave}, T_{visc})$ as $f_1(x(t), u(t))$ and it is understood that the system dynamics are a function of all the torques acting on the system. The electrical generated power P_{gen} is the difference of the mechanical absorbed power $P(t) = u(t)\dot{\theta}(t)$ and the total transmission loss in the PTO power train, P_{loss} . As such,

$$P_{gen} = P - P_{loss} .$$

The mathematical nature of P_{loss} , and its dependence on the response states of the WEC, will vary for different PTO topologies, and in many realistic scenarios can be rather complex. However, for now, it suffices to say that this model relates P_{loss} to absorbed power P , through a nonlinear algebraic equation.

10.2 Nonlinear MPC Problem Setup

The objective of MPC is to maximize the electrical generated power P_{gen} . At each instant t_0 , a cost-function $J(x, u)$ is minimized over a control horizon subject to motion constraints, limitations on the type of control (discrete or continuous), maximum applied control force and the ability to have bidirectional power flow. For continuous control with bi-directional power flow, the cost function $J(x, u)$ at a given time instant t_0 over the interval $t \in [t_0, t_0 + T_h]$ is defined as

$$\begin{aligned} J(x, u) &= \frac{1}{T_h} \int_{t_0}^{t_0+T_h} P_{gen}(t) dt \\ &= \frac{1}{T_h} \int_{t_0}^{t_0+T_h} (P(t) - P_{loss}(t)) dt \\ &= \frac{1}{T_h} \int_{t_0}^{t_0+T_h} (\dot{\theta}(t)u(t) - P_{loss}(t)) dt \end{aligned}$$

The MPC objective is to find the optimal control $u^*(t)$ that satisfies

$$\begin{aligned} \max_u J(x, u) \\ \text{s. t.} \quad & \bar{x}_0 - x(t_0) = 0 \\ & f_1(x(t), u(t)) - \dot{x} = 0, \quad t \in [t_0, t_0 + T_h] \\ & |\theta(t)| \leq p_{max}, \quad t \in [t_0, t_0 + T_h] \\ & |\dot{\theta}(t)| \leq v_{max}, \quad t \in [t_0, t_0 + T_h] \\ & |u(t)| \leq u_{max}, \quad t \in [t_0, t_0 + T_h] \end{aligned}$$

If P_{gen} can be written as a polynomial of the absorbed power such that,

$$P_{gen} = \Phi(P) = \alpha_0 + \alpha_1 P + \alpha_2 P^2 + \dots + \alpha_n P^n$$

then the cost function $J(x, u)$ can be written as

$$J(x, u) = \frac{1}{T_h} \int_{t_0}^{t_0+T_h} \Phi(P)(t) dt$$

As the generated power is represented as a function of the absorbed power, the optimization problem can now be solved using the chain rule while computing the Gradient and Hessian of the cost function.

10.3 Nonlinear MPC Algorithm and the Loss Model

The first step in solving the non-linear program (NLP) is to discretize the continuous-time problem over the control horizon $[t_0, t_0 + T_h]$ by dividing it into N smaller intervals $[t_k, t_{k+1}]$ with a constant time step δt . Assuming a zero-order hold condition, the continuous control input u is taken to be a constant u_k in each k^{th} interval. Similarly, the excitation forces and other external disturbances are discretized assuming a zero-order hold. We also introduce a matching condition to impose the dynamics constraints at the end of each interval $[t_k, t_{k+1}]$, i.e.

$$\chi_k(x_{k+1}; x_k, u_k) - x_{k+1} = 0, \quad t = t_{k+1}$$

where χ_k represents the state-trajectory discretized over the interval. After discretization, the cost function can be written as

$$\begin{aligned} J_k(x_k, u_k) &= \frac{1}{N} \sum_{k=0}^{N-1} L_k(x_k, u_k) \\ &= \frac{1}{N} \sum_{k=0}^{N-1} (P(x_k, u_k) - P_{loss}(x_k, u_k)) \\ &= \frac{1}{N} \sum_{k=0}^{N-1} \Phi_k(P) \end{aligned}$$

The discretized non-linear programming (NLP) problem is then given by

$$\begin{aligned} \max_u & J_k(x_k, u_k) \\ \text{s. t.} & \quad \bar{x}_0 - x = 0 \\ & \quad c(x_k, x_{k+1}, u_k) = \chi_k(x_{k+1}; x_k, u_k) - x_{k+1} = 0, \quad k = 0, 1, \dots, N-1 \\ & \quad d(x_k, u_k) \geq 0, \quad k = 0, 1, \dots, N-1 \end{aligned}$$

The NLP can be solved using a sequential quadratic programming (SQP) approach. To setup the SQP for this cost function, let us define the vector of optimization variable, $W^T = [U^T \ X^T]^T$, where, $U^T = [u_0^T \ \dots \ u_{N-1}^T]$, $X = [x_0^T \ \dots \ x_{N-1}^T]$. At each iteration of i , we use an appropriate initial guess for the optimization variable w_0 and Lagrange multiplier λ_0 for the constraints and solve the following quadratic programming (QP) problem instead of solving the NLP:

$$\max_{\Delta w} \frac{1}{2} \Delta w^T B^{(i)} \Delta w + b^{(i)T} \Delta w$$

$$s. t. \quad C^{(i)} \Delta w + c^{(i)} = 0$$

$$D^{(i)} \Delta w + d^{(i)} \geq 0$$

Where $B(i)$ is the Hessian of $L_k(x_k, u_k)$ and $b(i)$ is the cost function gradient, evaluated at the current iteration i . The constraint matrices are obtained by evaluating

$$C^{(i)} = \nabla_w c(w)|_{w^i}, \quad c^{(i)} = c(w^{(i)})$$

$$D^{(i)} = \nabla_w d(w)|_{w^i}, \quad d^{(i)} = d(w^{(i)})$$

The solution is then updated as follows

$$w^{(i+1)} = w^{(i)} + \gamma \Delta w^*$$

Here Δw^* is the optimal solution of the QP problem, and $\gamma \in [0,1]$ can be determined using a line search algorithm. The algorithm is said to have converged when the norm $\|w^{(i+1)} - w^i\|$ is less than a prescribed tolerance.

10.4 Results of Nonlinear Model Predictive Control

		Tp (s)														
		5	6	7	8	9	10	11	12	13	14	15	16	17	18	19
Hs (m)	0.25	0.000	0.000	0.000	0.001	0.000	0.000	0.001	0.000	0.001	0.000	0.000	0.000	0.000	0.000	0.000
	0.75	0.005	0.017	0.028	0.034	0.025	0.019	0.015	0.011	0.007	0.004	0.001	0.000	0.000	0.001	0.000
	1.25	0.003	0.023	0.046	0.061	0.042	0.029	0.020	0.013	0.010	0.006	0.003	0.001	0.000	0.001	0.001
	1.75	0.001	0.007	0.030	0.051	0.035	0.018	0.008	0.009	0.008	0.005	0.002	0.002	0.002	0.001	0.000
	2.25	0.000	0.000	0.009	0.023	0.039	0.027	0.013	0.006	0.005	0.005	0.004	0.001	0.001	0.001	0.000
	2.75	0.000	0.000	0.001	0.006	0.022	0.026	0.021	0.008	0.005	0.003	0.001	0.001	0.001	0.001	0.000
	3.25	0.000	0.000	0.000	0.001	0.007	0.016	0.019	0.015	0.007	0.003	0.002	0.002	0.001	0.001	0.001
	3.75	0.000	0.000	0.000	0.000	0.000	0.004	0.011	0.020	0.009	0.004	0.002	0.000	0.000	0.000	0.000
	4.25	0.000	0.000	0.000	0.000	0.000	0.000	0.002	0.008	0.008	0.005	0.001	0.001	0.000	0.000	0.000
	4.75	0.000	0.000	0.000	0.000	0.000	0.000	0.000	0.000	0.001	0.002	0.003	0.002	0.001	0.000	0.000
	5.25	0.000	0.000	0.000	0.000	0.000	0.000	0.000	0.000	0.000	0.001	0.001	0.001	0.001	0.001	0.000
	5.75	0.000	0.000	0.000	0.000	0.000	0.000	0.000	0.000	0.000	0.000	0.000	0.000	0.000	0.000	0.000

Figure 21- Yakutat scatter diagram

The numerical model of the flap was used to simulate two control strategies (a) Coulomb damping (baseline) (b) Non-linear Model Predictive Control with bi-directional power flow. The shallow water reference site near Yakutat, Alaska was chosen for computing the annual energy captured for both control methods. Subsequently, a 10% reduction in performance was taken to account for the effects of shallow water. Each sea state occurring in the Yakutat scatter diagram (see Figure 21) was simulated for 1200s. The

average value of absorbed power and generated power was calculated for each sea state. The Annual Energy Captured (AEC) in Mega Joules (MJ) was calculated according to the formula given below:

$$AEC = \sum_i^{N_s} \min(P_{gen}(i), P_{rated}) \times p(i) \times 24 \times 365 / 1000$$

Here i denotes a given sea state, $P_{gen}(i)$ is the average generated power (kW), $p(i)$ is the probability of occurrence of a sea state, N_s is defined as the total number of sea states in the scatter diagram and P_{rated} is the rated power of the flap (kW).

The Normalized Annual Energy Captured (NAEC) for a given control method (j) was obtained by using the annual captured energy for Coulomb damping as baseline.

$$NAEC(j) = AEC(j)/AEC(Coulomb\ damping)$$

The following table compares the normalized annual captured energy for the two control methods. It is evident from these results that Non-linear MPC offers significant improvement over the baseline Coulomb damping control. However, in cases where the effect of nonlinear drag forces dominates the system's dynamical response, the performance of MPC deteriorates and the relative improvement in performance is diminished.

Table 7 - Performance of Coulomb damping (baseline) and Non-linear MPC (continuous control, two-way power flow) for an example flap-type WEC

Control method	Normalized performance
Coulomb damping (baseline)	100%
Non-linear MPC (continuous control, two-way power)	188%

For more details on the Non-linear Model Predictive Control algorithm, PTO configurations, and derivation of a “controls-oriented” loss model for MPC, please refer to our paper [6] entitled “Non-linear Model Predictive Control of Wave Energy Converters with Realistic Power Take-off Configurations and Loss Model” authored by Anantha Karthikeyan, Mirko Previsic, Jeffrey Scruggs and Allan Chertok. This paper was published in the proceeding of the 3rd *IEEE Conference on Control Technology and Applications*, held in Hong Kong, from Aug 19-21, 2019.

11 Causal Control

11.1 Discrete-Time Causal Control with Nonlinear Stroke Protection

A detailed description of discrete-time optimal causal control with non-linear stroke protection is available in our paper [7] entitled “Discrete-time causal control of WECs with finite stroke, in stochastic waves” authored by Jeffrey Scruggs, Yejun Lao, Mirko Previsic and Anantha Karthikeyan. This paper was presented at the 13th European Wave and Tidal Energy Conference (EWTEC 2019) which was held between 1st – 6th of September 2019 in Napoli, Italy.

11.2 Optimal Causal Control with Nonlinear Dynamics and Loss Model

Detailed derivation of optimal causal controllers and simulation results for four different PTO configurations can be found in our paper [8] entitled “Optimal causal control of wave energy converters in stochastic waves – Accommodating nonlinear dynamic and loss models” authored by Rudy Nie, Jeff Scruggs, Allan Chertok, Darragh Clabby, Mirko Previsic and Anantha Karthikeyan. This paper was published in the International Journal of Marine Energy in 2016.

12 Power Take-Off Configurations

One of the core constraints in the overall system is the Power Take-off (PTO). Because the PTO is a key cost driver, imposing reasonable constraints on its capabilities will help contain cost. Constraints that can affect PTO cost include position, velocity, acceleration, force/torque, and power flow amplitude and direction. For example, a hydraulic PTO may use a hydraulic piston pump as the primary actuator, which has a stroke limit that must never be exceeded. This can be introduced as a position constraint in the optimization problem and be used in combination with a force constraint to avoid end-stop violations that would otherwise affect the mechanical integrity of the PTO and device structure. In a similar way, velocity and acceleration constraints can be used to keep the PTO within an envelope of acceptable limits, satisfying reliability concerns. Power flow constraints can be imposed to limit instantaneous power flow, which directly affects the cost of the PTO as well as power flow direction. A positive power flow constraint, for example, precludes the transport of reactive energy for maximizing power capture, which would require a more costly PTO to implement. Finally, PTOs may be able to produce only discrete force levels – typical in hydraulic systems, where a fixed displacement pump pressures fluid in an accumulator at fixed pressure. To better understand the trade-offs with different types of PTO capabilities, we have categorized all the PTOs into four different categories. This categorization allows us to establish fundamental trade-offs and

subsequently refine them based on the specifics of the physical system. These four options are illustrated below.

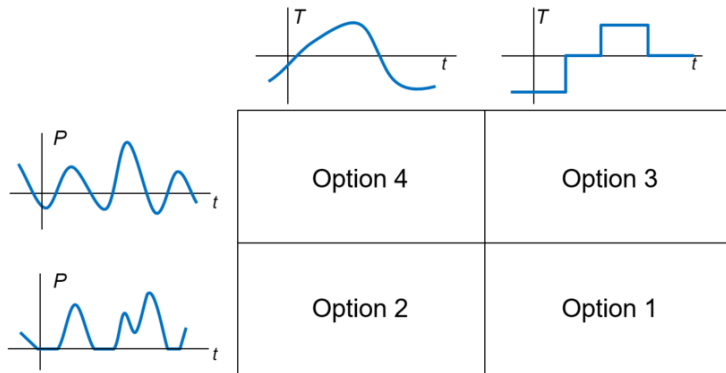


Figure 22 - PTO Options 1-4

Option 1 – Uni-directional power flow (damping only) with discrete force/torque values. This topology would be representative of a very simple hydraulic PTO, where the PTO force is given by a fixed system pressure. We still allow for that force to be switched between high and low and optimize the timing of these switching events.

Option 2 – Uni-directional power flow (damping only) with continuous force values. In this case, the force can be continuously varied, but only positive power flow is allowed. This uni-directional power flow constraint allows us to model PTOs that cannot act as an actuator (i.e., return power to the sea to maximize performance).

Option 3 – Same as Option 1 but allowing for bi-directional power flow.

Option 4 – Same as Option 2 but allowing for bi-directional power flow.

PTO capability and cost increase as PTO topology becomes progressively more complex from Option 1 to 4. This increased complexity can also be associated with higher failure rates. If properly weighted in a techno-economic model, these attributes can be translated into LCoE, allowing for an identification of the optimal topology for a given WEC design. While the complexity of the physical PTO increases with increasing capability, it is much easier to implement an optimal control algorithm for such an unconstrained system than for a heavily constrained one or one involving only discrete force levels. The following illustrations show the time domain behavior of the control forces for Options 1-4 using optimal control. Responses were computed using Model Predictive Control and are meant to illustrate these different response types for a flap type WEC.

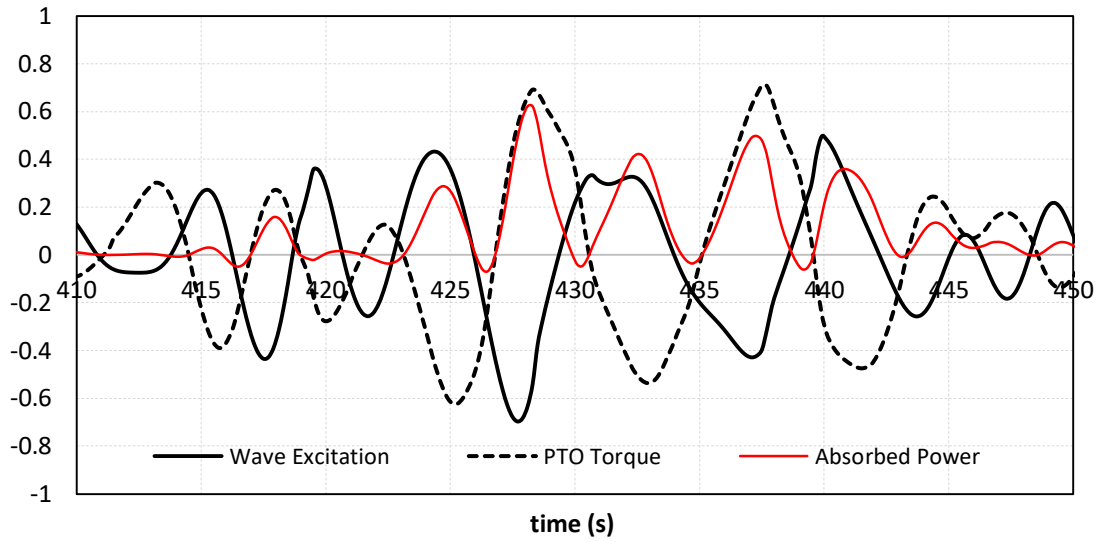


Figure 23 - Normalized response of surge WEC under control option 4 (Note: negative power flow)

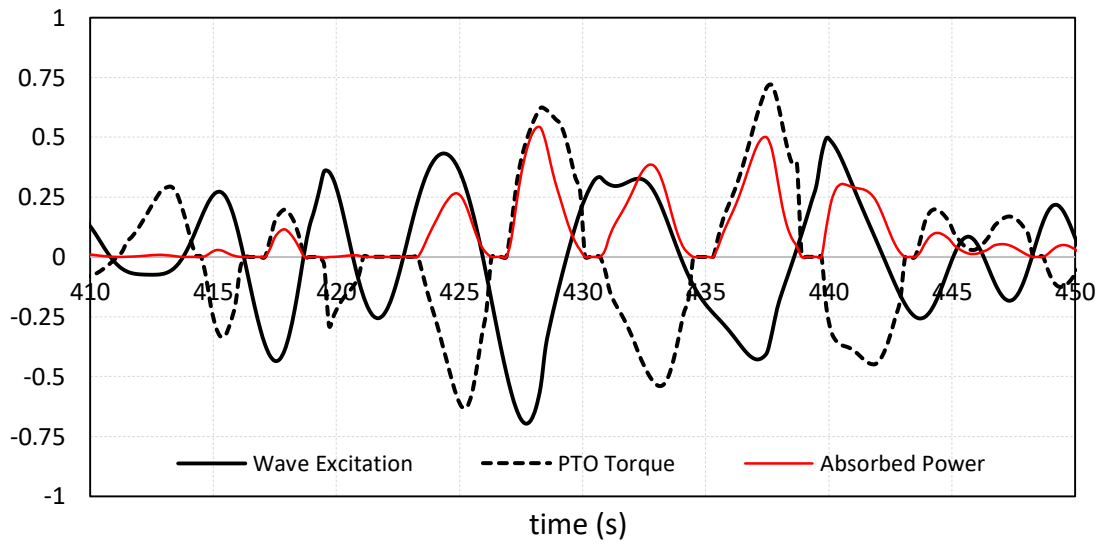


Figure 24 - Normalized Response of Surge WEC under Control Option 2 (Note: no negative power flow)

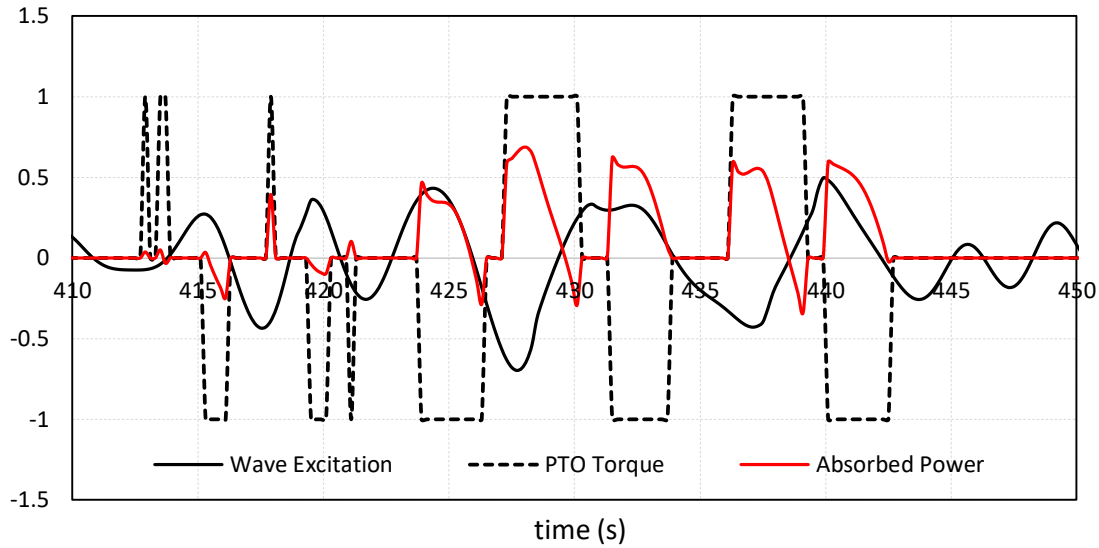


Figure 25 - Normalized Response of Surge WEC under Control Option 3 (Note: negative power flow allowed)

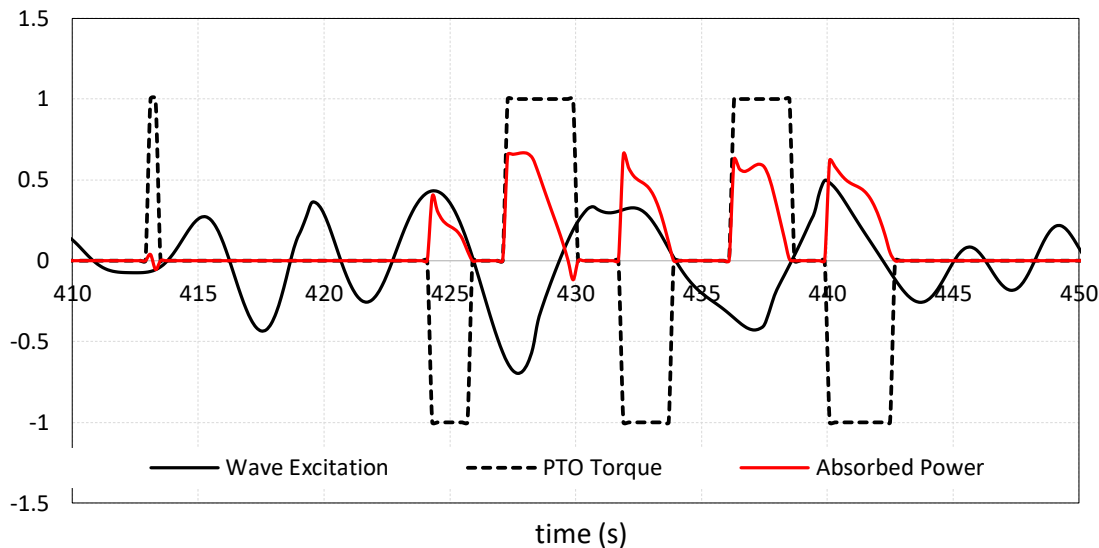


Figure 26 - Normalized Response of Surge WEC under Control Option 1 (Note: no negative power flow allowed)

13 System Identification Methods

System dynamics model for WEC devices are typically developed from frequency domain data that are obtained from Boundary Element Method (BEM) codes, such as WAMIT, Nemoh, or analytical models. Frequency domain data is then augmented in the time domain with non-linear terms for viscous damping and other non-linearities. These models are typically not directly suited for controls development purposes, and a reduced-order model is required to make it fast-enough in the optimization process. This proved

particularly challenging for the oscillating water column (BBDB), which has four heavily coupled oscillatory modes that must be described in the dynamic system.

In order to design controllers (both causal and MPC) for the oscillating water column, it was first necessary to develop an accurate linear finite-dimensional state-space model. By “linear finite-dimensional,” we mean that, at any given time t , the dynamics of the system can be described by a system of ordinary differential equations of the form:

$$\begin{aligned}\dot{x}(t) &= Ax(t) + Bu(t) \\ y(t) &= Cx(t) + Du(t)\end{aligned}$$

where $x(t)$ is a continuous, finite-dimensional vector of coordinates, $u(t)$ is a four-dimensional vector of incident wave forces on the BBDB system, defined as

$$u = \begin{bmatrix} \text{incident heave force} \\ \text{incident surge force} \\ \text{incident pitch force} \\ \text{incident chamber pressure} \end{bmatrix}$$

and $y(t)$ is a four-dimensional vector of response velocities co-located with these forces. This is a challenge because the true physical system is the consequence of partial differential equations, which may be thought of loosely as an infinite-dimensional state-space. Consequently, any finite-dimensional model, as described above, constitutes an approximation, and the goal is to find the best approximation for a given dimensionality of x . The dimension of x should be as small as possible to enhance the efficiency and practicality of the control designs based on this model. However, because the accuracy of the model decreases with dimensionality, there is a trade-off between accuracy and practicality.

One of the things that make MPC challenging for the BBDB is that the finite-dimensional model has four inputs and four outputs. There are consequently 16 input/output channels, all of which must be estimated accurately by the finite-dimensional model. A reasonable approximation without any model reduction techniques yielded a total of about 190 states, which proved detrimental to the computational efficiency of the MPC algorithm.

To address this issue, we refined a subspace-based system identification technique ([9]) to generate the finite-dimensional model. Subspace techniques are analytically sophisticated but very widely used methods for generating such models. They have the distinct advantage of being scalable to systems with many inputs and outputs, as well as systems requiring higher-dimensional state vectors to achieve desired modeling

accuracy. The drawback to these techniques is that the physical meaning of the internal states becomes lost. Figure 27 illustrates how accuracy improves as the number of states is increased. A reasonably accurate model is identified with about 50 states, representing a four-fold reduction in states compared with the original model. More details on model order reduction techniques can be found in [10] and [11].

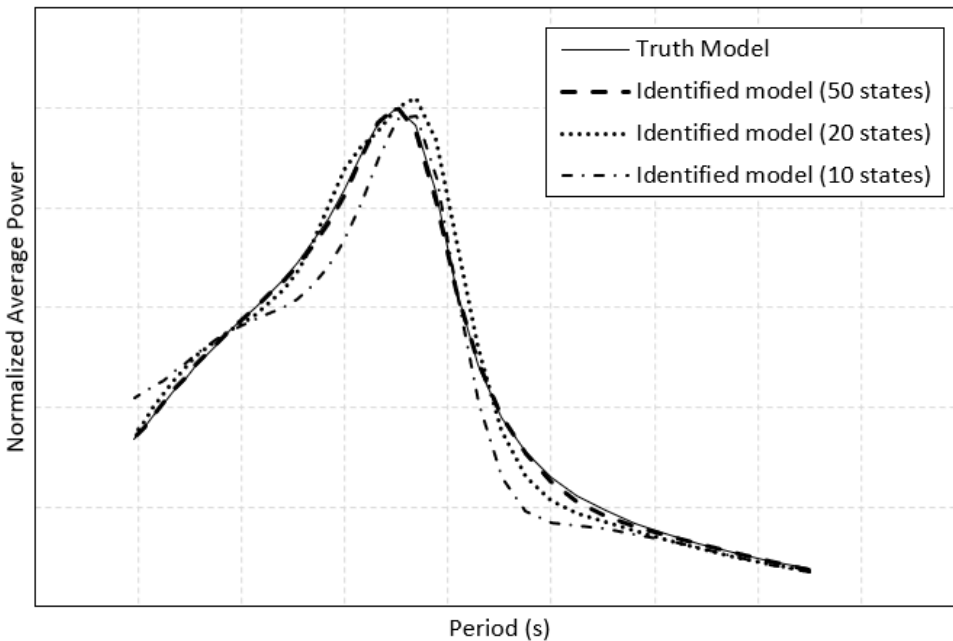


Figure 27 - Comparison of truth model vs identified model for different states

14 References

- [1] K. Budal and J. Falnes, "A Resonant Point Absorber of Ocean Waves," *Nature*, vol. 256, pp. 478-479, 1975.
- [2] J. Newman, "The Interaction of Stationary Vessels With Regular Waves," in *Proceedings of the 11th Symposium on Naval Hydrodynamics*, London, 1976.
- [3] K. Budal and J. Falnes, "Optimum Operation of Improved WavePower Converter," *Marine Science Communications*, vol. 3, no. 2, pp. 133-150, 1977.
- [4] K. Budal and J. Falnes, "Interacting Point Absorbers With Controlled Motion," in *Power From Sea Waves (B. Count, ed.)*, London, Academic, 1980, pp. 381-399.

- [5] J. Hals, J. Falnes and T. Moan, "Constrained optimal control of a heaving buoy wave-energy converter," *Journal of Offshore Mech. Arctic Eng.*, pp. 011401-1-011401-15, 2011.
- [6] A. Karthikeyan, M. Previsic, J. Scruggs and A. Chertok, "Non-linear Model Predictive Control of Wave Energy Converters with Realistic Power Take-off Configurations and Loss Model," in *IEEE Conference on Control Technology and Applications*, Hong Kong, 2019.
- [7] J. Scruggs, Y. Lao, M. Previsic and A. Karthikeyan, "Discrete-time causal control of WECs with finite stroke, in stochastic waves," in *13th European Wave and Tidal Energy Conference (EWTEC2019)*, Napoli, Italy, 2019.
- [8] R. Nie, J. Scruggs, A. Chertok, D. Clabby, M. Previsic and A. Karthikeyan, "Optimal causal control of wave energy converters in stochastic waves - Accommodating nonlinear dynamic and loss models," *International Journal of Marine Energy*, vol. 15, pp. 41-55, 2016.
- [9] J. Scruggs, S. Lattanzio, A. Taflanidis and I. Cassidy, "Optimal causal control of a wave energy converter in a random sea," *Applied Ocean Research*, vol. 42, pp. 1 - 15, 2013.
- [10] K. Glover, "All Optimal Hankel Norm Approximation of Linear Multivariable Systems, and Their L_{∞} - error Bounds," *International Journal of Control*, vol. 39, no. 6, pp. 1145-1193, 1984.
- [11] M. Safonov and R. Chiang, "A Schur Method for Balanced Model Reduction," *IEEE Transactions on Automatic Control*, vol. 34, no. 7, pp. 729-733, 1989.

Control Optimization – SPA II

Heaving Buoy Test Results



DOE Award Number: DE-EE0007173
Project Period: 01/01/2016 to 09-30-2018
Report Date: 6-29-17

Author

Daewoong Son

Principal Investigator

Mirko Previsic

mirko@re-vision.net

916-977 3970 ext. 200

Recipient Organization

Re Vision Consulting, LLC

1104 Corporate Way

Sacramento, CA 95831

Acknowledgment: “This report is based upon work supported by the U. S. Department of Energy under Award No. DE-EE0007173”.

Disclaimer: “Any findings, opinions, and conclusions or recommendations expressed in this report are those of the author(s) and do not necessarily reflect the views of the Department of Energy”. This document was prepared by the organizations named below as an account of work sponsored or cosponsored by the U.S. Department of Energy (DoE). Neither DoE, RE vision consulting, LLC (RE vision), any cosponsor, the organization (s) below, nor any person acting on behalf of any of them:

(A) Makes any warranty or representation whatsoever, express or implied, (I) with respect to the use of any information, apparatus, method, process or similar item disclosed in this document, including merchantability and fitness for a particular purpose, or (II) that such use does not infringe on or interfere with privately owned rights, including any party’s intellectual property, or (III) that this document is suitable to any particular user’s circumstance; or

(B) Assumes responsibility for any damages or other liability whatsoever (including any consequential damages, even if RE Vision or any RE Vision representative has been advised of the possibility of such damages) resulting from your selection or use of this document or any other information, apparatus, method, process or similar item disclosed in this document.

The views and opinions of authors expressed herein do not necessarily state or reflect those of the United States Government or any agency thereof, or RE Vision Consulting, LLC.

Proprietary Data Notice: If there is any patentable material or protected data in the report, the recipient, consistent with the data protection provisions of the award, must mark the appropriate block in Section K of the DOE F 241.3, clearly specify it here, and identify them on appropriate pages of the report. Other than patentable material or protected data, reports must not contain any proprietary data (limited rights data), classified information, information subject to export control classification, or other information not subject to release. Protected data is specific technical data, first produced in the performance of the award, which is protected from public release for a period of time by the terms of the award agreement. Reports delivered without such notice may be deemed to have been furnished with unlimited rights, and the Government assumes no liability for the disclosure, reproduction or use of such reports. This report is considered protected material in its entirety.

Document Prepared by:
RE Vision Consulting, LLC
www.re-vision.net
Project Manager: Mirko Previsic
Email Address: mirko@re-vision.net

Content

Content	3
List of Tables	5
List of Figures	6
1 Introduction	9
2 Test Objective	10
3 Test Facility	11
3.1 Wave Maker	13
4 Scaled Model Description	14
4.1 Device description	14
4.1.1 Full-scale device	14
4.1.2 Model-scale device	14
4.2 Power Take-Off description	16
4.3 Device properties	17
4.4 Froude scaling	18
5 Test Matrix and Schedule	19
5.1 Test matrix	19
5.2 Test schedule	19
6 Experimental Set Up and Methods	21
6.1 Installation	21
6.2 Instrumentation	22
7 Data Processing and Analysis	25
7.1 Data quality assurance	25
7.2 Data processing in real-time	25
7.3 Control modes	27
8 Experimental Results and Validation	28
8.1 Nomenclature	28
8.2 Numerical results	29
8.3 Free-decay test	29
8.4 Wave-excitation force	31

8.5	Power performance in regular waves.....	32
8.5.1	PTO force control	32
8.5.2	Power extraction performance results	33
Appendix A:	Specifications – motor.....	49
Appendix B:	Specifications – sensor	51
Appendix C:	specifications –speedgoat	52
Appendix D:	Instrumentation wiring	56
Appendix F:	Linmot-talk setting.....	57
Appendix G:	Test runs.....	59

LIST OF TABLES

Table 1. Specifications of OSU wave maker.....	13
Table 2. Critical properties of the buoy	17
Table 3. Froude scaling law.....	18
Table 4. Test matrix.....	19
Table 5. Test waves	19
Table 6. Testing schedule – Test Campaign I	19
Table 7. Testing schedule - Test Campaign II	20
Table 8. Testing schedule – Test Campaign III	20
Table 9. Sensors	22
Table 10. OSU wave gauge calibration slope and position.....	24
Table 11. Parameters on control panel.....	26
Table 12. Nomenclature of all variables and constant	28
Table 13. Summary of free-decay test results	31

LIST OF FIGURES

Figure 1. Overview of the DWB, OSU.....	11
Figure 2. General schematic of the DWB layout.....	12
Figure 3. Overview of the wave tank, RFS.....	12
Figure 4. Performance curves of the OSU wave maker.....	13
Figure 5. Schematic of the heaving buoy.....	14
Figure 6. Prospective view of overall system(left) and buoy (right) for 1:25 scale model.....	15
Figure 7. Engineering view of 1:25 scale heaving buoy.....	15
Figure 8. Detailed view of the transducer assembly.....	17
Figure 9. Installed device in the OSU wave basin.....	21
Figure 10. Installed device in the RFS wave tank.....	22
Figure 11. Calibration curve of force sensor.....	23
Figure 12. Layout of the installed device and probe in OSU wave basin.....	24
Figure 13. Data flow and processing steps.....	25
Figure 14. Workflow of Speedgoat.....	26
Figure 15. Front panel of real-time controller.....	27
Figure 16. Hydrodynamic coefficients in model-scale from full-scale WAMIT analysis.....	29
Figure 17. Time history of the buoy position after initial position.....	30
Figure 18. Wave-excitation force comparison.....	32
Figure 19. Schematic of PTO control loop.....	32
Figure 20. Time history of motion response with different linear damping values – Test Campaign I.....	33
Figure 21. Time history of PTO force between input and feedback with linear damping – Test Campaign I.....	34
Figure 22. Time history of PTO force between input and feedback with MPC– Test Campaign I.....	34
Figure 23. Time history of displacement between simulation and measurement with MPC- Test Campaign I.....	35
Figure 24. Time history of velocity between simulation and measurement with MPC – Test Campaign I.....	35
Figure 25. Time history of absorbed power between simulation and measurement with MPC – Test Campaign I.....	36
Figure 26. Time-averaged power performance with MPC – Test Campaign I.....	36
Figure 27. Heave response amplitude of operator for different linear damping - Test Campaign II ...	37
Figure 28. Time history of PTO force between input and feedback with linear damping - Test Campaign II.....	38
Figure 29. Linear damping optimization - Test Campaign II.....	38
Figure 30. Performance with linear damping in time series - Test Campaign II.....	39
Figure 31. Performance with causal control in time series - Test Campaign II.....	39
Figure 32. Performance with MPC in time series - Test Campaign II.....	40
Figure 33. Time-averaged power performance - Test Campaign II.....	40
Figure 34. Linear damping optimization - Test Campaign III.....	41
Figure 35. Optimal linear damping for each wave period.....	42

Figure 36. Performance for linear damping in time series - Test Campaign III 42

Figure 37. Performance for causal control in time series - Test Campaign III 43

Figure 38. Performance for linear MPC in time series - Test Campaign III 43

Figure 39. Position comparison between simulation and experiment with MPC – Test Campaign III. 44

Figure 40. Velocity comparison between simulation and experiment with MPC - Test Campaign III .44

Figure 41. PTO force comparison between simulation and experiment with MPC - Test Campaign III
..... 45

Figure 42. Power comparison between simulation and experiment with MPC - Test Campaign III 45

Figure 43. Time-averaged power performance - Test Campaign III 46

Figure 44. Heave response amplitude of operator - Test Campaign III 46

Figure 45. Performance with optimal linear damping in irregular waves 47

Figure 46. Performance with MPC in irregular waves 48

This page intentionally left blank

1 INTRODUCTION

This testing program measures the performance of a 1-DoF heaving wave-energy converter device to validate control strategies as part of our efforts under our SPA-II project to develop optimal controls approaches.

The core objectives of this project is to improve the power capture of three different wave energy conversion (WEC) devices by more than 50% using an advanced control system and validate the attained improvements using wave tank and full scale testing. In parallel, we will bring along the development of a wave prediction system that is required to enable effective control and test it at full scale. Development efforts will start at a TRL 3 and end at a TRL6.

The purposes of this report are to:

- Plan and document the 1/25th scale device testing at the wave-tank facility;
- Document the test article, setup and methodology, sensor and instrumentation, mooring, electronics, wiring, and data flow and quality assurance;
- Communicate the testing results between the associated members;
- Facilitate reviews that will help to ensure all aspects (risk, safety, testing procedures, etc.);
- Provide a systematic guide to setting up, executing and decommissioning the experiment.

2 TEST OBJECTIVE

The main objective of the 1/25th scale point-absorber type heaving buoy is to obtain the necessary measurements required for validate the performance of different control strategies. This includes:

- Validate the hydrodynamic coefficients such as wave-excitation force, radiation damping, drag coefficient of the device;
- Validate the numerical results from WAMIT;
- Measure the power-extraction performance of the WEC device with different control strategies (Linear damping, Causal control, MPC).

3 TEST FACILITY

Testing was mainly conducted in the Directional Wave Basin (DWB) at O. H. Hinsdale Wave Research Laboratory of Oregon State University (OSU), Corvallis, Oregon. The DWS is an indoor basin having an overall length of 48.8 m (160 ft.), a width of 26.5 m (87 ft.) and a depth of 1.37 m (4.5 ft.). A photo of the DWB can be found in Figure 1. The basin has an instrumentation carriage spanning the width of basin. The opposite end of wavemaker is 1:10 removable steel beach. Uni-strut inserts are placed in rows with 1.2 m spacing to affix wave gauge and model in floor of the basin. Figure 2 shows general schematic of the DWB layout.

The second testing was performed in the Richmond Field Station (RFS) of University of California at Berkeley, which is shown in Figure 3. The RFS wave-tank has 68 m length, 2.4 m width, and 1.8 m depth with a flap-type wave maker. A carriage can travel along with the length of the tank.



Figure 1. Overview of the DWB, OSU

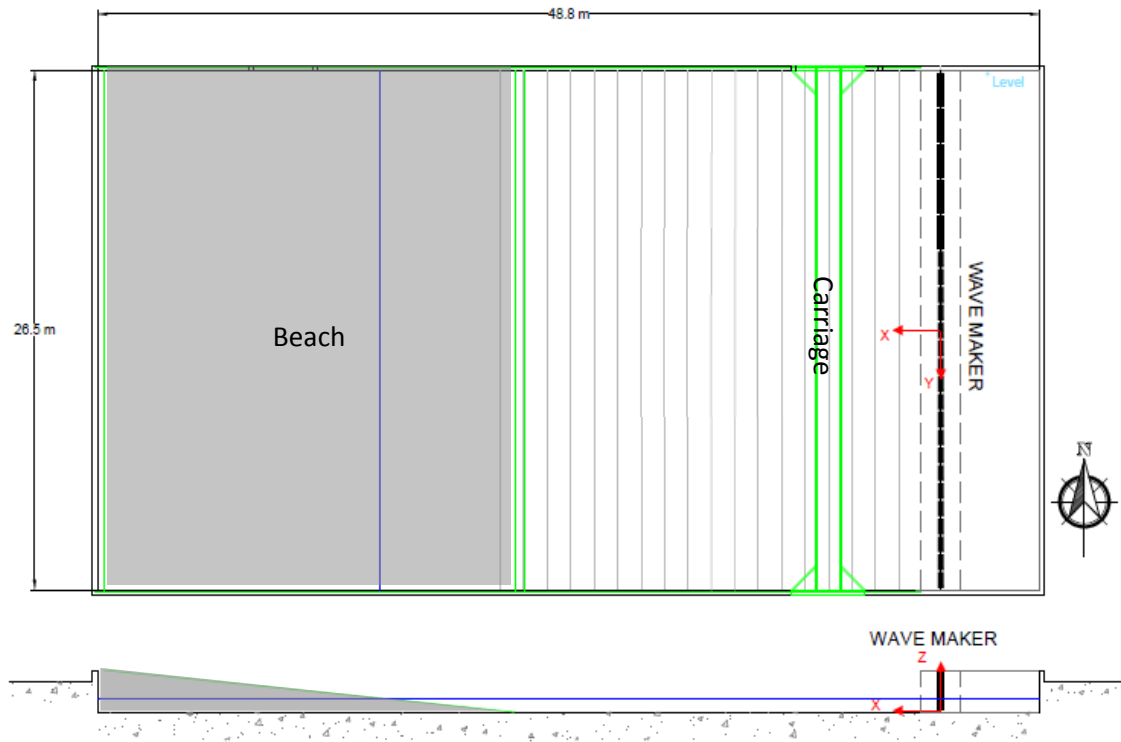


Figure 2. General schematic of the DWB layout

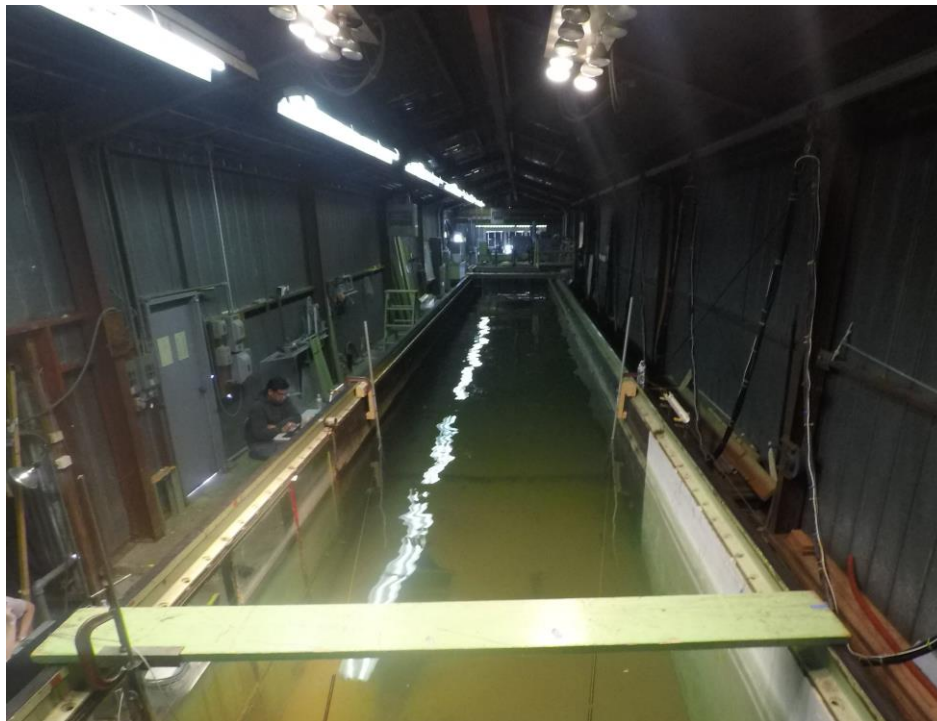


Figure 3. Overview of the wave tank, RFS

3.1 WAVE MAKER

The OSU wave maker is a piston-type system made of 29 boards with up to 2.1 m long stroke. The 29 boards of 2 m (6.6 feet) height are driven by electrical motors. The facility has been designed to generate regular, irregular, Tsunami and multidirectional waves. Detailed specifications of the OSU wave maker are list in Table 1.

Table 1. Specifications of OSU wave maker

Parameter	Value
Period range	0.5 to 10 sec
Max. wave	0.75 m (2.5 ft.) in 1.37 m (4.5 ft.) depth
Max. stroke	2.1 m (6.9 ft.)
Max. velocity	2.0 m/s (6.6 ft./s)

Figure 4 shows the performance curves of the OSU wave maker as functions of wave height (h)/water depth (H) and wave height (h)/wave length (L). Based on this performance curves, wave conditions, i.e., periods and height, were selected to retain linear-wave theory.

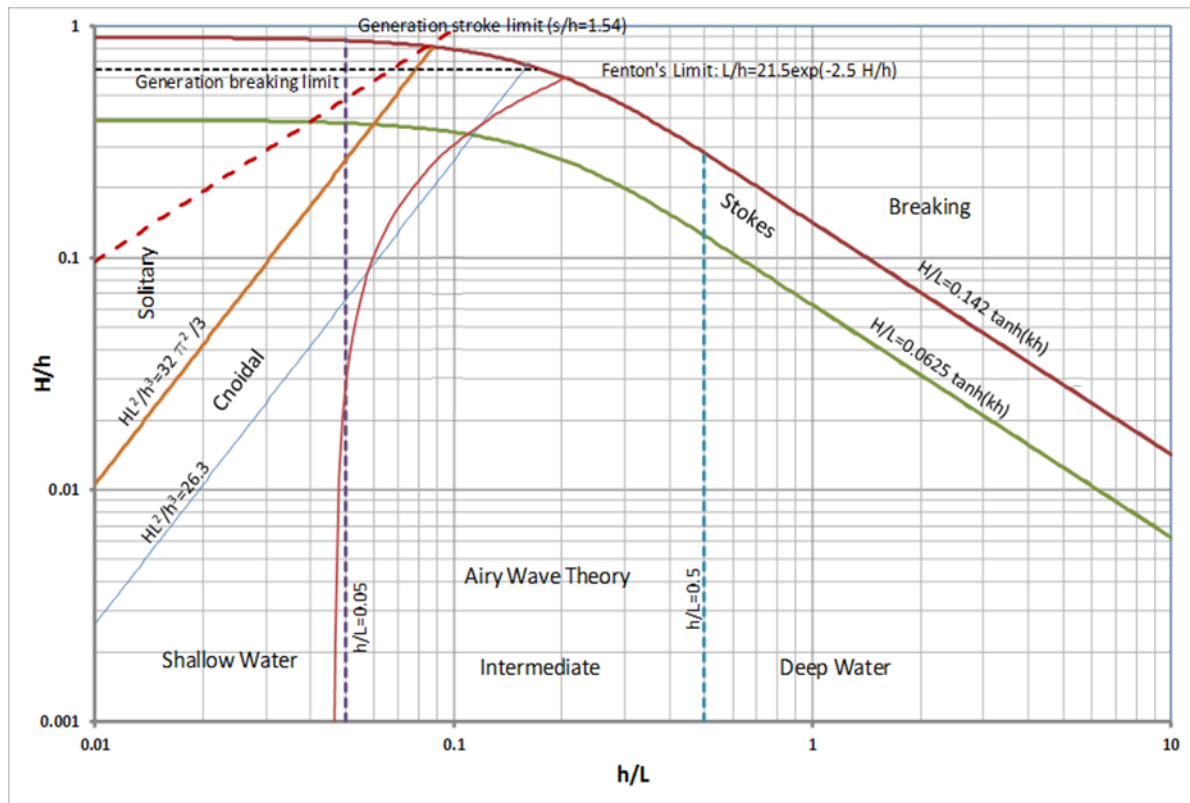


Figure 4. Performance curves of the OSU wave maker

4 SCALED MODEL DESCRIPTION

4.1 DEVICE DESCRIPTION

4.1.1 Full-scale device

The heaving buoy designed by RE Vision Consulting, LLC., is a heaving point-absorber wave-energy converter (WEC). A single body is constrained to move vertically in response to incident waves. The relative vertical motion with respect to the fixed structure or platform is utilized to capture wave energy. The buoy has an axisymmetric body, with conical bottom shape. The general concept of the heaving buoy is illustrated in Figure 5.

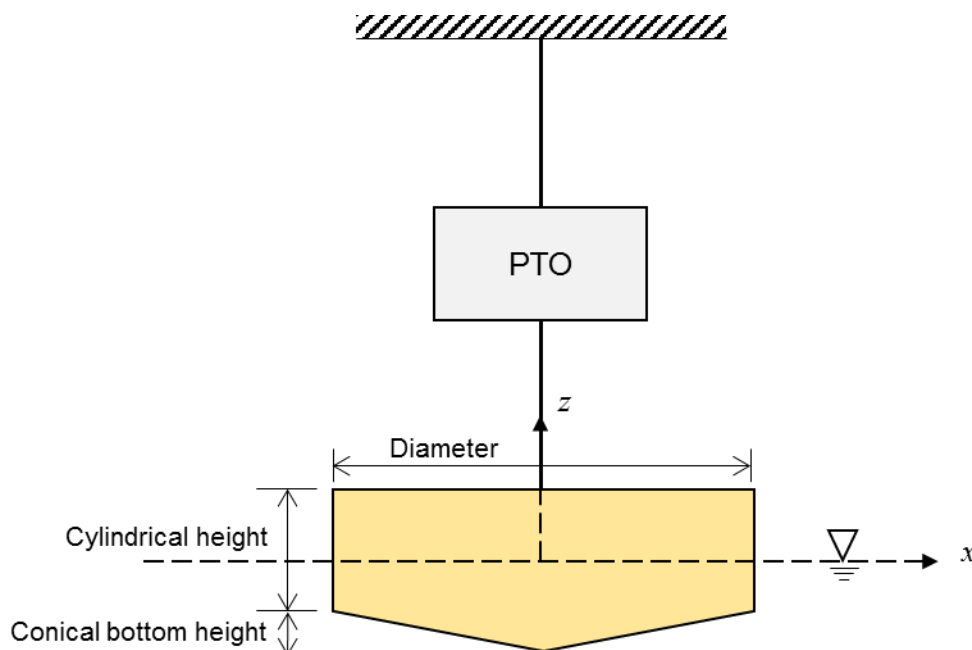


Figure 5. Schematic of the heaving buoy.

The full-scale device is expected to be deployed in intermediate or deep water, and dimensions are a diameter of 11 m, a cylindrical height of 4 m, and conical bottom height of 1.2 m (30% of the cylindrical height).

4.1.2 Model-scale device

For testing in the wave basin, the device was scaled down by 25X from the full-scale design. A SolidWorks rendered image of the 1:25 scale model and proposed arrangement for testing at wave tank are shown in Figure 6. An engineering view of the heaving buoy is also shown in Figure 7.

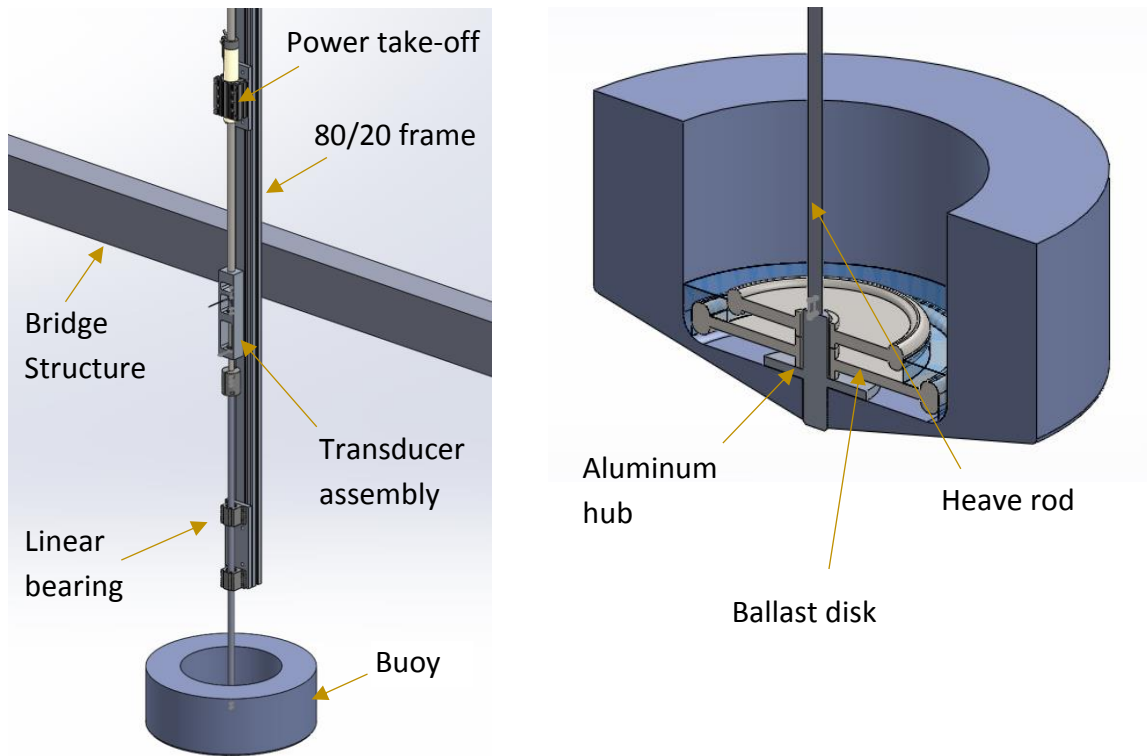


Figure 6. Prospective view of overall system(left) and buoy (right) for 1:25 scale model

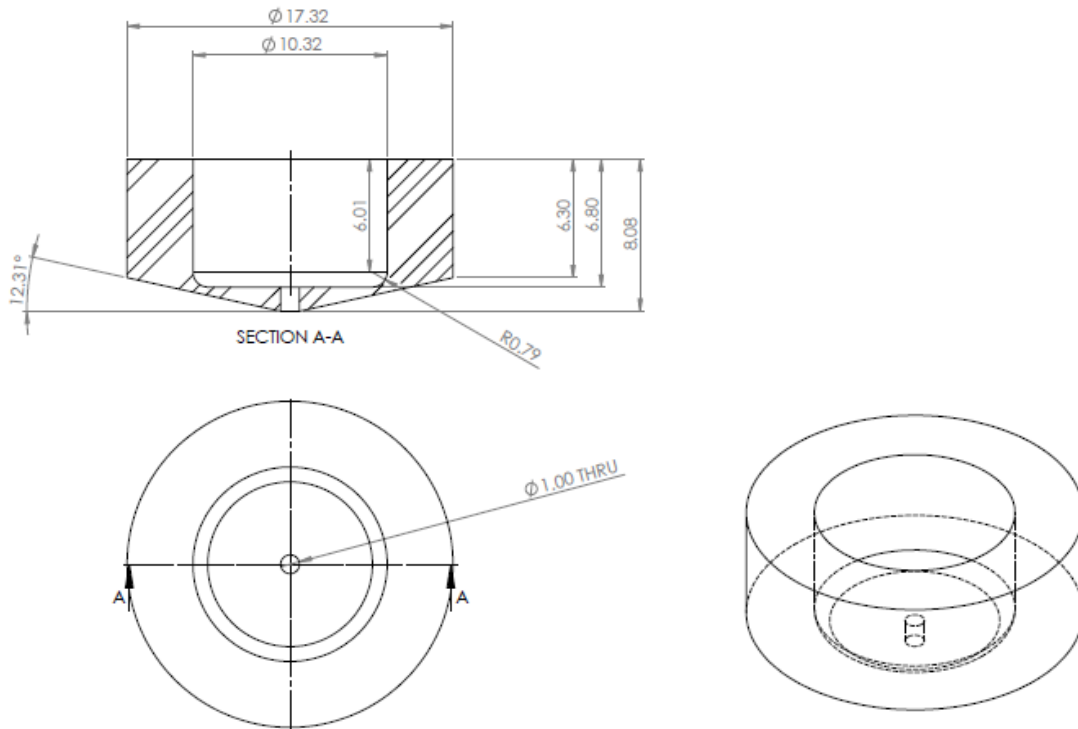


Figure 7. Engineering view of 1:25 scale heaving buoy

The elements of the model-scale WEC device for tank testing are as follows:

- The buoy: moving part of the device made by Foam and Fiberglass for surface;
- The power take-off: permanent magnet linear motor consisting of stator and slider;
- The transducer assembly: contains a load cell and connects the slider to the heave rod;
- The ballast disk: weights to match desired draft of the buoy, 15 lbs (6.8 kg);
- The heave rod: (1) 8" (length) x 0.5" (diameter) shaft for compatibility with load cell carrier;
(2) 36" (length) x 0.625" (diameter) shaft connected to the center of buoy.

The power take-off and linear bearings for heave rod are mounted on 80/20 frame, which is attached to the platform or carriage using C-clamps.

4.2 POWER TAKE-OFF DESCRIPTION

The power take-off (PTO) is a direct-drive permanent magnet linear motor PS01x37-120C with PL01-20x1600/1520-LC slider manufactured by LinMot. It provides a maximum 163 N reaction force. Specifications of motor and drive is included in [Appendix A](#).

The moving part of magnet or slider is connected to the buoy, while the stator is mounted on the bridge. The motor force is controllable via an analog signal provided by the motor drive which allows real-time force control loops to be implemented. The load cell is positioned between the slider and the heave rod as shown in Figure 8, thus measuring the total linear force between the buoy and the PTO. Linear bearings isolate the forces transferred to the load cell to 1-DoF and insure off-axis loads.

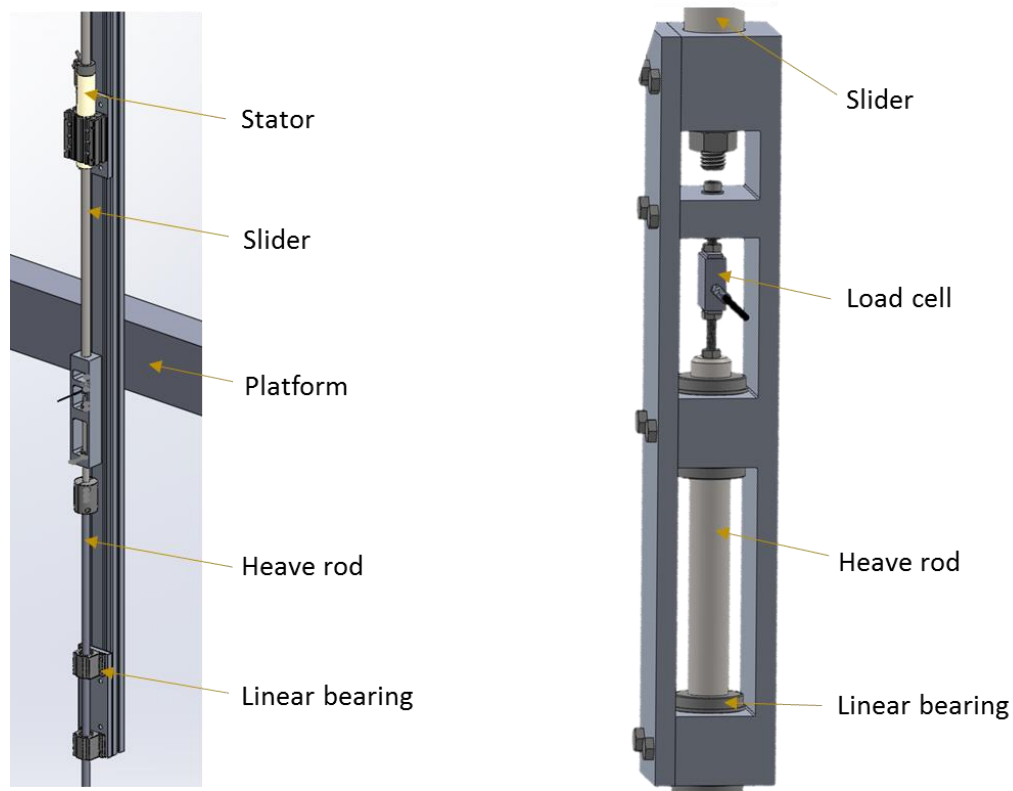


Figure 8. Detailed view of the transducer assembly

The motor drive provides position measurements in form of a simulated encoder output. A encoder to voltage converter manufactured by Laurel Electronics, provides the user scalable analog output 0-10V from digitally transmitted pulse counts.

4.3 DEVICE PROPERTIES

The full-scale and 1:25th model-scale buoy properties are listed in Table 2. Definition of geometrical parameters of the buoy is shown in Figure 5.

Table 2. Critical properties of the buoy

	Full-scale	Model-scale
Diameter (m)	11	0.44
Cylindrical height (m)	4	0.16
Conical bottom height (m)	1.2	0.048
Draft (m)	3.2	0.128

Water depth (m)	35	1.365
Displaced mass (kg)	228079.6	14.60
Submerged volume (m ³)	228.08	0.146

4.4 FROUDE SCALING

Device linear dimensions and properties are scaled per Froude scaling laws, listed in Table 3 below.

Table 3. Froude scaling law

Quantity	Units	Scaling
Wave height and length	m	s
Wave period and time	sec	$s^{0.5}$
Wave frequency	Hz	$s^{-0.5}$
Linear displacement	m	S
Linear velocity	m/s	$s^{0.5}$
Force	N	s^3
Power	W	$s^{3.5}$
Mass	Kg	s^5
Linear stiffness	N/m	s^2
Linear damping	N/(m/s)	$s^{-2.5}$

5 TEST MATRIX AND SCHEDULE

5.1 TEST MATRIX

The performed tests of the 1/25th scale device at wave-tank listed in Table 4, and incident-wave conditions for testing are shown in Table 5. Detailed test runs are listed in [Appendix G](#).

Table 4. Test matrix

ID	Tests	Measurements	Device	Wave
1	Free-decay	. Position	-	-
2	Wave-excitation force	. Force . Incident-wave elevation	Fixed	Regular
3	Power performance	. Force . Position . Incident-wave elevation	-	Regular

Table 5. Test waves

Type	Period	Height	Test ID
Regular	1.0/1.4/1.8/2.2/2.6/3.0/3.4 sec	4 cm	2. 3
	5/7/9/11/13/15/17 sec	1 m	(Full scale)
h/L (OSU)	0.87/0.45/0.28/0.21/0.17/0.14/0.12	0.03 (H/h)	

5.2 TEST SCHEDULE

TEST CAMPAIGN I was carried out at the Oregon State University (OSU) tank facility from March 6 (Monday) to March 8 (Wednesday), 2017, as shown in Table 6.

Table 6. Testing schedule – Test Campaign I

Date/Time	Event
Monday	WEC installation and work-in
08:00 – 14:00	Assembling and installation of the device, set up for testing and verifying operation
14:00 – 17:00	Force control loop debugging

Tuesday	Full Test Day
08:00 – 15:30	Force control loop debugging
15:30 – 17:00	Wave-excitation force test
Wednesday	Full Test Day
08:00 – 08:30	Free-decay test
08:30 – 10:00	Wave-excitation force test
10:00 – 17:00	Performance test in regular waves with linear damping and MPC

TEST CAMPAIGN II was carried out at the Richmond Field Station (RFS) of the UC Berkeley from April 19 (Wednesday) to April 21 (Friday), 2017, as shown in Table 7.

Table 7. Testing schedule - Test Campaign II

Date/Time	Event
Wednesday	WEC installation
18:00 – 20:00	Assembling and installation of the device, set up for testing and verifying operation
Thursday	Full Test Day
09:00 – 15:30	Performance test in regular waves with linear damping
15:30 – 20:00	Performance test in regular waves with MPC
Friday	Full Test Day
09:00 – 14:00	Performance test in regular waves with MPC
14:00 – 19:00	Performance test in regular waves with Causal control
19:00 – 21:00	Decommissioning the model

TEST CAMPAIGN III was carried out at the OSU from May 24 (Wednesday) to May 26 (Friday), 2017, as shown in Table 8.

Table 8. Testing schedule – Test Campaign III

Date/Time	Event
Wednesday	WEC installation and work-in
12:00 – 15:30	Assembling and installation of the device, set up for testing and verifying operation
15:30 – 17:00	Performance test in regular waves with linear damping
Tuesday	Full Test Day
08:00 – 11:00	Performance test in regular waves with MPC
11:00 – 12:00	Performance test in regular waves with Causal control
12:00 – 17:00	Performance test in regular waves with linear damping
Wednesday	Full Test Day
08:00 – 11:00	Performance test in regular waves with Causal control
11:00 – 16:30	Performance test in regular waves with MPC
16:30 – 17:30	Decommissioning the model

6 EXPERIMENTAL SET UP AND METHODS

6.1 INSTALLATION

The slider, transducer assembly, and heave rod need to be connected sequentially. Figure 9 and Figure 10 show the installed device in the Oregon State University (OSU) wave basin and the Richmond Field Station (RFS) wave tank, respectively. One of wave gauges is aligned with the center of buoy, and another one is positioned the device ahead.

After installing the device in wave tank, a fundamental functionality test should be done to check force control mode of LinMot motor and to confirm direction of the force and position. The positive PTO force moves the buoy up (positive position).

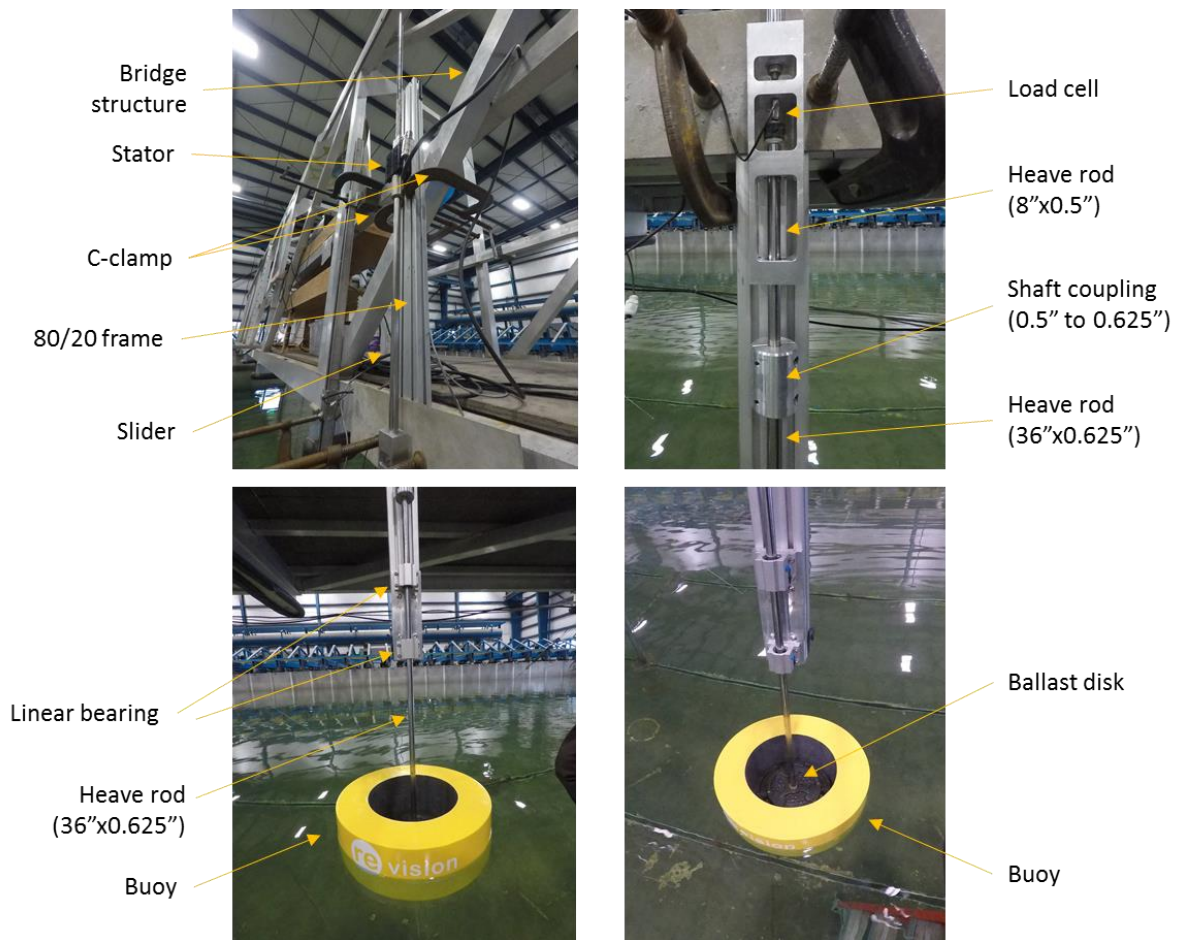


Figure 9. Installed device in the OSU wave basin

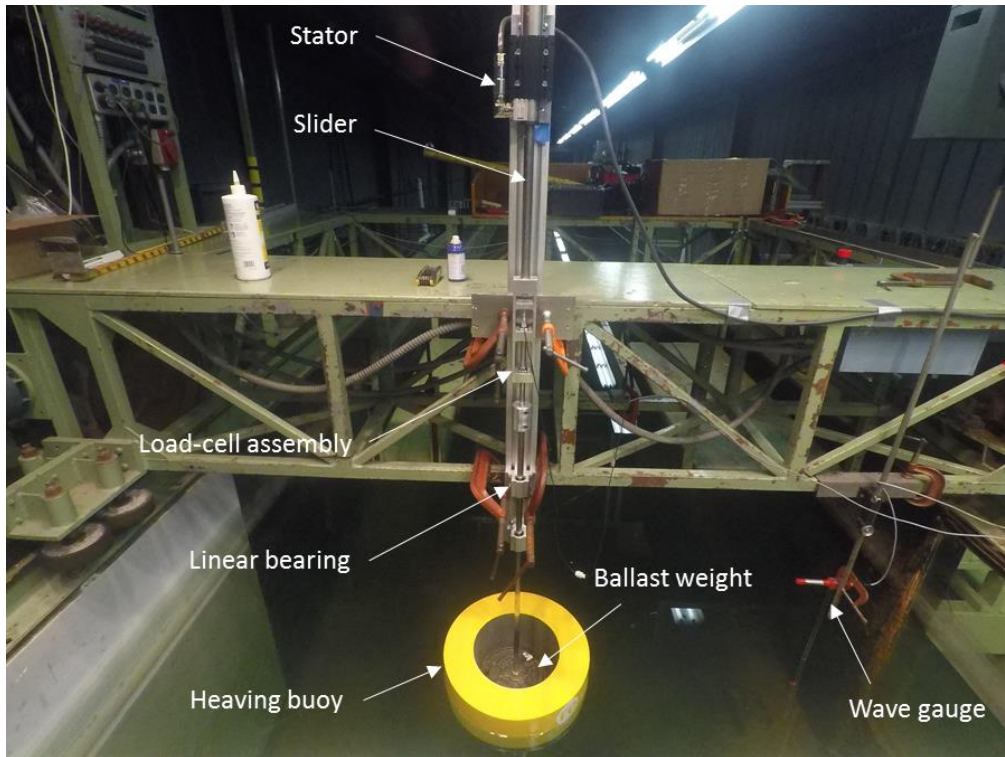


Figure 10. Installed device in the RFS wave tank

6.2 INSTRUMENTATION

The sensors used for testing are listed in Table 9 below:

Table 9. Sensors

Function	Sensor	Maker	Units
PTO force	LSB200 – 50lb	Futek	N
Linear position	LT61QD	Laurel Electronics, Inc.	m
Wave elevation	Twin-wire resistance wave gauge (OSU) Capacitance wave gauge (RFS)	-	m

The following points should be noted in relation to the interface with sensor systems:

- Force feedback is provided by way of a dedicated load cell, which is connected to a strain gauge amplifier manufactured by Mantracourt Electronics. An output in volts from the sensor is provided in the calibration curve, which is shown in Figure 11. Detailed information of the load cell and amplifier is included in [Appendix B](#).

- Linear position is provided by way of a simulated quadrature encoder outputs, providing A/B/Z TTL signals from the LinMot drive. The connected Laurel transmitter provides analog output for position from quadrature encoder signal by digital-to-analog converter. To scale analog output, two endpoints of output range needs to be set. After calibration, a slope of -11.913 mm/V was used at +/- 3000 count range of the encoder, with 10 um resolutions.
- OSU provided the wave gauge of twin-wire resistance type. Seven wave probes were installed around the device in semicircle as shown in Figure 12. The provided conversion slope between the voltage output and wave elevation in meter is listed in Table 10. At the RFS facility, wave gauges of capacitor type were installed with 18.05 m distance between them. In addition, wave maker signal is also provided, which is 5 volts from 0 volt when it starts.

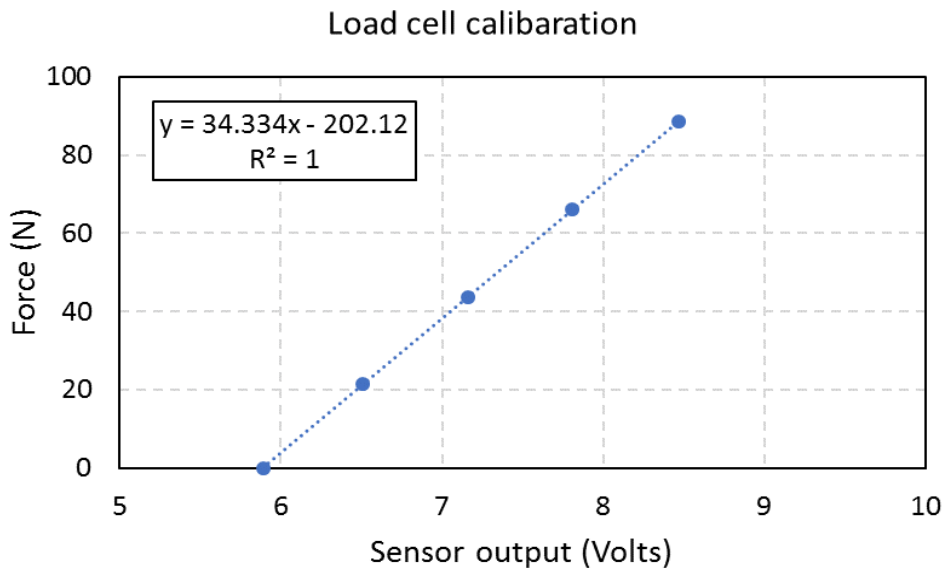


Figure 11. Calibration curve of force sensor

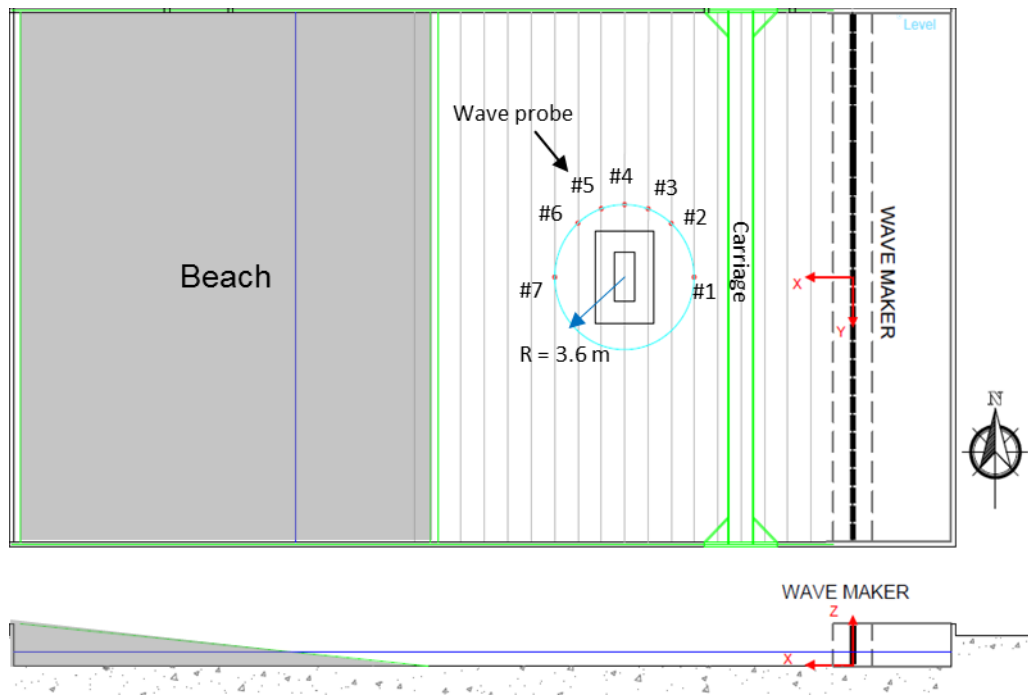


Figure 12. Layout of the installed device and probe in OSU wave basin

Table 10. OSU wave gauge calibration slope and position

Wave probe #	Slope	Slope unit	X-Position (m)	Y-Position (m)
1	0.231	m/V	9.477	0.003
2	0.228	m/V	10.704	2.687
3	0.227	m/V	11.909	3.427
4	0.346	m/V	13.141	3.624
5	0.228	m/V	14.351	3.414
6	0.239	m/V	15.574	2.697
7	0.230	m/V	16.779	-0.006

7 DATA PROCESSING AND ANALYSIS

7.1 DATA QUALITY ASSURANCE

Data collection started just before wave maker started and continued until wave generation stopped. This ensure that the data captures the initial conditions and ramp-up/down as well as the trigger signal to enable subsequent time synchronization.

Raw data from the wave gauges and from the sensors were collected by the same data acquisition system and stored in a .mat file for each test run. The data quality assurance was checked at three points: 1) visually in real-time during each test, 2) in-between test runs through the initial processing, and 3) data analysis after testing. Corrective action was taken if any issues in the data and device were observed.

7.2 DATA PROCESSING IN REAL-TIME

The data flow and processing steps are shown in Figure 13. The tests were performed using pre-written scripts that run on a Speedgoat system. These scripts load the data, perform initial processing, and create figures for review. Post-processing and analysis were completed using achieved data file after testing was complete.

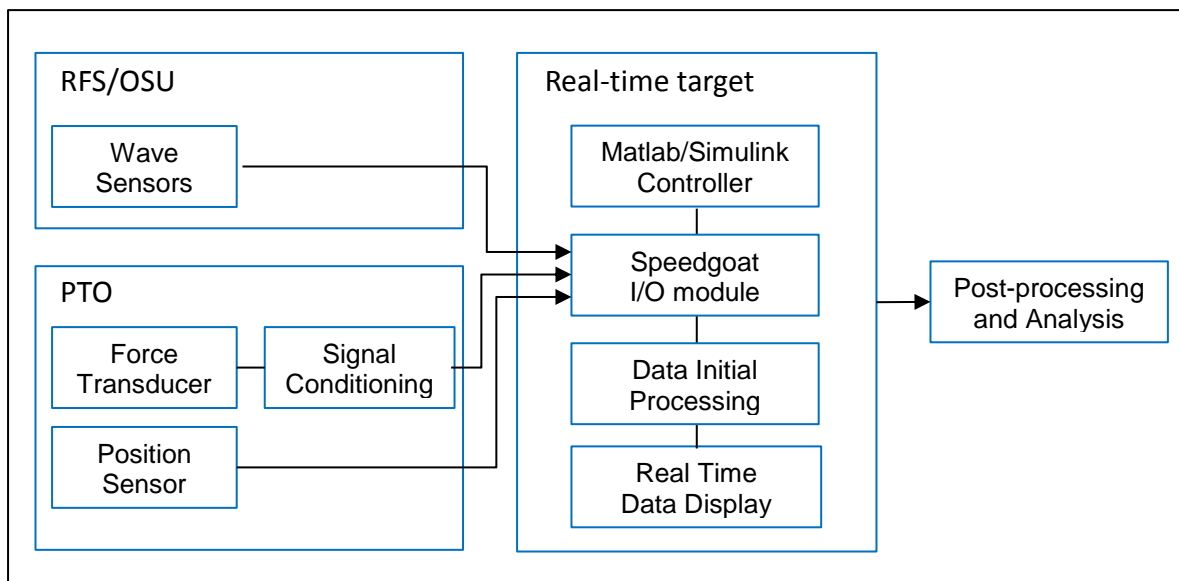


Figure 13. Data flow and processing steps.

For real-time data assessment and control prototyping, Speedgoat was used. Speedgoat is a real-time target machine that allowed us to execute Simulink models in real-time. Specifications of the Speedgoat system is included in [Appendix C](#). This Speedgoat system allows live parameter tuning, signal monitoring and execution control. Workflow of the Speedgoat system is illustrated in Figure 14. Wiring to sensors via I/O module of the Speedgoat is illustrated in [Appendix D](#).

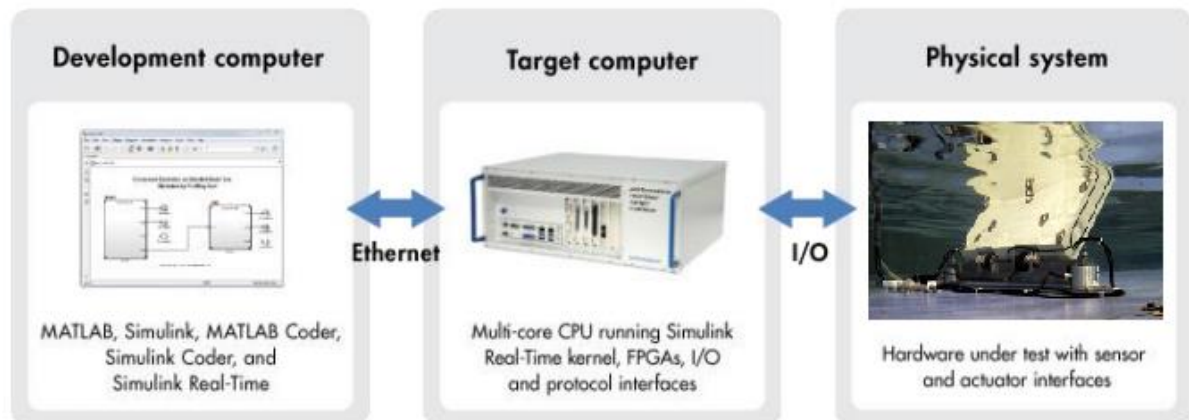


Figure 14. Workflow of Speedgoat.

A screen-shot of the front panel for real-time data processing and different control mode is provided in Figure 15. It should be noted that all input values from control panel should be full-scale values, and are then converted into model-scale values in Simulink. The parameters implemented on the front panel as follows:

Table 11. Parameters on control panel

Parameter	Description	Units
Control Modes	1: Linear damping, 2: Causal control, 3: Safe damping, 4: MPC	
Set loop gain	Loop gain for all control modes	
Damper	Used to set PTO damping value for linear damping (Test 5)	N/(m/s)
Safe damper	PTO damping value for safe operation	N/(m/s)

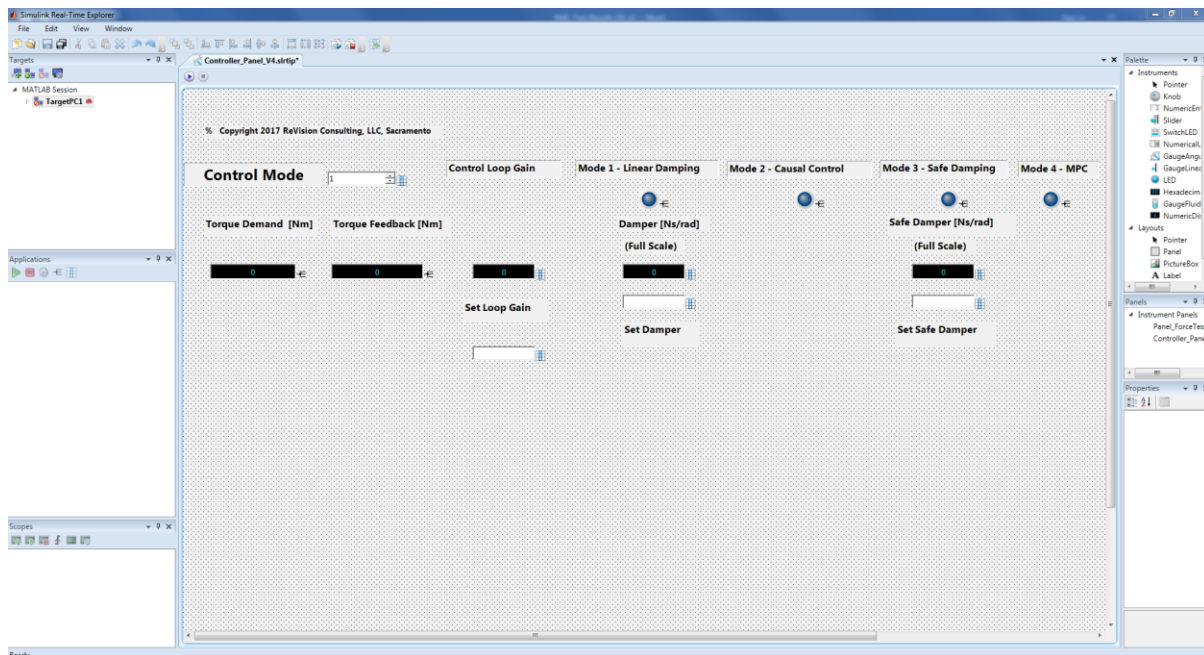


Figure 15. Front panel of real-time controller

7.3 CONTROL MODES

Three different control modes are considered in this work: Linear damping, Causal, and MPC. These control strategies are implemented on the real-time target machine, Speedgoat.

For linear damping control mode, the PTO is assumed to be linear damper system. This mode uses velocity feedback, and provide a force demand by multiplying linear damping value into the PTO. A damping value is constant and continuous value, which can be controlled on the front panel.

Causal control uses both position and velocity feedback signals, and provides a force demand signal into the PTO. Optimal tuning parameters needs to be set for different wave conditions.

MPC simply applies pre-determined PTO force-demand, which is optimized using an offline MPC optimization. For this purpose, wave information from wave gauge aligned with the device is needed in advance. In experiment, the optimized force time series is synchronized using the wave-maker trigger signal.

8 EXPERIMENTAL RESULTS AND VALIDATION

8.1 NOMENCLATURE

Table 12. Nomenclature of all variables and constant

	Symbol	Unit
Displaced mass	M	kg
Added mass	M_a	kg
Radiation damping	B	N/(m/s)
Viscous damping	B_{vis}	N/(m/s)
Total damping	$B_T=B+B_{vis}$	N/(m/s)
Hydrostatic stiffness	K_P	N/m
Damping ratio	ζ	-
Logarithmic decrement	δ	-
Damped natural period	T_d	sec
Damped natural frequency	ω_d	Rad/s
Natural frequency	ω_n	Rad/s
Wave number	k	m^{-1}
Water density	ρ	Kg/m^3
Drag coefficient	C_D	-
Water-plane area of the buoy	A	m^2
Wave amplitude	a	m
Group velocity	V_g	m/s
Wave-excitation force	F_{exc}	N

8.2 NUMERICAL RESULTS

The first step for determining hydrodynamic performance of the device is to obtain the hydrodynamic coefficients including; added mass M_a , radiation damping B , and wave-excitation force F_{exc} . The numerical hydrodynamic coefficients for given geometrical properties of the buoy in full scale were computed by WAMIT, which is plotted in Figure 16.

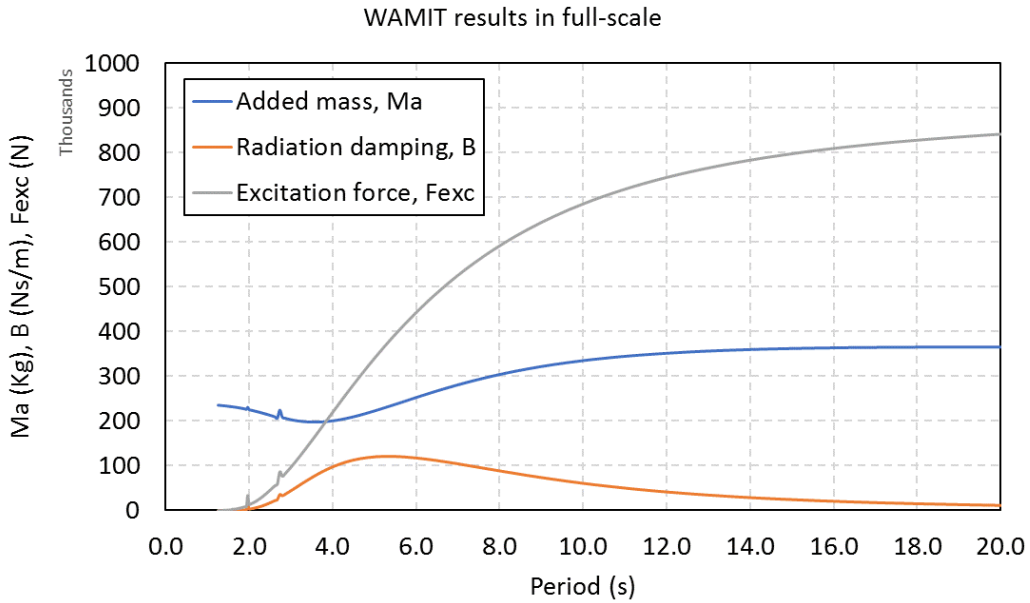


Figure 16. Hydrodynamic coefficients in model-scale from full-scale WAMIT analysis.

8.3 FREE-DECAY TEST

The oscillation of the buoy gradually decreases to its steady-state position after releasing from a certain initial displacement, which shows a typical underdamped mechanical system. The decaying period reveals the natural resonance frequency of the device using the logarithmic decrement method.

The damped mechanical system typically has the following form:

$$M\ddot{x} + B\dot{x} + K_p x = 0 \Rightarrow \ddot{x} + 2\zeta\omega_n\dot{x} + \omega_n^2 x = 0$$

where M , B and K_p are mass, damping and spring coefficient, respectively. Also, ζ and ω_n are the damping ratio and the natural frequency:

$$\zeta = \left(\frac{B}{M}\right)\left(\frac{1}{2\omega_n}\right)$$

$$\omega_n = \sqrt{\frac{K_p}{M}} = \frac{\omega_d}{\sqrt{1-\zeta^2}} = \frac{2\pi}{T_d\sqrt{1-\zeta^2}}$$

where ω_d represents the damped natural frequency.

In addition, the logarithmic decrement δ is obtained from the successive peaks and related to the damping ratio:

$$\delta = \ln\left(\frac{y_n}{y_{n+1}}\right) = \zeta\omega_n T_d = \zeta\omega_n \frac{2\pi}{\omega_d} = \frac{2\pi\zeta}{(1-\zeta^2)}, \text{ or } \zeta = \frac{\delta}{\sqrt{4\pi^2 + \delta^2}}$$

Thus, the natural frequency is obtained from the oscillation data of the device over time as shown in Figure 17. With the use of the added mass coefficients from WAMIT, the spring stiffness and damping value considering a linear-viscous damping term in real fluid were deduced:

$$\omega_n = \sqrt{K_p / (M + M_a)} \Rightarrow K_p = \omega_n^2 (M + M_a)$$

$$B_T = B + B_{vis} = 2\zeta\omega_n (M + M_a)$$

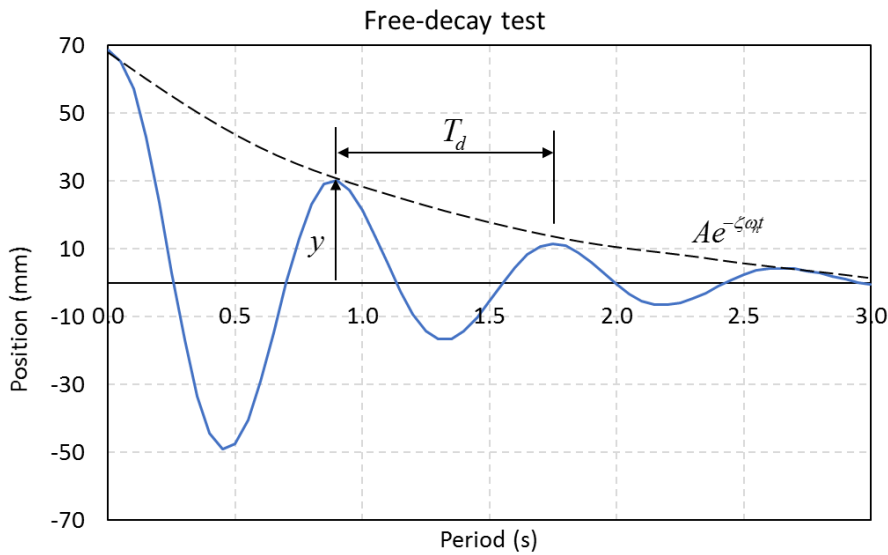


Figure 17. Time history of the buoy position after initial position

A summary of the free-decay test results is listed in Table 13. Initially, a linear drag or viscous damping value was assumed as follows:

$$B_{vis} = 0.5 \times C_D \times \rho \times A$$

where $C_D = 0.5$, $\rho = 1025 \text{ kg/m}^3$, and A is the water-plane area.

It turns out that the measured resonance frequency matches well with prediction, and measured linear viscous damping value is close to the prediction.

Table 13. Summary of free-decay test results

	Full-scale (WAMIT)	Model-scale (WAMIT)	Model-scale (Experiment)
Natural resonance period (s)	4.5	0.9	0.88
Natural resonance frequency (rad/s)	1.40	7.0	7.17
Displaced mass, M (kg)	233781.62	14.96	14.96
Added mass at resonance freq., M_a (kg)	210100	13.45	
Hydrostatic restoring stiffness, K_p (N/m)	899275.7	1438.8	1460.1
Radiation damping at resonance freq., B (N/(m/s))	111801.5	35.78	
Total damping including viscous effects, $B_T=B+B_{vis}$	-	-	47.97
Linear-viscous damping, B_{vis}	24352.25	7.79	12.19

8.4 WAVE-EXCITATION FORCE

With a fixed position of the buoy, measured wave-excitation force was measured and compared to the WAMIT results as a function of incident-wave period in full scale, which is shown in Figure 18. Measurements match well with predictions.

The Haskind's relation represents reciprocity relation between wave-excitation force and damping:

$$F_{exc} = a \left[\frac{4\rho g V_g}{k} B \right]^{1/2}$$

where a is the incident-wave amplitude, V_g is the group velocity, k is the wave number, and B is the radiation damping.

The computed wave-excitation force from the Haskind's relation has the same results with numerical results. Thus, it proves that the radiation damping between the prediction and the experiment agrees well.

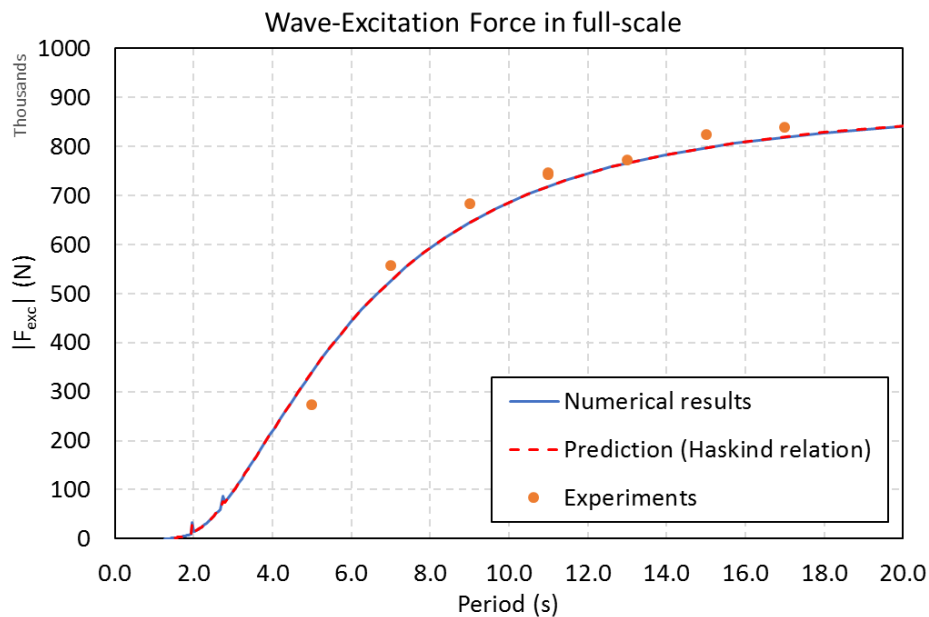


Figure 18. Wave-excitation force comparison

8.5 POWER PERFORMANCE IN REGULAR WAVES

8.5.1 PTO force control

Reaction force of the PTO affects the motion response of the buoy to incident waves as well as power extraction. Thus, the PTO force was controlled during the test to investigate the motion response and power extraction performance. With use of the permanent magnet linear motor as the PTO, internal PI algorithm of LinMot drive was used for the force control loop. The purpose of the force control loop is to match actual force to desired force demand. PI gains are adjustable on the motor drive, and set to $P=0.1$ and $I=2$ for experiments. A schematic of the PTO force control loop is illustrated in Figure 19.

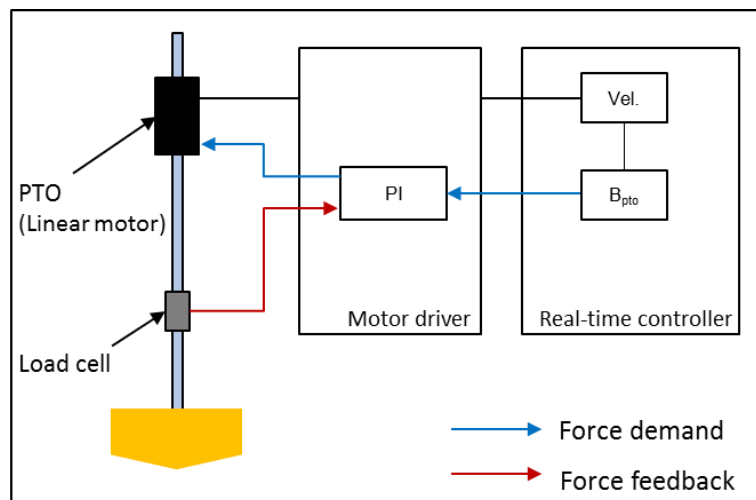


Figure 19. Schematic of PTO control loop

8.5.2 Power extraction performance results

A) TEST CAMPAIGN I

During Test Campaign I, a few performance tests performed to verify operation of the device in different control modes. In testing with linear damping control mode, two things were observed: (1) increasing motion response with increasing PTO damping shown in Figure 20; (2) time delay in force feedback from force input shown in Figure 21.

It is expected that motion response decreases with increasing PTO damping because PTO force applies against motion velocity. It turns out that force input direction of the PTO was wrong during the testing, thus feeding power into waves not extracting power from waves. The time delay between force input to the PTO and feedback from load cell was also observed in MPC mode trials, which can be found in Figure 22, as an example of $T = 11$ sec (2.2 sec in model scale). In addition, measured motion response and absorbed power lag simulation results when compared in time domain as shown in Figure 23 to Figure 25. However, experimental results have a similar amplitude with simulation results, so measured time-averaged power extraction agrees with simulation as shown in Figure 26. The time delay issue on feedback signal was resolved by updating IO module driver of the Speedgoat after Test Campaign I was complete.

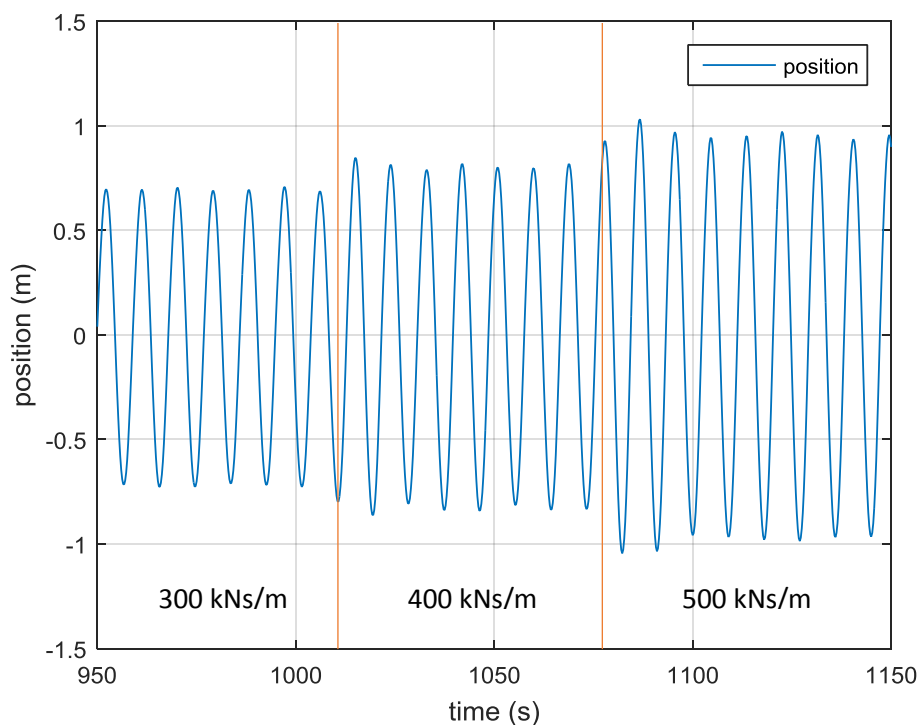


Figure 20. Time history of motion response with different linear damping values – Test Campaign I

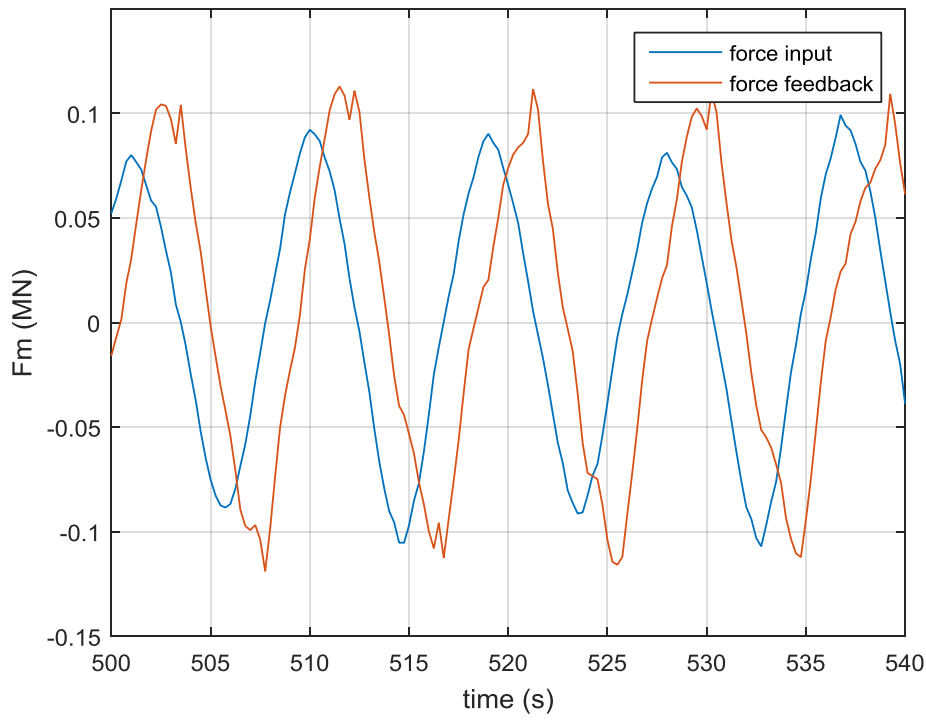


Figure 21. Time history of PTO force between input and feedback with linear damping – Test Campaign I

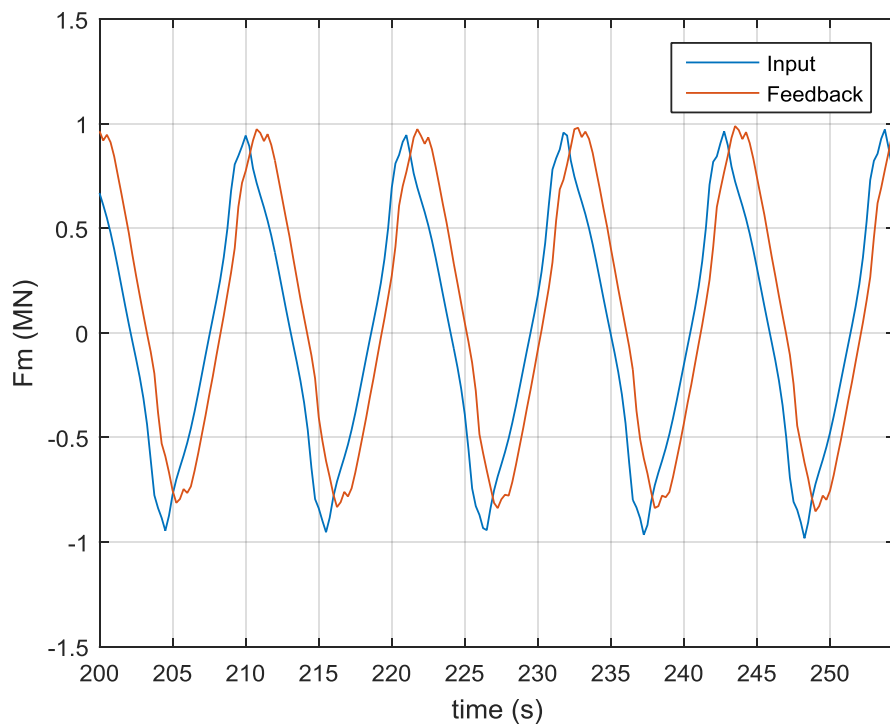


Figure 22. Time history of PTO force between input and feedback with MPC– Test Campaign I

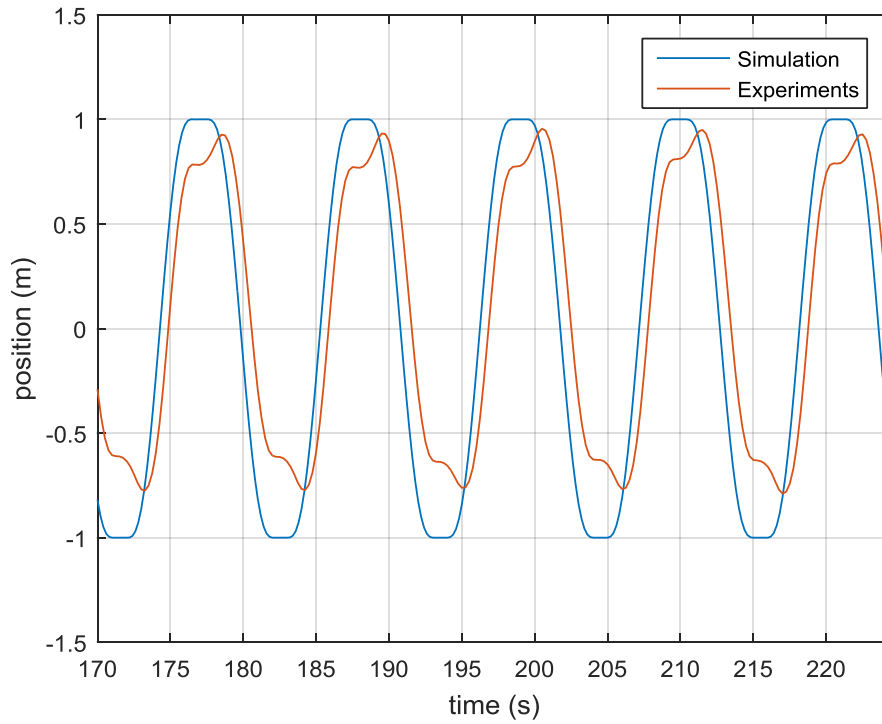


Figure 23. Time history of displacement between simulation and measurement with MPC- Test Campaign I

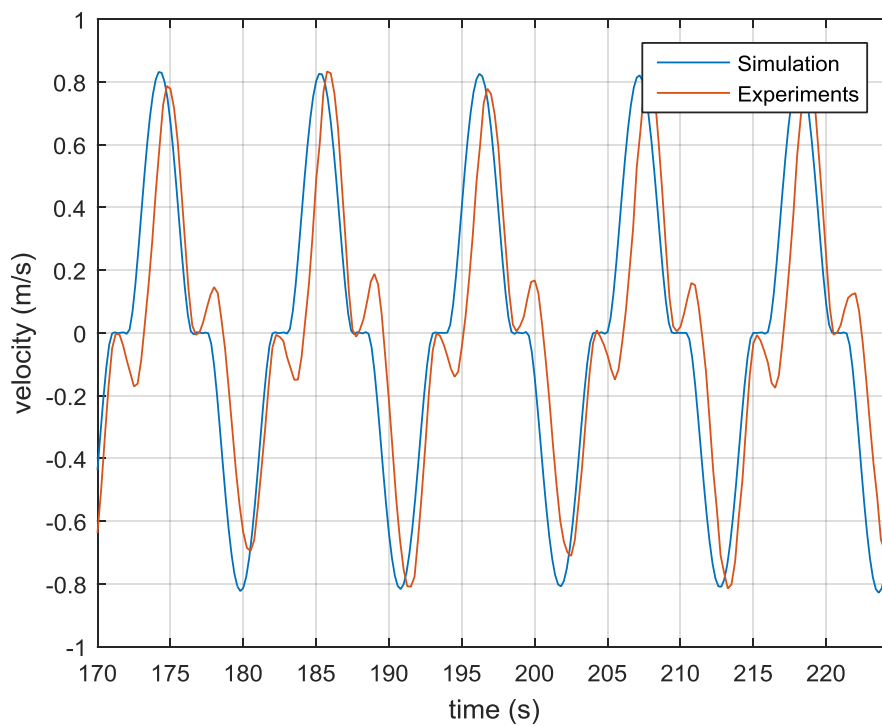


Figure 24. Time history of velocity between simulation and measurement with MPC – Test Campaign I

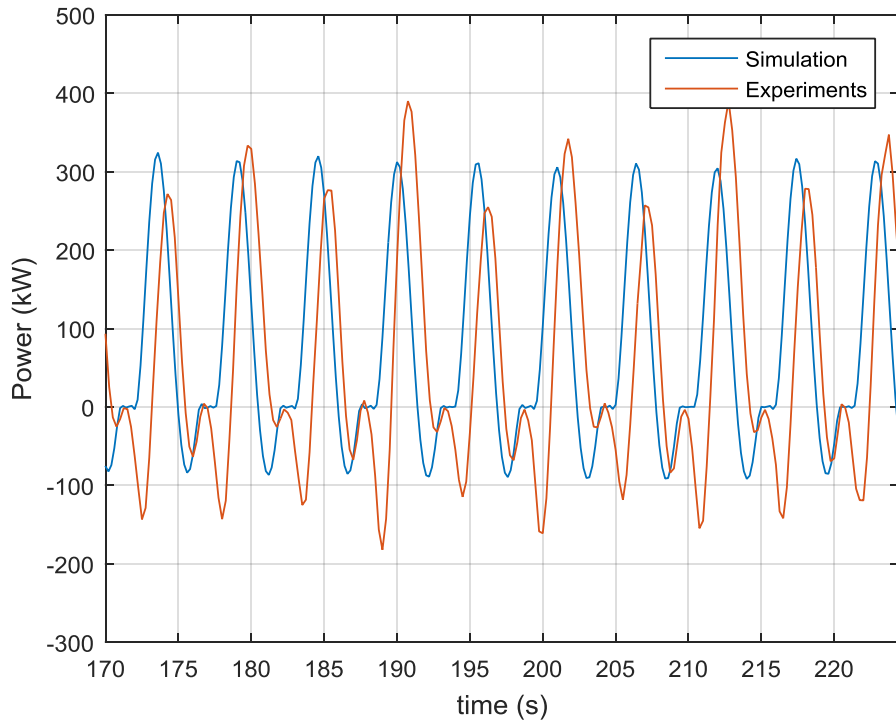


Figure 25. Time history of absorbed power between simulation and measurement with MPC – Test Campaign I

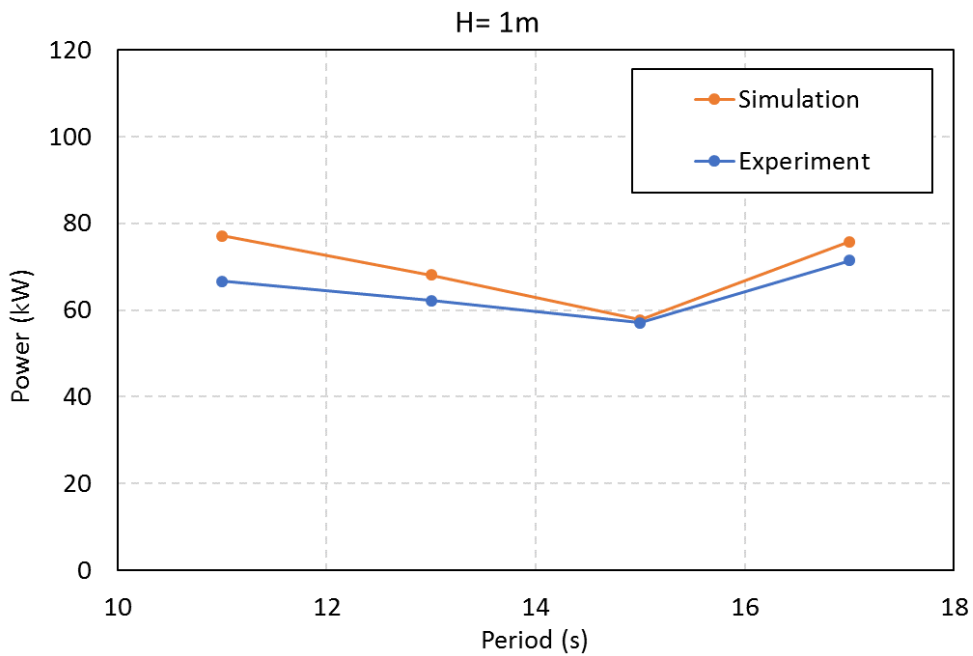


Figure 26. Time-averaged power performance with MPC – Test Campaign I

B) TEST CAMPAIGN II

By fixing the force input direction of the PTO and updating the hardware driver of the target machine, the issues observed in Test Campaign I disappeared. The heave response amplitude of operator (RAO), amplitude of motion response with respect to amplitude of incident wave, decreases with increasing PTO damping value, as shown in Figure 27. The phase shift between force input to PTO and feedback from load cell is significantly reduced and is negligible, which is shown in Figure 28.

Each frequency has a different optimal PTO damping at which maximum power is captured. By sweeping different PTO damping values for given frequencies, an optimal linear damping was found as shown in Figure 29. As an example of $T = 9$ sec, Figure 30 shows instantaneous power, applied PTO force, and motion responses with the optimal damping value of 1200 kN/(m/s) in time domain. In addition, time histories of performance for causal control and MPC are plotted in Figure 31 and Figure 32.

As a summary of this Test Campaign II, time-averaged power absorption for 1m incident-wave height as a function of frequency with different control methods is plotted in Figure 33. Obviously, the causal control and MPC improve performance of the power capture when compared to the constant linear damping control. For the simulation results, an actual wave data measured from wave gauge was used not to overestimate performance with ideal sinusoidal waves. Overall trends between experiment and simulation agree for all control modes, but fine tuning of developed numerical model is needed for better matching with experimental results.

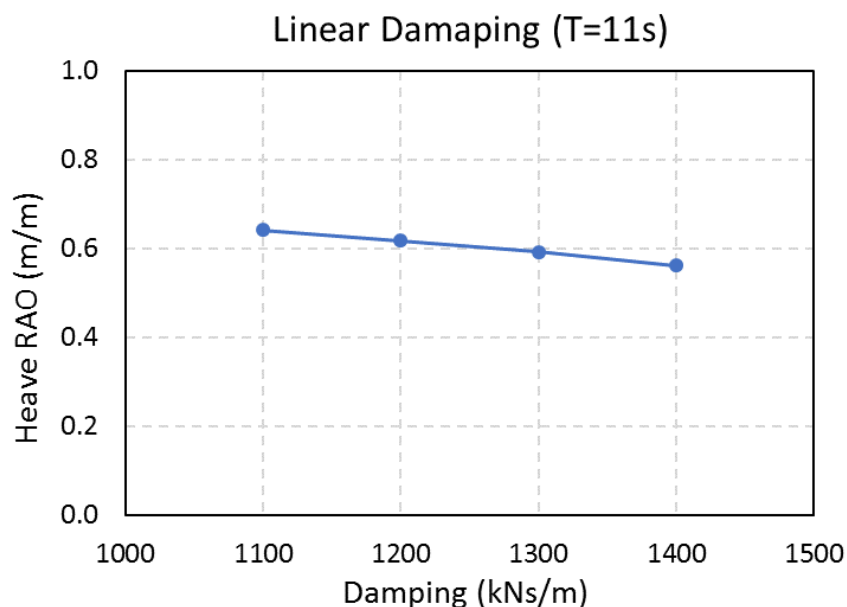


Figure 27. Heave response amplitude of operator for different linear damping - Test Campaign II

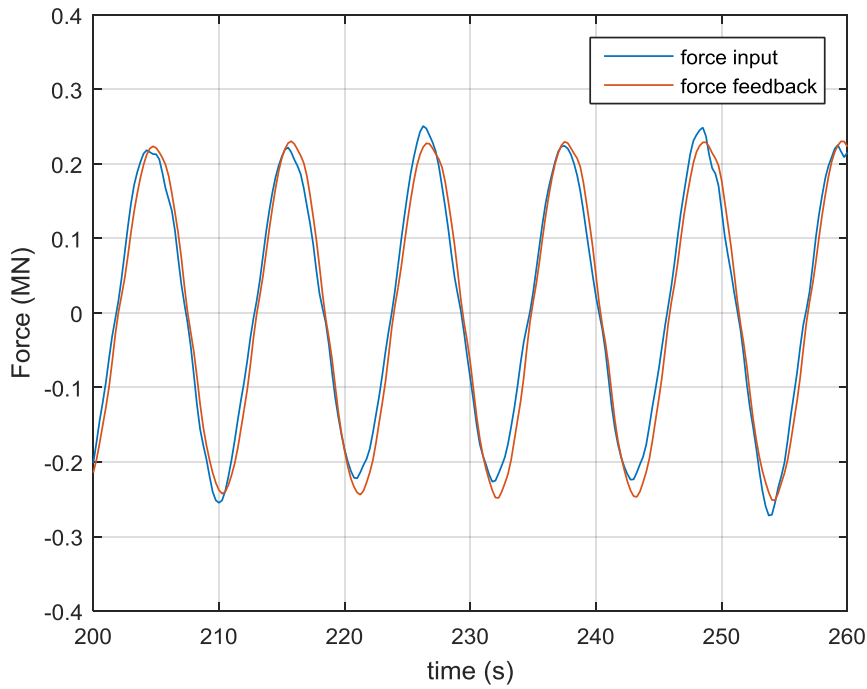


Figure 28. Time history of PTO force between input and feedback with linear damping - Test Campaign II

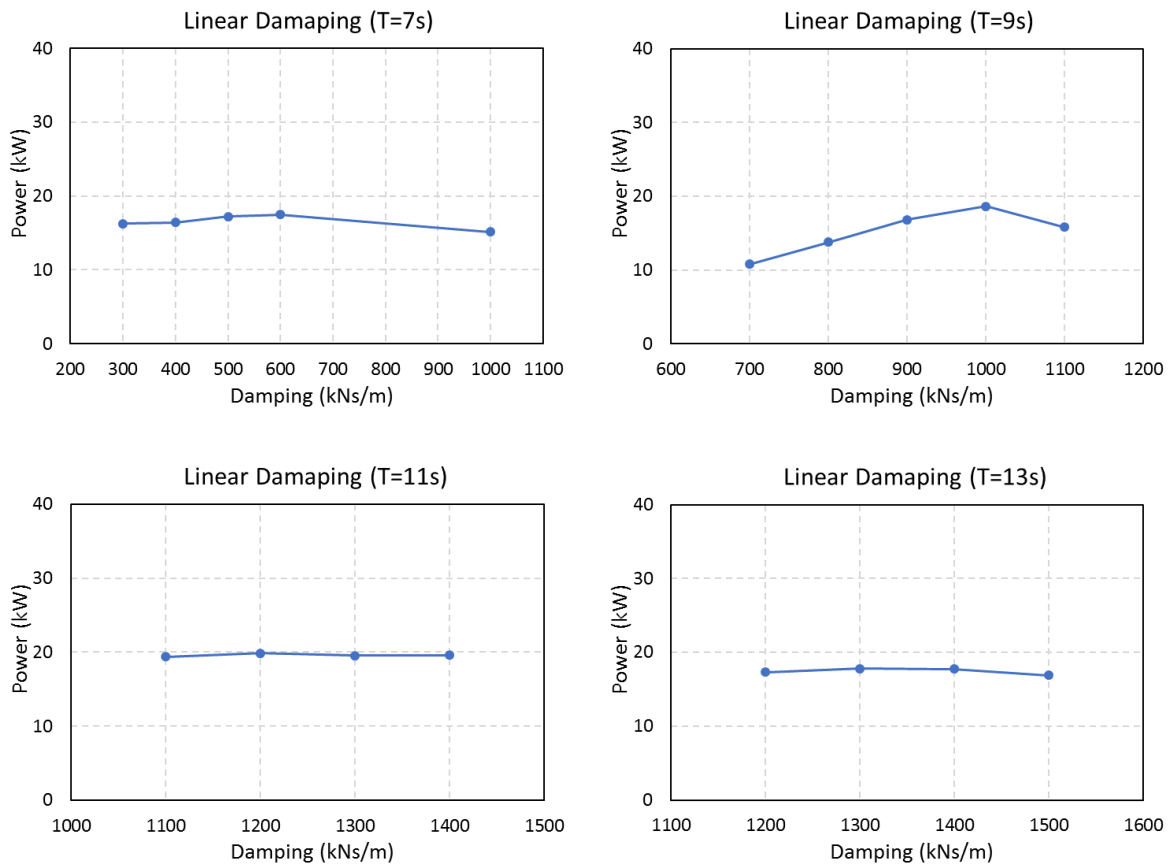


Figure 29. Linear damping optimization - Test Campaign II

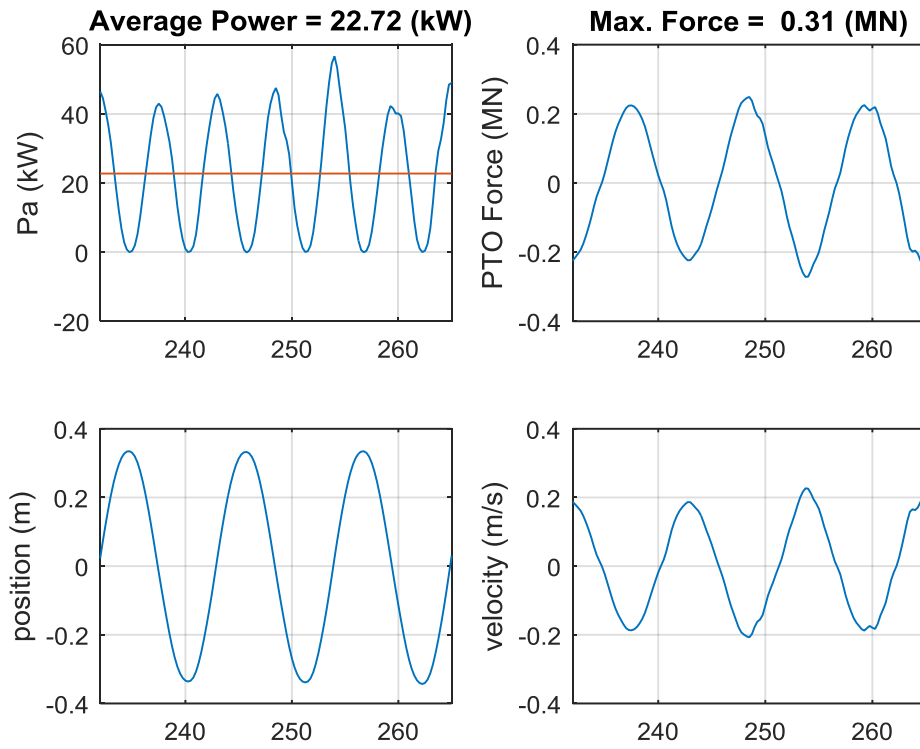


Figure 30. Performance with linear damping in time series - Test Campaign II

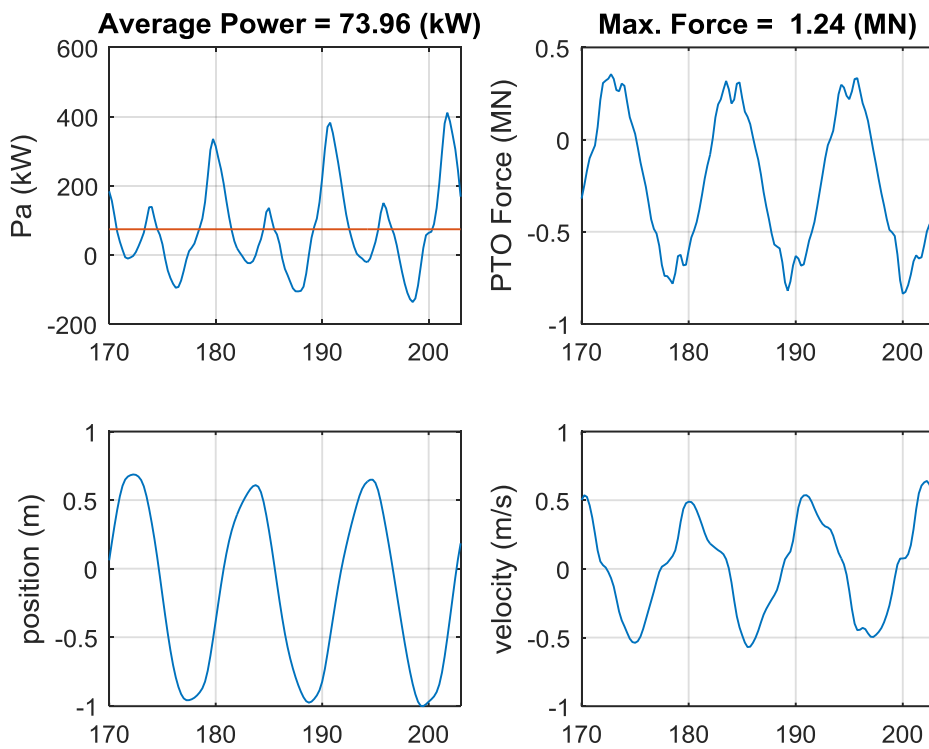


Figure 31. Performance with causal control in time series - Test Campaign II

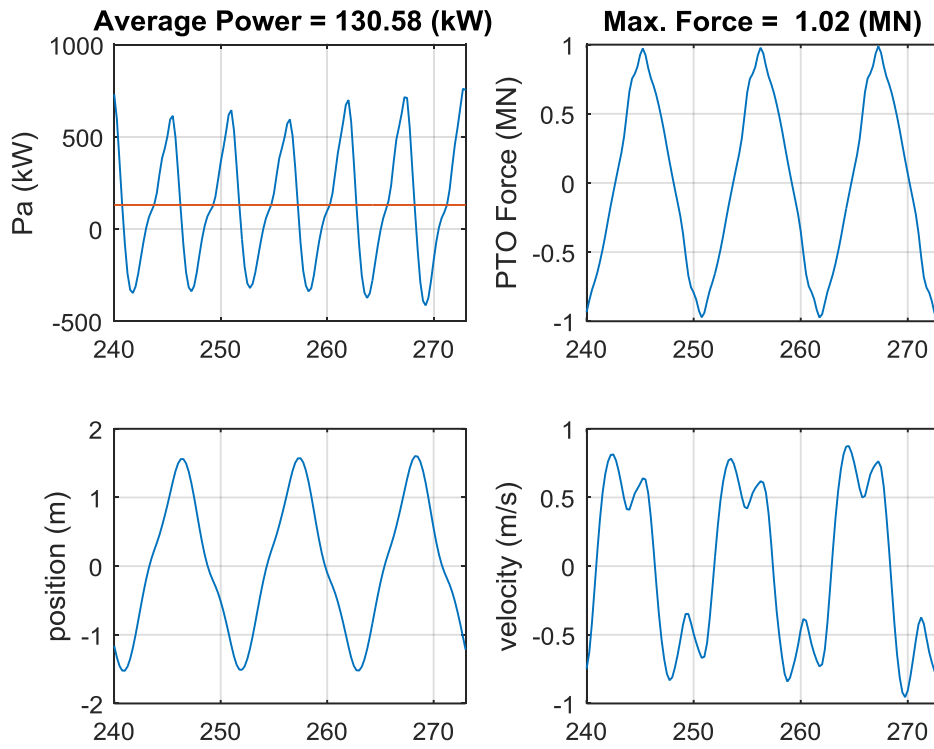


Figure 32. Performance with MPC in time series - Test Campaign II

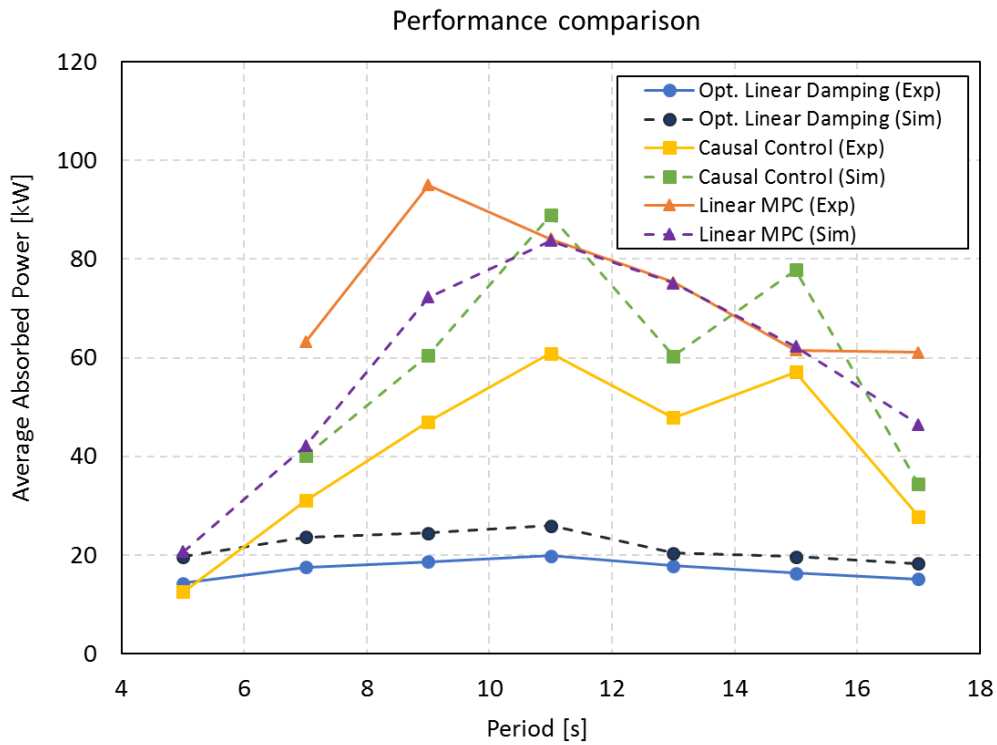


Figure 33. Time-averaged power performance - Test Campaign II

C) TEST CAMPAIGN III

The Test Campaign III repeated previous test matrix, but with tuned numerical model parameters, to verify the performance improvement by causal control and MPC than that of linear damping control. Figure 34 shows searching of the optimal damping at each frequency, and compares with predicted power computed by simulation. A found optimal linear damping from experimental results has the same with one from simulation results as well as time-averaged power value. Absorbed power, PTO force, and motion responses in time domain for three different control methods are plotted in Figure 36 to Figure 38, which is at 11 sec wave periods. For the MPC, measurements and simulation results for selected periods are compared through Figure 39 to Figure 42. It shows good agreement between them, even in latching-like velocity behavior.

Figure 43 presents time-averaged power as a function of frequency. At a glance, causal control and MPC improve performance in power extraction, especially 9 sec wave periods onward. The causal control and MPC lead to maximum 3-fold and 5-fold power performance respectively when compared to the optimal linear damping control. Figure 44 is the heave response amplitude of operator (RAO) in the same way with power comparison. It is consistent with power performance results, and can explain power improvement by the causal control and MPC.

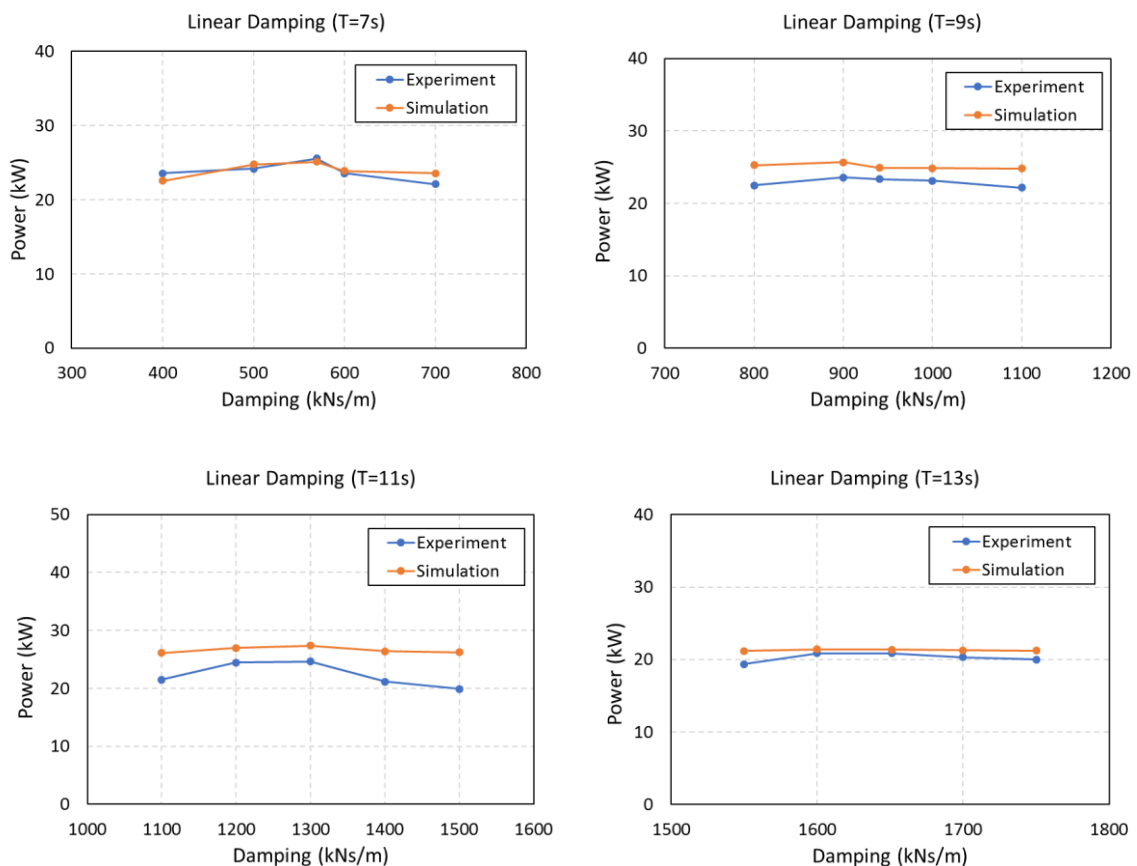


Figure 34. Linear damping optimization - Test Campaign III

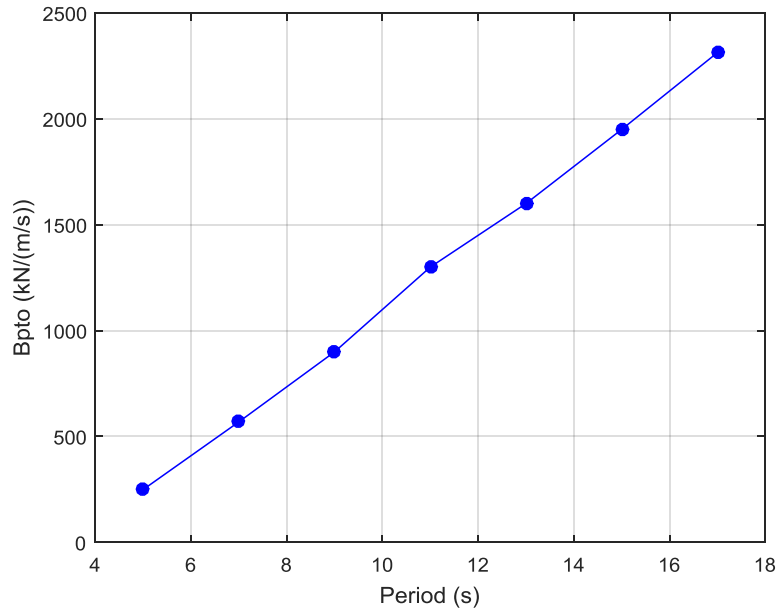


Figure 35. Optimal linear damping for each wave period

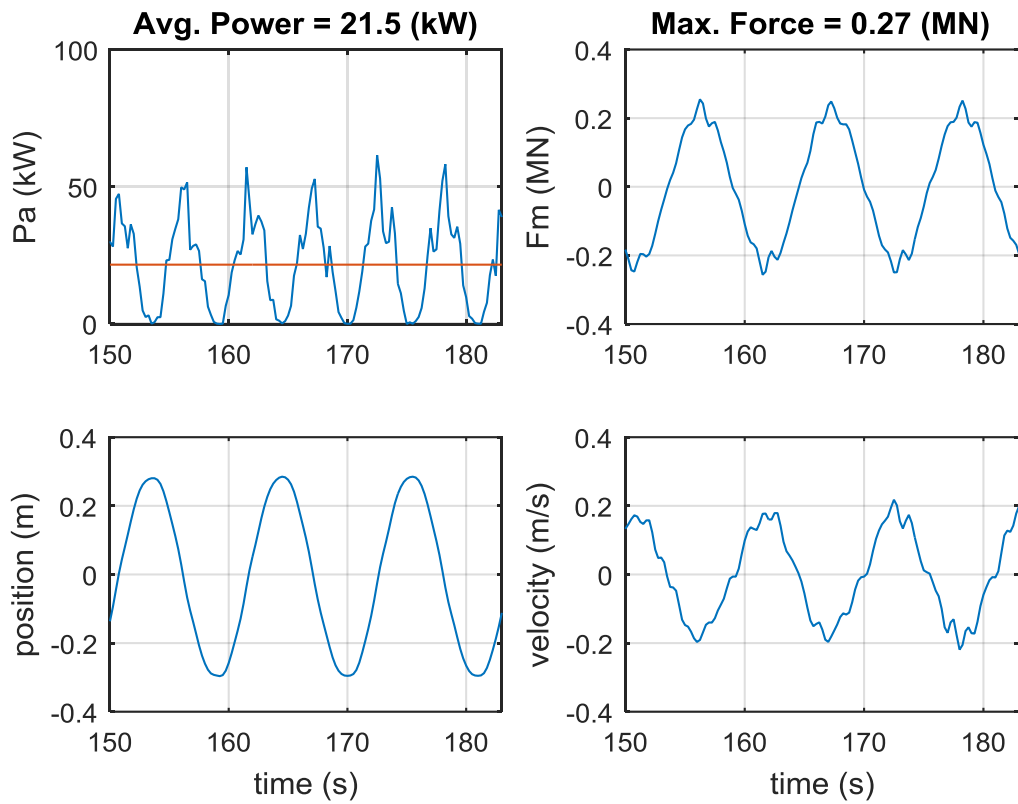


Figure 36. Performance for linear damping in time series - Test Campaign III

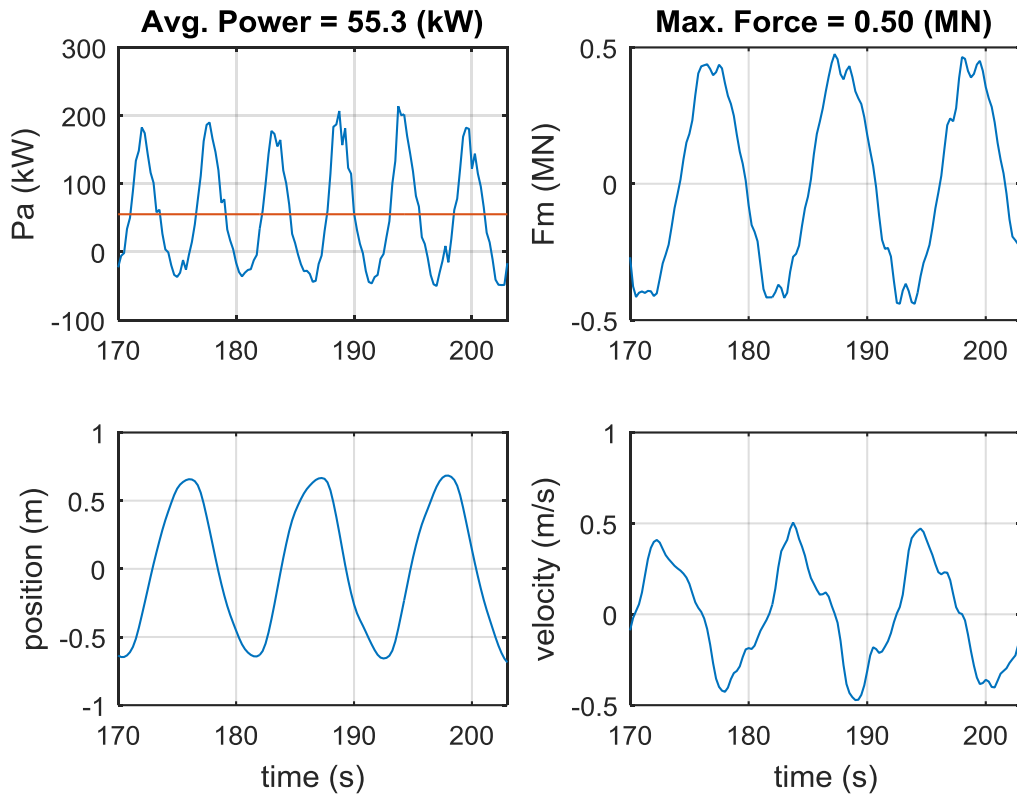


Figure 37. Performance for causal control in time series - Test Campaign III

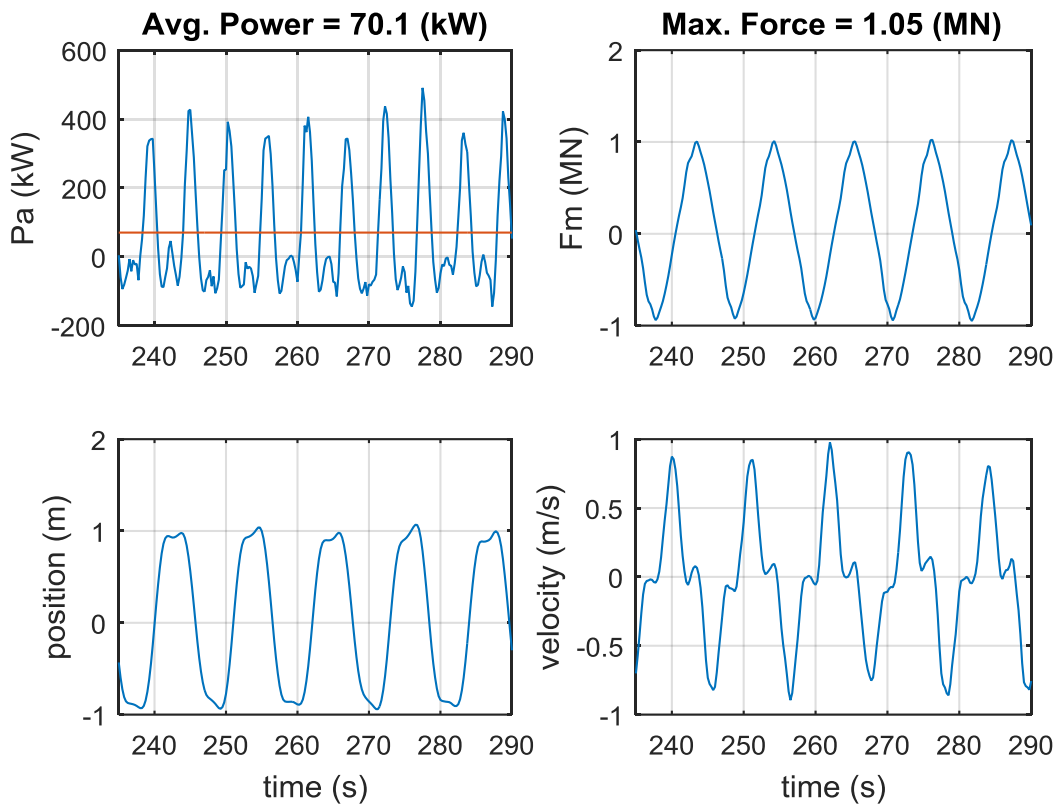


Figure 38. Performance for linear MPC in time series - Test Campaign III

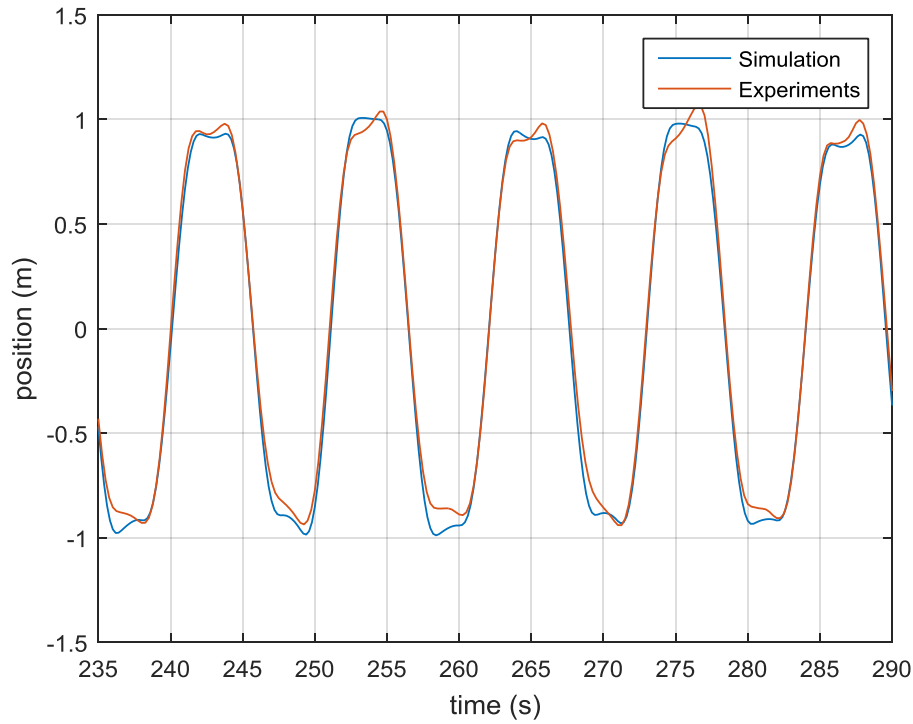


Figure 39. Position comparison between simulation and experiment with MPC – Test Campaign III

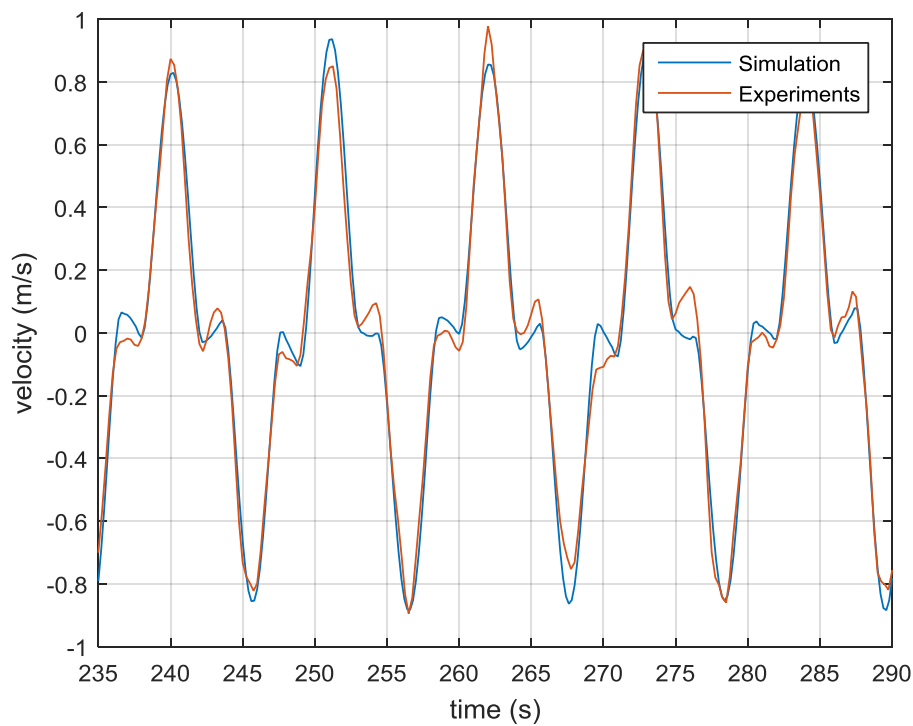


Figure 40. Velocity comparison between simulation and experiment with MPC - Test Campaign III

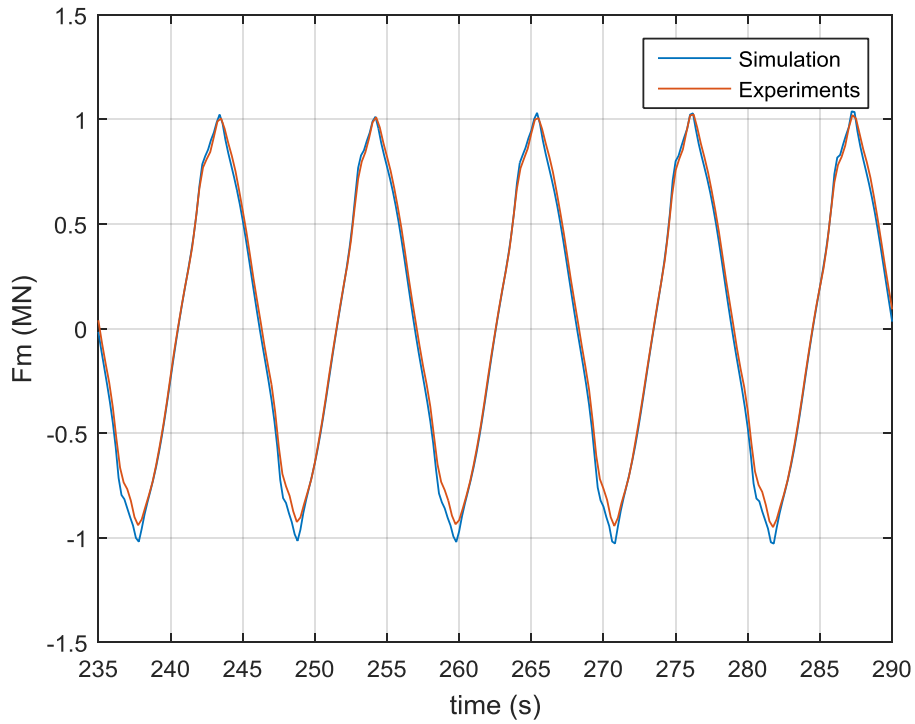


Figure 41. PTO force comparison between simulation and experiment with MPC - Test Campaign III

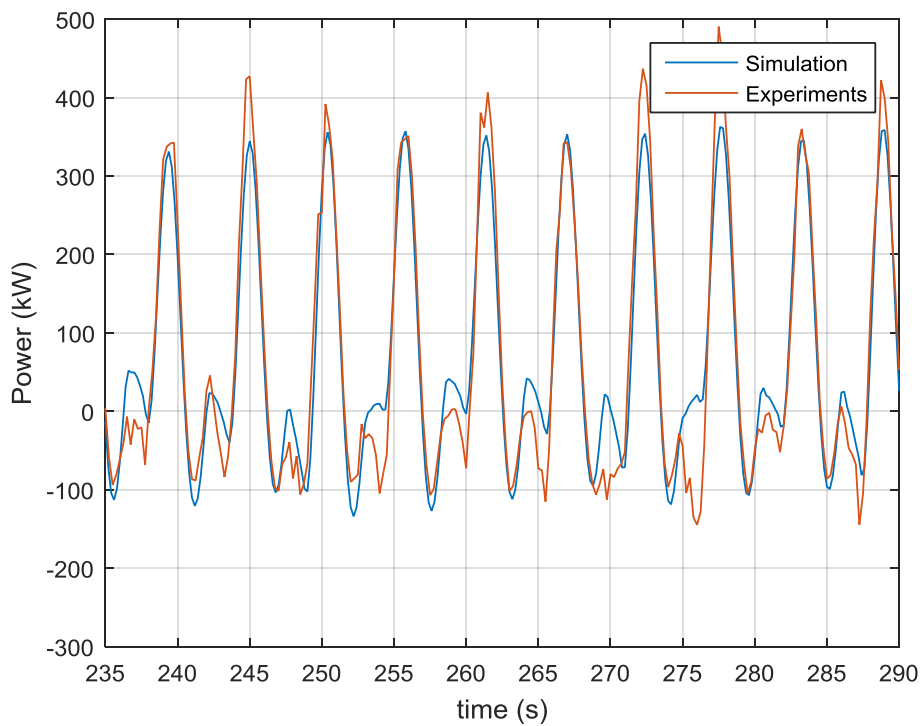


Figure 42. Power comparison between simulation and experiment with MPC - Test Campaign III

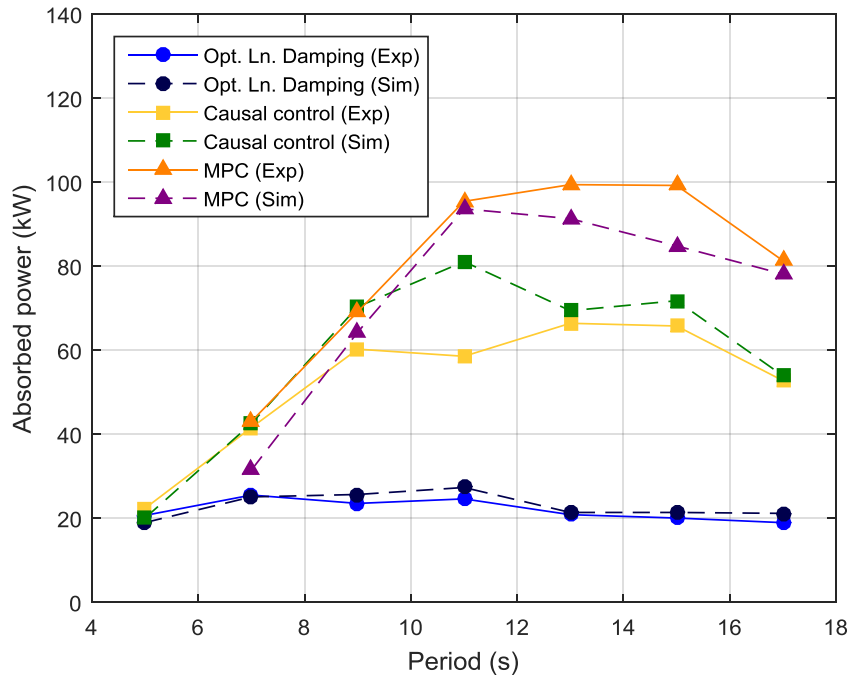


Figure 43. Time-averaged power performance - Test Campaign III

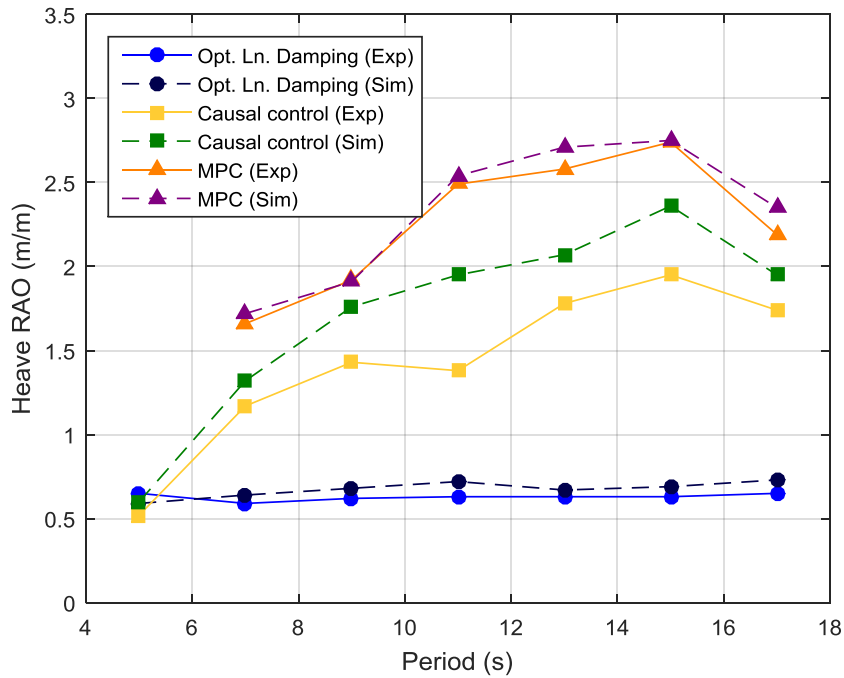


Figure 44. Heave response amplitude of operator - Test Campaign III

In order to confirm the power performance improvement brought by the MPC, tests were also performed in irregular waves. For this purpose, a JONSWAP spectrum with significant wave height of 1m and peak period of 11s in full scale was used. An optimal damping of 1013600 Ns/m was found from simulation study for linear damping control, and performance for certain time window is plotted in Figure 45. In the same way, performance controlled by MPC can be found in Figure 46. Those results indicate the MPC significantly improves absorbed power by factor of about 4; measured mean power absorption for [100s, 2500s] is about 10kW by linear damping control and 38kW by MPC.

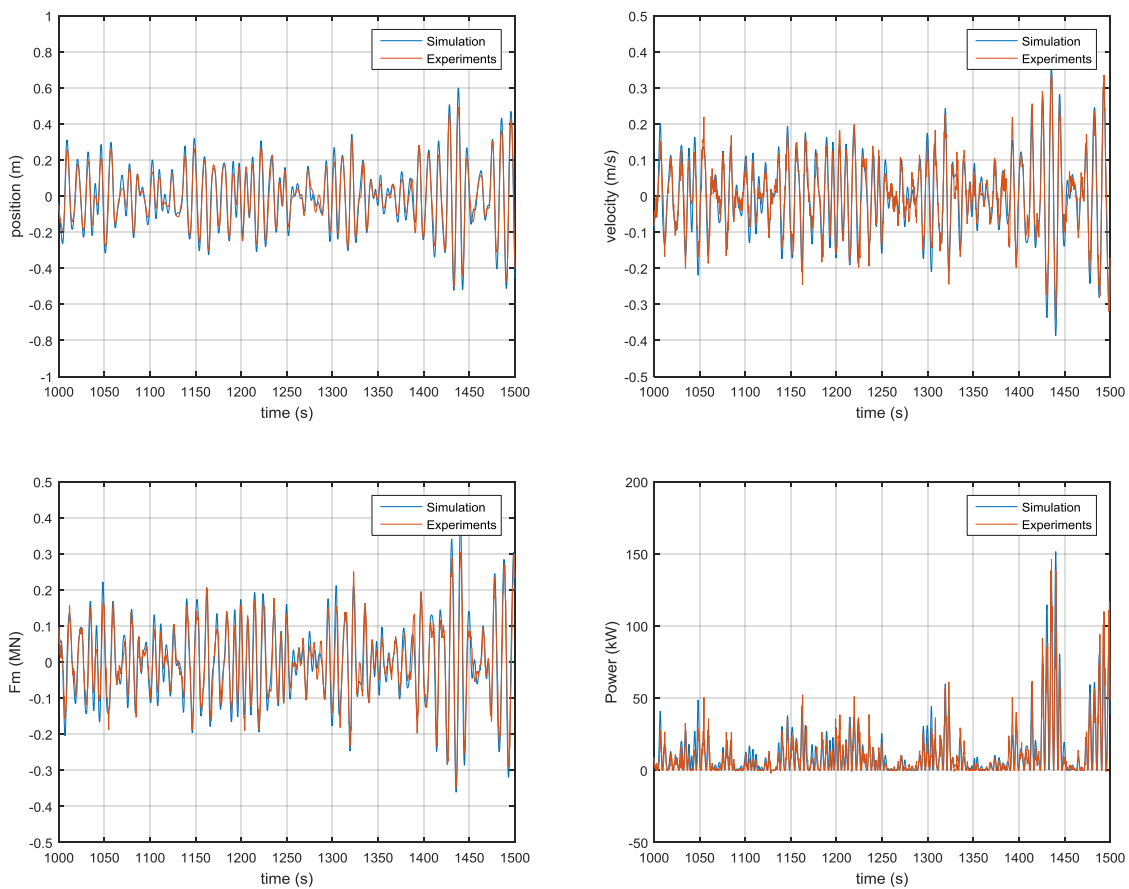


Figure 45. Performance with optimal linear damping in irregular waves

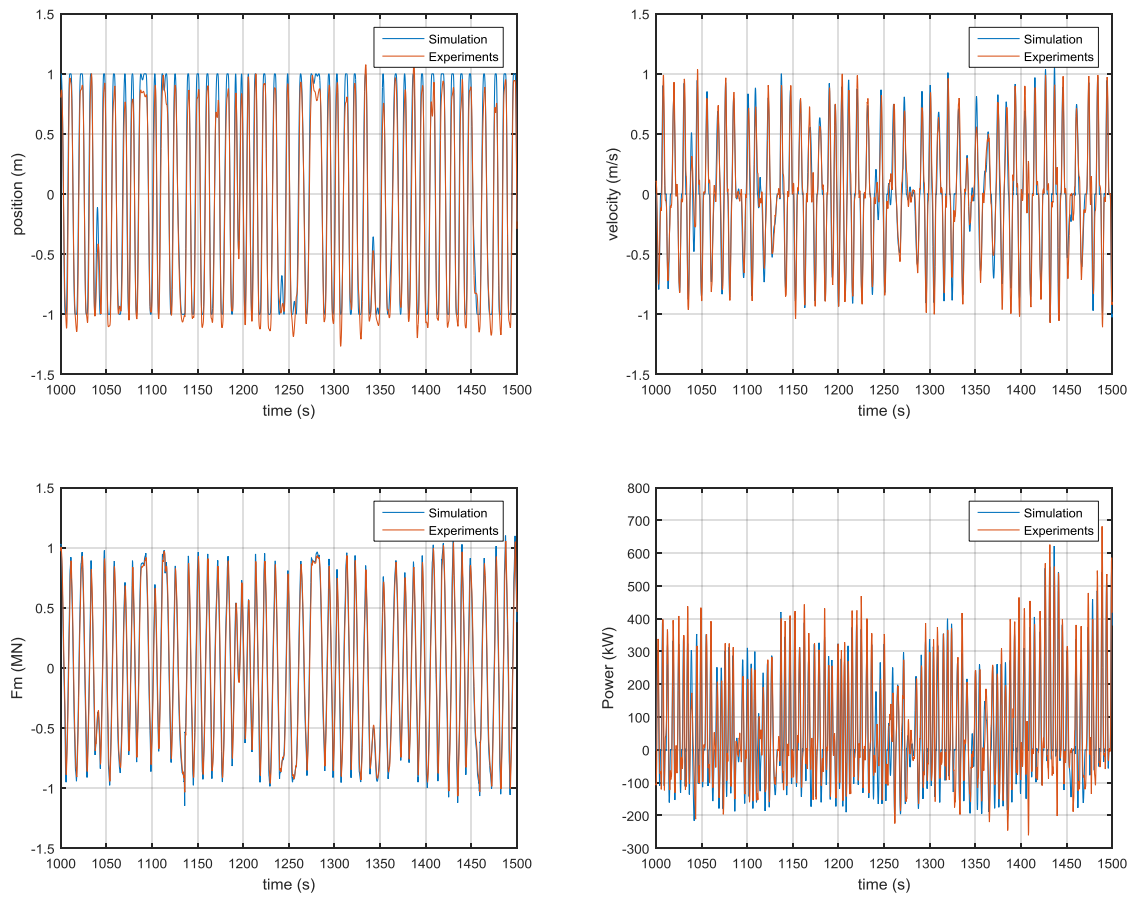


Figure 46. Performance with MPC in irregular waves

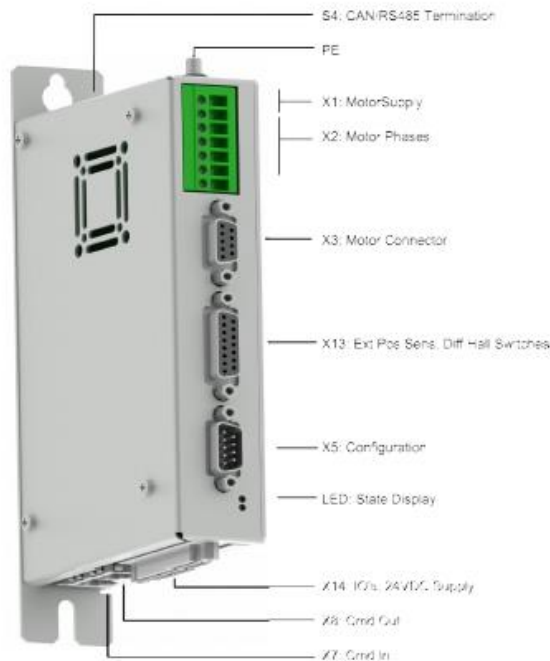
APPENDIX A: SPECIFICATIONS – MOTOR

1. PS01-37x120C

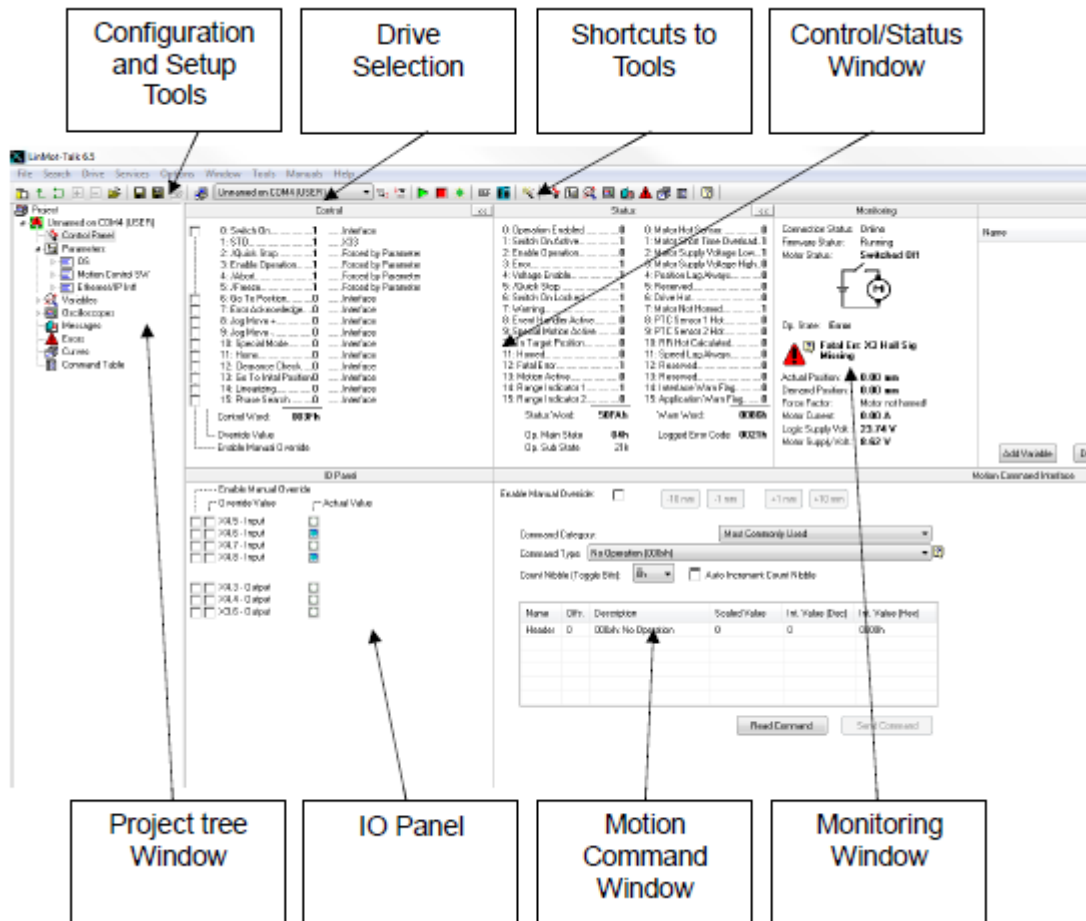
Motor Specification

	P01-	Connector Type	Cable Type
		37x120/1380x1460-C	37x120/1380x1460-P150 37x120/1380x1460-C20
Extended Stroke ES	mm (in)	1460 (57.48)	1460 (57.48)
Standard Stroke SS	mm (in)	1380 (54.33)	1380 (54.33)
Peak Force E1100-HC	N (lbf)	163 (36.7)	163 (36.7)
Peak Force E1100 / E1001	N (lbf)	163 (36.7)	163 (36.7)
Cont. Force	N (lbf)	29 (6.5)	29 (6.5)
Cont. Force Fan cooling	N (lbf)	54 (12.2)	54 (12.2)
Border Force	%	67	67
Force Constant	N/A (lbf/A)	20.4 (4.59)	20.4 (4.59)
Max. Current @ 72VDC	A	8.0	8.0
Max. Current @ 48VDC	A	6.3	6.3
Max. Velocity @ 72VDC	m/s (in/s)	3.2 (128)	3.2 (128)
Max. Velocity @ 48VDC	m/s (in/s)	2.2 (85)	2.2 (85)
Phase Resist. 25/80 °C	Ohm	6.2/7.5	6.2/7.5
Phase Inductance	mH	3.1	3.1
Thermal Resistance	°K/W	3.6	3.6
Thermal Time Const.	sec	2900	2900
Stator Diameter	mm (in)	37 (1.46)	37 (1.46)
Stator Length	mm (in)	216 (8.50)	227 (8.94)
Stator Mass	g (lb)	740 (1.63)	740 (1.63)
Slider Diameter	mm (in)	20 (0.79)	20 (0.79)
Slider Length	mm (in)	1600 (62.99)	1600 (62.99)
Slider Mass	g (lb)	3622 (7.99)	3622 (7.99)
Position Repeatability	mm (in)	±0.05 (±0.0020)	±0.05 (±0.0020)
Linearity	%	±0.10	±0.10
Repeatability with EPS	mm (in)	±0.01 (±0.0004)	±0.01 (±0.0004)
Linearity with EPS	mm (in)	±0.01 (±0.0004)	±0.01 (±0.0004)

2. B1100-GP drive



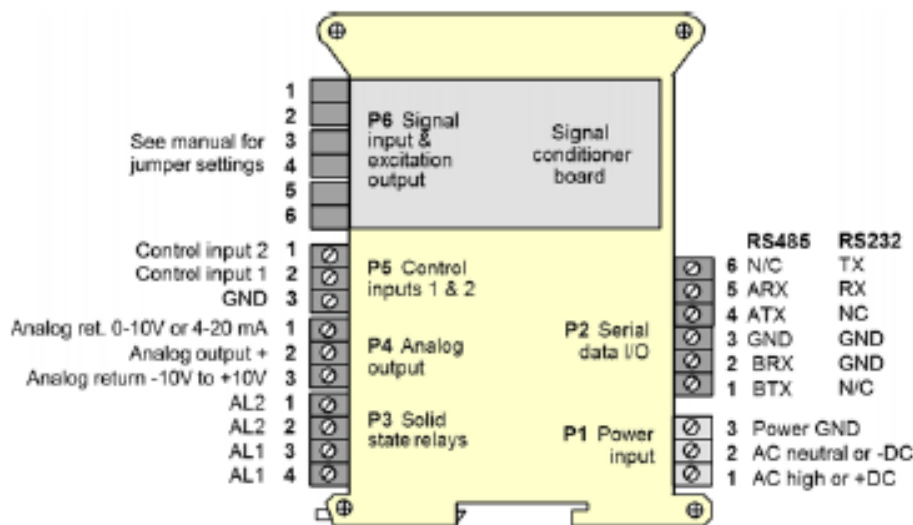
3. LinMot-Talk



The screenshot shows the LinMot-Talk 6.5 software interface. It features a menu bar at the top, a toolbar, and several main panels. Callouts point to various components:

- Configuration and Setup Tools:** Points to the 'Control' panel on the left, which lists various control actions like 'Switch On', 'Stop', 'Go To Position', etc.
- Drive Selection:** Points to the 'IO Panel' in the center, which shows digital and analog input/output status.
- Shortcuts to Tools:** Points to the 'Motion Command Window' at the bottom center, which includes a dropdown for 'Command Category' and a table for command parameters.
- Control/Status Window:** Points to the 'Status' panel on the right, which displays real-time motor data and a 'Fatal Error' warning.
- Project tree Window:** Points to the 'Project' tree on the far left.
- Monitoring Window:** Points to the 'Monitoring' panel on the far right, which shows connection status and motor status.

4. Pinout for position measurement – LT61QD



APPENDIX B: SPECIFICATIONS – SENSOR

1. LSB200 load cell (S/N 660406)

SPECIFICATIONS	
PERFORMANCE	
Nonlinearity	±0.1% of RO
Hysteresis	±0.1% of RO
Nonrepeatability	±0.05% of RO
ELECTRICAL	
Rated Output (RO)	See chart on third page
Excitation (VDC or VAC)	10 max
Bridge Resistance	See chart on third page
Insulation Resistance	≥500 MOhm @ 50 VDC
Connection	#29 AWG, 4 conductor, spiral shielded silicone cable, 5 ft [1.5 m] long
Wiring/Connector Code	WC1
MECHANICAL	
Weight (approximate)	0.3 oz [9 g]
Safe Overload	1000% of RO 200% tension only (50–100 lb)
Material	Aluminum (10 g–10 lb), stainless-steel (25–100 lb)
IP Rating	IP40
TEMPERATURE	
Operating Temperature	-60 to 200°F [-50 to 93°C]
Compensated Temperature	60 to 160°F [15 to 72°C]
Temperature Shift Zero	±0.01% of RO/°F [0.018% of RO/°C]
Temperature Shift Span	±0.02% of Load/°F [0.036% of Load/°C]
CALIBRATION	
Calibration Test Excitation	5 VDC
Calibration (standard)	5-pt Tension
Calibration (available)	Compression

2. Wiring color code

WIRING CODE (WC1)	
RED	+ EXCITATION
BLACK	- EXCITATION
GREEN	+ SIGNAL
WHITE	- SIGNAL
SHIELD	FLOATING

APPENDIX C: SPECIFICATIONS —SPEEDGOAT

1. Real-time target machine

Housing	
Enclosure	4U 19"-compatible aluminium chassis / I/O front-accessible (standard) I/O front or rear accessible (deep option)
Color	Silver powder-coated, natural aluminium
External dimensions	Height: 177.8mm (4U) Width: 440mm, 480mm (including rack mounts) Depth (standard): 360mm (400mm including handles) Depth (deep option): 440mm (480mm including handles)
Weight	12kg (excluding I/O modules, cables, and terminal boards)
Power supply	400W, 100-240V, 50-60Hz, fan-less, zero-noise
Fans	Two at rear (outtake), high quality, low-noise Papst fans
Handles	2 for desktop use 2 for rack installation
Certification	CE and FCC certified

Mainboard & CPU	
Processor	Intel Core i3 3.3GHz (standard) Intel Core i7 3.4GHz (option) Intel Core i7 3.5GHz (option)
Form factor	ATX
Chipset	Intel C216
Bus	PCI, 32-bit/33MHz
Memory	2048MB DDR3 RAM 4096MB (option)
Graphics	Intel HD Graphics 400P onboard
USB	4 x USB 3.0 and 1 x USB 2.0 at front 6 x USB 2.0 internal
Ethernet	2 x Gigabit at front
Serial Ports (for baud rates up to 115kb/s only)	1 x RS232/422/485 at front 1 x RS232/422/485 and 4 x RS232 internal
Keyboard & mouse	1 x PS/2 at front
BIOS	American Megatrend Inc. (AMI)
Number of slots for I/O modules	3 PCI 4 x PCIe 1 x Mini PCIe

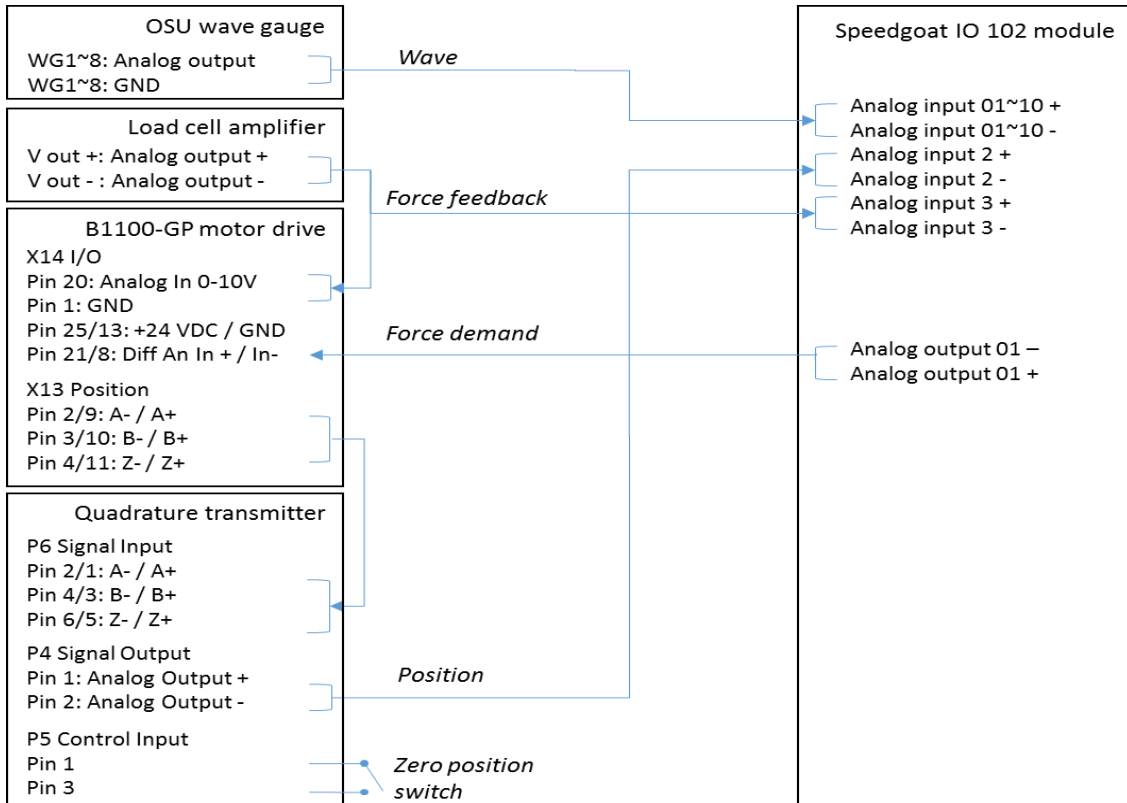
Drives	
Standard (for storing real-time application, Simulink Real-Time kernel, and logged data)	1 x 60GB SSD (read transfer rates up to 450MB/s, write transfer rates up to 450MB/s)
Options:	500GB or 1TB HDD 256GB SSD (read transfer rates up to 540MB/s, and write transfer rates of up to 520MB/s)
Power	
Power inlet	AC 100-240V, 50/60Hz, at rear
Power switch	at rear
Secondary power switch	at front
Reset button	none (secondary power switch)
Power LED	at front (combined with secondary power switch)
Environment	
Temperature	0° to +60°C (operating)
Humidity	10-90%, non-condensing
Software	
OS / RTOS	FreeDOS / Simulink Real-Time™ kernel, preinstalled on CompactFlash or Hard Disk for current release of MathWorks software
Development computer	Utilities for kernel transfer, I/O drivers and Simulink test models for your selected I/O modules

2. IO 102 module

Physical	
Form factor	PMC
Power requirements	+5VDC \pm 0.2 VDC at 1.4 Amps, maximum, 0.9 Amps typical
PCI bus	32bit / 33MHz
Connector	68-way SCSI3 Cable connectors: Tyco Electronics Board connector: Tyco Electronics part no. 5749069-7
Environmental	
Operating temperature	0 to 70°C (extended temperature variant: -40°C to +85°C)
Relative humidity	0 to 95%, non-condensing
Analog inputs (at 25°C)	
Number of inputs	Standard variant: 32 input lines, configurable as 32 single-ended or 16 differential channels, one A/D converter for all channels HV variant: 16 input lines, configurable as 16 single-ended or 8 differential channels, one A/D converter for all channels
Resolution	16 Bits (0.0015 percent of FSR)
Channel conversion time	3.3 μ s, maximum
Sampling mode	Sequential; 2, 4, 8, 16, or 32 channels per scan (32 channels available only in single-ended mode)
Voltage Ranges	Driver configurable as \pm 10V, \pm 5V or \pm 2.5V (HV variant: \pm 60V, \pm 30V or \pm 15V)
Input impedance	1MOhm line-to-ground, 2MOhm line-to-line, in parallel with 100pF (HV variant: 180K line-to-ground)
Bias current	80nA, maximum
Crosstalk rejection	85dB, DC-10kHz
Signal/Noise ratio (SNR)	80dB typical
Common mode rejection	60dB DC-60Hz, differential input mode
Over voltage protection	\pm 30V with power applied, \pm 15 Volts with power removed (HV variant: \pm 70 Volts).
DC accuracy (maximum composite error after autocalibration)	Standard variant: \pm 10V range: \pm 3.2mV (midscale accuracy), \pm 4.2mV (full scale accuracy) \pm 5V range: \pm 2.3mV (midscale accuracy), \pm 2.8mV (full scale accuracy) \pm 2.5V range: \pm 1.6mV (midscale accuracy), \pm 2mV (full scale accuracy) HV variant: \pm 60V range: \pm 30mV (midscale accuracy), \pm 6% of range (full scale accuracy) \pm 30V range: \pm 17mV (midscale accuracy), \pm 6% of range (full scale accuracy) \pm 15V range: \pm 10mV (midscale accuracy), \pm 6% of range (full scale accuracy)
Integral nonlinearity	\pm 0.003 percent FSR (FSR = fullscale range; e.g.: 20V on \pm 10V range)
Differential nonlinearity	\pm 0.0015 percent FSR

Analog outputs (at 25°C)	
Configuration	4 single-ended output channels
Resolution	16 Bits (0.0015 percent of FSR)
Settling time	8 μ s to 1LSB, typical 50% fullscale step
Voltage ranges	Same as selected for analog inputs: ± 10 , ± 5 or ± 2.5 V
Output resistance	1.0 Ohm maximum at I/O connector pins
Output protection	Withstands sustained short-circuiting to ground
Load current	Zero to ± 3 mA per channel
Load capacitance	Stable with 0 to 2000pF shunt capacitance
Noise	1.0mV-RMS, 10Hz-1MHz typical
Glitch Impulse	5 nV-Sec, typical on ± 2.5 V range
DC Accuracy (Max error, no-load):	± 10 V range: ± 2.7 mV (midscale accuracy), ± 3 mV (full scale accuracy) ± 5 V range: ± 1.9 mV (midscale accuracy), ± 2.3 mV (full scale accuracy) ± 2.5 V range: ± 1.3 mV (midscale accuracy), ± 1.7 mV (full scale accuracy)
Crosstalk rejection	85 dB minimum, DC - 1000 Hz
Integral nonlinearity	± 0.004 percent of FSR, maximum
Differential nonlinearity	± 0.0015 percent FSR
Digital I/O (at 25°C)	
Ports	16 bidirectional lines, configurable in groups of 8
Levels	Standard TTL
Output load	8mA

APPENDIX D: INSTRUMENTATION WIRING



APPENDIX F: LINMOT-TALK SETTING

1) Motor Wizard

Step 5/9; Additional Load Mass 1308 g

Step 7/9; Speed: 0.01 m/s, Mode: Actual Position

Step 8/9; Distance A: 750 mm

Step 9/9; HP: 0 mm, IP: 0 mm

2) Force feedback control setting

Project tree window: Parameters > Motion control SW > Protected Technology Functions > Analog Force Feedback Control

> Input Selection: Analog Input On X14.20

> Analog Force Feedback Config

0 V: -183.7 N (negative)

10 V: 157.8 N (positive)

Note: values are from calibration slope, but it should be tuned to have zero measured force at neutral position. (To check measured force, go to the Project tree windows: Variables > MC SW Force Control)

> Force Control Parameters

P Gain: 0.2 A/N

I Gain: 2 A/(N*s)

3) Command table setting (X14.16)

Entry ID: 10

Motion Command Type: VAI Go To Pos With Higher Force Ctrl Limit and Target Force

Target Position: -20 mm

Max. Velocity: 0.01 m/s

Acceleration: 0.1 m/s²

Force Limit: -0.9 N

Target Force: -1 N

4) Encoder setting for position (LT61QD)

Running a IS2 program after connecting a RS232 cable between the encoder and PC.

Output type: +/- 10 V

Output reading range: +/- 3000 (During the TEST III, it is changed to +/- 300 with 100 um resolution value of encoder simulation in LinMot-talk)

5) Force control operating

After homing the motor (check both 0. Switch on and 11. Home) first, uncheck the 11. Home of override value side.

After that, check both X14.16 in IO panel. If the motor is now in force control mode, the 9. Special Motion Active in Status window indicates on (1).

APPENDIX G: TEST RUNS

1) TEST CAMPAIGN I

Full Scale	Input		
Run#	Wave Height (m)	Wave Period (s)	Comments
20	1	5	Excitation Test
21	1	7	Excitation Test
22	1	9	Excitation Test
23	1	11	Excitation Test
24	1	13	Excitation Test
25	1	15	Excitation Test
26	1	17	Excitation Test
27	1	11	Excitation Test
28	1	5	Excitation Test
30			Free-Decay Test
40	1	9	Linear Damping
41	1	7	Linear Damping
42	1	11	Linear Damping
52	1	11	MPC
53	1	13	MPC
54	1	15	MPC
55	1	17	MPC

2) TEST CAMPAIGN II

Full Scale	Input			
Run#	Wave Height (m)	Wave Period (s)	Linear Damping	Comments
703	1	5	100000	Linear Damp.
704	1	5	200000	Linear Damp.
705	1	5	300000	Linear Damp.
706	1	5	400000	Linear Damp.
707	1	5	500000	Linear Damp.
708	1	7	300000	Linear Damp.

709	1	7	400000	Linear Damp.
710	1	7	500000	Linear Damp.
711	1	7	600000	Linear Damp.
712	1	7	1000000	Linear Damp.
713	1	9	700000	Linear Damp.
714	1	9	800000	Linear Damp.
715	1	9	900000	Linear Damp.
716	1	9	1000000	Linear Damp.
717	1	9	1100000	Linear Damp.
718	1	11	1100000	Linear Damp.
719	1	11	1200000	Linear Damp.
720	1	11	1300000	Linear Damp.
721	1	11	1400000	Linear Damp.
722	1	13	1500000	Linear Damp.
723	1	13	1400000	Linear Damp.
724	1	13	1300000	Linear Damp.
725	1	13	1200000	Linear Damp.
726	1	15	1700000	Linear Damp.
727	1	15	1800000	Linear Damp.
728	1	15	1900000	Linear Damp.
729	1	17	2000000	Linear Damp.
730	1	17	2100000	Linear Damp.
731	1	17	2200000	Linear Damp.
732	1	7	700000	Linear Damp.
733	1	7	800000	Linear Damp.
734	1	9	1200000	Linear Damp.
735	1	11	1500000	Linear Damp.
736	1	13	1100000	Linear Damp.
737	1	15	1600000	Linear Damp.
738	1	15	2000000	Linear Damp.
739	1	15	2100000	Linear Damp.
740	1	15	2200000	Linear Damp.
741	1	13	1600000	Linear Damp.

742	1	5	1000000	Linear Damp.
743	1	11	1000000	Linear Damp.
744	1	13	1000000	Linear Damp.
745	1	15	1000000	Linear Damp.
746	1	17	1000000	Linear Damp.
802	1	5		Causal control
803	1	7		Causal control
804	1	9		Causal control
805	1	11		Causal control
806	1	13		Causal control
807	1	15		Causal control
808	1	17		Causal control
900	1	11		Linear MPC
901	1	13		Linear MPC
902	1	13		Linear MPC
903	1	15		Linear MPC
904	1	17		Linear MPC
905	1	5		Linear MPC
906	1	7		Linear MPC
907	1	9		Linear MPC
908	1	11		Linear MPC
910	1	7		Uni-MPC
911	1	9		Uni-MPC
912	1	11		Uni-MPC
913	1	13		Uni-MPC
914	1	15		Uni-MPC
915	1	17		Uni-MPC
916	1	5		Uni-MPC
920	1	7		Uni-MPC (Neg)
921	1	9		Uni-MPC (Neg)
922	1	11		Uni-MPC (Neg)
923	1	13		Uni-MPC (Neg)
924	1	15		Uni-MPC (Neg)

925	1	17		Uni-MPC (Neg)
926	1	5		Uni-MPC (Neg)
930	1	7		Nonlinear (opt2)
931	1	9		Nonlinear (opt2)
932	1	11		Nonlinear (opt2)
933	1	13		Nonlinear (opt2)
934	1	15		Nonlinear (opt2)
935	1	5		Nonlinear (opt2)
940	1	7		Nonlinear (opt4)
941	1	9		Nonlinear (opt4)
942	1	11		Nonlinear (opt4)
943	1	5		Nonlinear (opt4)
944	1	7		Nonlinear (opt4)
945	1	9		Nonlinear (opt4)
946	1	11		Nonlinear (opt4)
947	1	13		Nonlinear (opt4)
948	1	15		Nonlinear (opt4)

3) TEST CAMPAIGN III

Full Scale	Input			
Run#	Wave Height (m)	Wave Period (s)	Damping (Ns/m)	Comments
H=1m				
6026	1	5	150000	Linear Damp.
6000	1	5	200000	Linear Damp.
6036	1	5	238476	Linear Damp.
6034	1	5	250000	Linear Damp.
6035	1	5	300000	Linear Damp.
6061	1	6	402436	Linear Damp.
6037	1	7	400000	Linear Damp.
6001	1	7	500000	Linear Damp.
6038	1	7	569476	Linear Damp.
6039	1	7	600000	Linear Damp.

6040	1	7	700000	Linear Damp.
6062	1	8	749936	Linear Damp.
6041	1	9	800000	Linear Damp.
6002	1	9	900000	Linear Damp.
6042	1	9	940976	Linear Damp.
6043	1	9	1000000	Linear Damp.
6044	1	9	1100000	Linear Damp.
6063	1	10	1117436	Linear Damp.
6045	1	11	1100000	Linear Damp.
6046	1	11	1200000	Linear Damp.
6003	1	11	1300000	Linear Damp.
6047	1	11	1400000	Linear Damp.
6048	1	11	1500000	Linear Damp.
6064	1	12	1482436	Linear Damp.
6049	1	13	1550000	Linear Damp.
6004	1	13	1600000	Linear Damp.
6050	1	13	1650976	Linear Damp.
6051	1	13	1700000	Linear Damp.
6052	1	13	1750000	Linear Damp.
6065	1	14	1824936	Linear Damp.
6053	1	15	1900000	Linear Damp.
6054	1	15	1950000	Linear Damp.
6005	1	15	2000000	Linear Damp.
6055	1	15	2050000	Linear Damp.
6056	1	15	2100000	Linear Damp.
6066	1	16	2136936	Linear Damp.
6057	1	17	1950000	Linear Damp.
6006	1	17	2000000	Linear Damp.
6058	1	17	2312476	Linear Damp.
6059	1	17	2500000	Linear Damp.
6060	1	17	2550000	Linear Damp.
H=2m				
6007	2	5	2000000	Linear Damp.

6008	2	7	500000	Linear Damp.
6009	2	9	900000	Linear Damp.
6010	2	11	1300000	Linear Damp.
6011	2	13	1600000	Linear Damp.
6012	2	15	2000000	Linear Damp.
6019	1	5		Linear MPC
6073	1	6		Linear MPC
6020	1	7		Linear MPC
6074	1	8		Linear MPC
6014	1	9		Linear MPC
6075	1	10		Linear MPC
6015	1	11		Linear MPC
6076	1	12		Linear MPC
6016	1	13		Linear MPC
6077	1	14		Linear MPC
6017	1	15		Linear MPC
6078	1	16		Linear MPC
6018	1	17		Linear MPC
6019	1	5		Linear MPC (re-run sim.)
6020	1	7		Linear MPC (re-run sim.)
6014	1	9		Linear MPC (re-run sim.)
6015	1	11		Linear MPC (re-run sim.)
6016	1	13		Linear MPC (re-run sim.)
6017	1	15		Linear MPC (re-run sim.)
6018	1	17		Linear MPC (re-run sim.)
6019	1	5		Linear MPC (re-run sim.)
6020	1	7		Linear MPC (re-run sim.)
6014	1	9		Linear MPC (re-run sim.)
6015	1	11		Linear MPC (re-run sim.)
6016	1	13		Linear MPC (re-run sim.)
6017	1	15		Linear MPC (re-run sim.)
6018	1	17		Linear MPC (re-run sim.)
6086	1	5		Linear MPC (Uni-Pos)

6087	1	7		Linear MPC (Uni-Pos)
6088	1	9		Linear MPC (Uni-Pos)
6089	1	11		Linear MPC (Uni-Pos)
6090	1	13		Linear MPC (Uni-Pos)
6091	1	15		Linear MPC (Uni-Pos)
6092	1	17		Linear MPC (Uni-Pos)
6079	1	5		Nonlinear MPC (opt 4)
6080	1	7		Nonlinear MPC (opt 4)
6081	1	9		Nonlinear MPC (opt 4)
6082	1	11		Nonlinear MPC (opt 4)
6083	1	13		Nonlinear MPC (opt 4)
6084	1	15		Nonlinear MPC (opt 4)
6085	1	17		Nonlinear MPC (opt 4)
6093	1	5		Nonlinear MPC (opt 2)
6094	1	7		Nonlinear MPC (opt 2)
6095	1	9		Nonlinear MPC (opt 2)
6096	1	11		Nonlinear MPC (opt 2)
6097	1	13		Nonlinear MPC (opt 2)
6098	1	15		Nonlinear MPC (opt 2)
6099	1	17		Nonlinear MPC (opt 2)
6068	1	5	$\alpha=4, \gamma=1e2$	Causal (re-run)
6028	1	7	$\alpha=1, \gamma=2e4$	Causal
6071	1	9	$\alpha=4, \gamma=1e2$	Causal (re-run)
6030	1	11	$\alpha=4, \gamma=1e2$	Causal
6031	1	13	$\alpha=2, \gamma=5e1$	Causal
6032	1	15	$\alpha=2, \gamma=5e1$	Causal
6033	1	17	$\alpha=2, \gamma=5e1$	Causal
6200	1	9	756600	Irregular (Lin. Damping)
6201	1	11	1013600	Irregular (Lin. Damping)
6205	1	9		Irregular (Linear MPC)
6206	1	11		Irregular (Linear MPC)